On the dynamics of nonstructural carbohydrates in woody plants

by

Scott Oswald

(Under the Direction of Doug P. Aubrey)

Abstract

The major products of photosynthesis in plants are nonstructural carbohydrates, sugars and starch. Sugars serve as transport molecule and intermediate in cell metabolism while starch acts a storage molecule, sequestering the energy and carbon for later use. Because they sit at the intersection of plant photosynthesis and the rest of plant metabolism, nonstructural carbohydrates interact with the major carbon fluxes in plant physiology such as photosynthesis and respiration. Furthermore, excess photosynthesis need not be all allocated to growth. Observations of nonstructural carbohydrate dynamics might indicate the status of plant carbon balance or the priority of storage relative to growth. Despite a number of experiments over more than 20 years, many aspects of nonstructural carbohydrate dynamics remain mysterious. We study these dynamics in an effort to render the mysterious obvious. We present three main results. The first is that simple feedbacks can create a number of dynamical phenomena (such as lag or hysteresis) in seasonal nonstructural carbohydrate dynamics. The second is an experiment on the post-drought change in seasonal nonstructural carbohydrate dynamics, for which we employ the first result. The third is that feedbacks provide important structure for ecosystem models, especially when implementing nonstructural carbohydrate models. Taken together, these results suggest that a simple feedback loop is sufficient to describe much of the heretofore mysterious nonstructural carbohydrates dynamics; however, much work to confirm and elaborate on these ideas remains.

Index words: nonstructural carbohydrates, carbon storage, carbon dynamics, plant physiology, mathematical modeling

On the dynamics of nonstructural carbohydrates in woody plants

by

Scott Oswald

B.S. Biology, Goergia Southern University, 2016

A Dissertation Submitted to the Graduate Faculty of the
University of Georgia in Partial Fulfillment of the Requirements for the Degree.

Doctor of Philosophy

Athens, Georgia

2023

On the dynamics of nonstructural carbohydrates in woody plants

by

Scott Oswald

Major Professor:	Doug Aubrey
Committee:	Alex Bucksch
	Dan Johnson
	Joe O'Brien

Electronic Version Approved:

Ron Walcott
Dean of the Graduate School
The University of Georgia
May 2023

Dedication

To my parents and friends will supported me through out.

Acknowledgments

I would like to thank my fellow lab mates, my friends, and my family for their help over the years. We thank the USDA National Institute of Food and Agriculture, the U.S. Department of Energy, the Office of Science Graduate Student Research (SCGSR) program, the University of Georgia Research Foundation, and the U.S. Forest Service Savannah River for providing funding. We thank Old Castle Lawn & Garden Southeast (Atlanta, GA) for their donation of soil used in the experiment described in Chapter 3.

Contents

List of Figures

List of Tables

Chapter 1

Introduction

Plants are about 45% carbon by dry mass (Epstein, 2005; Ma et al., 2018). This proportion is not surprising given that carbohydrates are about 45% carbon by mass and that carbohydrates such as cellulose (44%), hemicelluloses (44%), sugars (40-42%), and starch (44%) comprise a large part of plant cells and wood. Carbon atoms form the structural backbone of all biological chemical compounds. Save a few exceptions, plants absorb all of the carbon in their bodies from the atmosphere by using light to reduce carbon dioxide into organic compounds. Carbon and oxygen assimilated by photosynthesis form the majority of plant biomass. Collectively, plants provide all of the carbon present in terrestrial ecosystems. Thus, terrestrial ecosystems represent half of all carbon assimilated on Earth, even if dry land only covers 25% of the total surface area (Bonan, 2008; Chapin et al., 2011). The absorption of carbon by land plants is great enough that we observe a seasonal oscillation with an amplitude $\approx$ 3-4 $\mu\mathrm{mol\,mol}^{-1}$ in worldwide atmospheric concentrations of carbon dioxide (Keeling et al., 1976). These oscillations occur in sync with the seasons of the northern hemisphere which contains a greater fraction of terrestrial surface area that the southern one and thus has large boreal forests that are behind this effect. For more than 200 years, the concentration of carbon dioxide has increased due to anthropogenic emission. This increase drives a change of climate and an acidification of the ocean which have negative effects for ecosystems and human societies.

Recognizing its importance in the carbon balance of the atmosphere, plant physiology has attracted great attention. Obviously, knowing photosynthesis and photosynthetic responses to environmental changes are mandatory for prediction, but by itself is insufficient. Essentially, we must predict whether forests will grow or recede in terms of surface area and biomass in order to know future carbon exchange. Despite a robust description of photosynthesis (Farquhar et al., 1980; von Caemmerer, 2013), we must admit photosynthesis is not growth. For example, a number of experiments on the free air carbon dioxide enrichment (FACE) demonstrate that an increase in photosynthesis does not always lead to an increase in plant growth (Ainsworth & Long, 2005; Norby et al., 2022; Norby & Zak, 2011). Besides its effect on the atmosphere, agricultural yields and plant resilience to environmental stressors stimulate research on the link between photosynthesis and growth. Thus, the study of the carbon balance between photosynthesis and various demands for photosynthate unites these three objectives.

The role of photosynthate in carbon balance is not only limited to its production and its consumption. There also exists the storage of photosynthate, thus raising a question: of what is produced, how much is stored? How much is consumed? There does not yet exist a final answer, but the present work describes certain results toward this end. The fruit of three projects are described (See Chapter2–4). To put these results in a wider context, the rest of this chapter summarizes the current situation of research on photosynthate storage and on the role of storage in carbon balance. In describing the main experimental facts and tracing the evolution of theoretical frameworks of the recent past, we seek to establish the current status of this science, and not to make a historical account. We address this body of science in the present work to note gaps in the theoretical development of nonstructural carbohydrates thereby sharpening it.

A short terminological detour will bring us to the beginning of this summary. Above, we use the photosynthate—that is what is produced or synthesized by photosynthesis—but it is not a precise term, grouping together several possible chemical compounds. We also speak of carbon reserves, carbon storage, and nonstructural carbon. These three terms effectively group together any chemical compound that serves as storage in a budget between supply (production) and demand (consumption); in other words, these terms define a class of compounds by their function. In fact, nonstructural carbon could be applied to any compound not used for plant structure, but it is applied to reserves in practice. Its origin seems to be the opposite of structural carbon, the carbon needed for growth (division and elongation of new cells). While general, it is difficult to measure the quantity of carbon reserves because one must choose whether each chemical compound is part of the reserves or not. This choice raises a theoretical problem, and we will examine it closely later in this summary. Practice is simpler to describe. We measure nonstructural carbohydrates, that is starch and sugars[1], Starch is a glucose chain of $\alpha(1 \rightarrow 4)$ bonds (amylose) and $\alpha(1 \rightarrow 6)$ bonds (amylopectin) unlike cellulose which is composed of glucose monomers with $\beta(1 \rightarrow 4)$ bonds[2]. While there is a great diversity of sugars in plants, hexoses and disaccharides are the most common forms, especially glucose, sucrose, fructose, and galactose. Using a chemical assay, the concentration of these compounds may be quantified, and thus one obtains a measurement of the total quantity contained in a tissue sample. Since they are what is measured, nonstructural carbohydrates occupy the center of research into storage and its role in carbon balance.

1.1 Storage as investment

To begin our summary, Chapin et al., 1990 presents a theory of storage that defines storage as the resources which accumulate and could support future biosynthesis and growth. These authors distinguish three classes of storage: accumulation, reserve formation, and recycling (Chapin et al., 1990). Accumulation is the increase of compounds that do not "promote" growth or plant defense (Chapin et al., 1990). They add that an excess of photosynthate supply relative to demands results in accumulation (Chapin et al., 1990). On the other hand, reserve formation diverts a part of this supply toward storage (Chapin et al., 1990). Recycling is the consumption of structural compounds (products of growth or defense) to support

[1] Cellulose and hemicellulose are structural carbohydrates.

[2] A matter of different orientations relative to the stereocenter.

new biosynthesis (Chapin et al., 1990). This classification by function has immediate problems, and even Chapin et al., 1990 admit that the same compound may be produced by accumulation or by reserve formation, and they recognize that the classification of compounds in these is difficult. However, this storage schema has survived in mutated forms. The central idea that forms the basis of the theory proposed by Chapin et al., 1990 is the economic analogy. As a company draws a profit if its revenue exceeds its costs, a plant earns a "profit" if carbon supply via photosynthesis exceeds the current metabolic demand needed to remain alive. As a company reinvests to increase its revenue, a plant reinvests the excess in growth to increase its ability to gather resources from the environment or to reproduce (Chapin et al., 1990). Even if storage competes with growth, according to Chapin et al., 1990, there exists three reasons for storage: to permit a lag in time between supply and demand, to avoid death following catastrophic tissue losses like fire or grazing, and to prepare for reproduction. In essence, to understand the allocation between various processes, one must understand the opportunity costs.

With this analogy, the authors discuss several phenomena (Chapin et al., 1990). To cite several examples, plants maintain a nearly constant efflux throughout the course of a diurnal cycle despite photosynthetic variations (Baysdorfer & Robinson, 1985; Fondy & Geiger, 1985; Fox & Geiger, 1984); and starch acts as storage to support this efflux at night (Chapin et al., 1990). However, leaves export photosynthate before mobilizing their starch reserves (Schulze et al., 1991) which shows that storage (starch synthesis) has an opportunity cost relative to export (Chapin et al., 1990). Likewise, mutants that do not produce starch exhibit a greater diurnal variation in sugars (Schulze et al., 1991) and thus an elevated respiration rate which brings about an overall decrease in growth (Chapin et al., 1990). Chapin et al., 1990 remark that the reserves of perennials growing within a seasonal environment decline throughout periods of high growth but recover whenever growth slows or stops. The opportunity cost forms a basis to understand the lifecycle of biannuals that accumulate a reserve during their first year to fuel rapid reproductive growth during the second year (Chapin et al., 1990). Chapin et al., 1990 also remark that the experiments needed to differentiate between their proposed hypotheses have yet to be performed.

Despite its effect on research, the 30 years since Chapin et al., 1990 raised these questions have not answered them. Even if this work is still cited and its ideas still stimulate research, it is difficult to classify a process as reserve formation or accumulation, or to measure opportunity costs. While Chapin et al., 1990 present this economic theory as a qualitative theory, and not a quantitative one, this analogy easily leads to a mathematical theory for calculating carbon allocation (Chiariello & Roughgarden, 1984; Cohen, 1966, 1971; Iwasa et al., 1984; Iwasa & Cohen, 1989; Klinkhamer et al., 1997; Kozłowski & Wiegert, 1986; Schaffer, 1983). Comparing opportunity costs becomes an optimality principle: maximize investment in reproduction. A model constructed according to this principle can reproduce the lifecycle of biannuals, using the same logic as the economic analogy (Chiariello & Roughgarden, 1984). Sometimes, a principle with a shorter time-scale is put forth, such as to maximize current carbon gain, and since Chapin et al., 1990, analyzing resource allocation, especially carbon, along an optimality principle has gone out of fashion (Dewar, 2009; Franklin et al., 2012; Franklin et al., 2020). Unfortunately, we are unaware of any case in which this scheme revealed an unknown phenomenon or described an unexpected observation.

1.2 From sources to sinks

In a review of nonstructural carbohydrates[3], Kozlowski, 1992 describes the transport and use of nonstructural carbohydrates with the help of a notion originating in studies on phloem transport, that of carbohydrate sources and sinks. A source is an organ (or a tissue, cell, etc.) that exports more carbohydrates than it receives, whereas a sink imports more than its own production. These terms designate differences between organs by their role in internal carbon balance; for example, a source leaf produces enough carbohydrate for its own metabolic needs and the surplus is exported by the phloem to a sink leaf that is too young, newly budded to support its own metabolic needs. Leaf development includes a transition from sink to source. Reserves can therefore play both roles, source and sink. Kozlowski, 1992 makes a distinction between reversible and irreversible sinks, the former being an organ which can become a source and the latter an organ which cannot become one. According to the Münch pressure flow hypothesis, phloem loading and unloading by each organ generates a gradient in sugar concentrations across the phloem (Dinant, 2008; Jensen, 2018; Jensen et al., 2012; Knoblauch et al., 2016; Stroock et al., 2014). Sources load sugars into the phloem and sinks unload them, and from this process, sugars are redistributed across the plant body.

Using this terminology, Kozlowski, 1992 exhaustively examines the role of carbohydrates in growth, respiration, transport, and storage. In describing carbohydrate physiology, Kozlowski, 1992 does not express a theory as such but its description echoes Chapin et al., 1990. The allocation of sugars between sources and sinks depends on the sink strength (sink activity) and its sink potential, that is the current or potential capacity of an organ to attract or absorb photosynthate (Kozlowski, 1992). A salient detail, Kozlowski, 1992 specifies that the import rate of carbohydrates by an organ changes if either its sink strength changes or the sink strength of another organ changes, and that a change in sink strength can modify the allocation between organs without changing the raw production of dry matter. Therefore, according to the definition, sink strength is not the carbohydrate flux from phloem unloading. Kozlowski, 1992 proposes the difference between local photosynthesis and respiration as an indicator of sink strength. To describe allocation, the utility of sink strength is not clear, Kozlowski, 1992 summarizes Chapin et al., 1990, stating that nonstructural carbohydrates accumulate if production exceeds use and they deplete if otherwise.

While Kozlowski, 1992 does not highlight it, carbon allocation between sources and sinks is linked to phloem mechanics (Dinant, 2008). Mathematical models of phloem transport (Jensen, 2018; Thompson & Holbrook, 2003) and especially those that describe the coupling of the xylem and phloem reveal that phloem loading ties the phloem sugar concentrations not only to those of adjacent tissues, but also to starch synthesis (Daudet et al., 2002; Lacointe & Minchin, 2008). If carbon allocation follows an optimality principle, its effect must be present in phloem transport and the link between nonstructural carbohydrates and the phloem must result from it. Effectively, reserves complicate the relationship between sources and sinks. Source leaves form a starch reserve during the day to export it at night; therefore they are part of reserves but do not change their source-sink status. On the other hand, roots (especially root parenchyma)

[3] This term had yet to take root at the time.

are sinks until the flux changes directions and their reserves are mobilized. Seasonal leaf-out or regrowth following a tissue loss causes this change in source-sink status. Therefore, root reserves must attract a large part of the internal allocation, but what causes this storage ? A surplus of supply in the leaves that exceeds the metabolic needs of the roots? Or if not, an elevated demand in the roots to form its reserves? And what stimulates this change from source to sink? A reduction of import or a phytohormone? Chapin et al., 1990 conclude that starch synthesis has an opportunity cost relative to transport which suggests that synthesis, transport, and mobilization must be regulated to anticipate whole-plant needs.

1.3 Carbon limitation

While studying possible plant responses to changes in the climate driven by an increase in atmospheric CO_2, Körner, 2003 examines nonstructural carbohydrates (and in limited fashion, nonstructural lipids) to ask the question: Are plants, especially wild trees, limited in their growth by a lack of carbon; that is a lack of photosynthate? If an increase in CO_2 stimulates photosynthesis, will it also stimulate plant growth worldwide? Körner, 2003 posits that nonstructural carbohydrates indicate the carbon balance according to the logic uttered by Chapin et al., 1990 and Kozlowski, 1992. Accumulation indicates a surplus of carbon while depletion indicates a deficit of carbon. According to Körner, 2003, the rate of change in nonstructural carbohydrates reflects the balance between source and sink activity, alluding to the terminology employed in Kozlowski, 1992. Briefly, Körner, 2003 concludes that growth is not limited by carbon supply (by neither photosynthesis nor nonstructural carbohydrates) because the concentrations of nonstructural carbohydrates remain elevated or even increase during periods of growth reduced by cold or drought (Hoch et al., 2003; Hoch et al., 2002). Moreover, an increase in CO_2 around leaves or the entire canopy leads to an increases in nonstructural carbohydrates in the leaves (Körner, 2003; Würth et al., 1998). Körner, 2003 also highlights that the starch increases more than the sugar after low temperatures or droughts, which contradicts the possibility of an effect via xylem transport.

This conclusion is based on a somewhat informal analysis of time series of nonstructural carbohdyrates, but more elaborated than in Chapin et al., 1990. The argument is well reasoned and persuasive but not without flaws. Concentrations are not fluxes, and thus a high or low concentration reveals little about carbon balance. Körner, 2003 remarks that his laboratory has never observed a case of complete depletion in carbon reserves even during periods of high demand, implying that nonstructural carbohydrates are abundant and do not limit growth. However, only a deficit yields a decrease in reserves, and if high demand is countered by high carbon supply, then carbon reserves remain constant. A feedback between the fluxes and nonstructural carbohydrates could prevent depletion by reducing demand given a weak supply. Likewise, a feedback could prevent supply from exceeding demand when larges reserves are already present.

In fact, we should expect such a feedback as we argue in Chapter 2. We show therein that maxima and minima in nonstructural carbohydrates are indicators for changes in the balance between supply and demand. Moreover, a constant concentration indicates equal carbon supply and demand. We also show that the magnitude of fluxes is linked to the time required for an equilibrium to be established. This is not

a contradiction of these conclusions but a sharpening. The primary goal of the present work is to study these questions. The derivation of results that we describe there led to the recognition of these problems.

1.4 Death by drought: a lack of carbon?

Before continuing the development of theories on nonstructural carbohydrates, we must detour through adjacent debate, the physiological causes of death during drought. When available water in the soil is depleted, plants risk death due to dehydration. Many species respond to this risk by closing their stomata which reduces the rate of carbon assimilation while conserving water. Drought influences plant carbon balance and thus the nonstructural carbohydrates. For this reason, it was proposed that carbon starvation is the cause of a certain fraction, possibly the majority of plant mortality during or after a drought (Mcdowell, 2011; Mcdowell & Sevanto, 2010; Mcdowell et al., 2013; Mcdowell et al., 2008). On one hand, this debate interests us because Chapter 3 presents a study on the effect of water stress on seasonal variation of nonstructural carbohydrates. On the other hand, if a lack of carbon triggers death during a drought, then nonstructural carbohydrates as carbon reserves grant protection against this risk (Mcdowell, 2011). In dry climates, the protection may be worth growth reductions depending on opportunity costs to echo Chapin et al., 1990.

This link is problematic given the observations reviewed by Körner, 2003; in other words, nonstructural carbohydrate seem to either increase or remain constant during drought, especially regular seasonal drought. Körner, 2003 explains this by the greater sensitivity to water stress (in particular decreases in water potential) of growth relative to photosynthesis (Fatichi et al., 2014; Körner, 2015). In fact, Mcdowell, 2011 assumes that photosynthesis is almost as sensitive as growth while maintenance respiration decrease slowly during several weeks such that it dominates the other fluxes (See Fig. 1 in Mcdowell, 2011). By supposing it so, the conclusion follows but is vacuous. Yet, this vacuous conclusion is not the only gap. Adams et al., 2017 provides an analysis of several studies concluding that while a loss of xylem conductance is always associated with mortality, a decrease in nonstructural carbohydrates is less tightly linked to mortality by drought.

It is possible that the effect is more complex than described, involving the role of sugars in water flux. Based on their observations, Sevanto et al., 2014 propose a difference between rapid and gradual droughts. The rapid onset of intense water stress causes xylem and phloem failure, which stops phloem transport, while gradual onset allows transport by the phloem of carbohydrates during drought (Sevanto et al., 2014). It is possible that the depletion of carbohydrates may drive the failure of phloem transport. In fact, Martínez-Vilalta et al., 2019; Sapés et al., 2019 argue that cell and tissue hydration is more important than water potential itself, and sugars contribute to osmotic potential throughout the plant body, affecting the water balance of cells as much as phloem transport. On a related note, Sapés et al., 2020 provide data that seem to show that nonstructural carbohydrate depletion may bring about a loss of turgor. As we have established, sugar gradients generate the necessary force to drive sugar from a source to sinks (Dinant, 2008; Stroock et al., 2014). Sevanto, 2018 detail several known or possible effects of water stress on phloem transport (Sevanto, 2014). In a model of coupled xylem and phloem transport, the transpiration

rate through the xylem affected the flux from sources to sinks and thus the overall allocation (Lacointe & Minchin, 2008). Briefly, nonstructural carbohydrates are tied to water stress, and thus might have opportunity costs between storage and growth, but to what degree remains unknown. It seems that the links are indirect, by way of the effect on growth and transport rather than photosynthesis.

1.5 Active or passive?

Responding to Körner, 2003 and his analysis, Sala et al., 2012 and Wiley and Helliker, 2012 present a theoretical framework that calls back to Chapin et al., 1990. Using the economic terminology, Sala et al., 2012 recognize that carbon storage results from the balance between carbon supply and demand, but they summarize the categories of Chapin et al., 1990 as active and passive. According to them, the problem in the analysis of Körner, 2003 is that he does not account for any possible regulation of storage, and that growth may be reduced to maintain a certain quantity of nonstructural carbohydrates. If reserves only result from the net difference in supply and demand, Sala et al., 2012 term them passive reserves, calling reserves active if they are regulated. A large fraction of nonstructural carbohydrates are not consumed during the course a year despite seasonal variations (Hoch et al., 2003; Martínez-vilalta et al., 2016), and thus it is possible that this reserve does not represent a surplus but rather a regulation of growth and metabolism (Sala et al., 2012). These reserves are kepr to meet any "unexpected" deficits. Sala et al., 2012 cite the example of rubber tree tapping where tapping stimulates a reduction in nonstructural carbohydrate concentrations (Silpi et al., 2007) whereas olive trees do not experience a similar decrease during years of high fruit and oil production (Bustan et al., 2011). The maintenance of carbohydrates does not indicate the absence of high demand, only that demand equals supply. Sala et al., 2012 also cite the coordination between leaf starch as reviewed by A. M. Smith and Stitt, 2007 (see below). By examining the possible roles in the xylem system, regrowth, and chemical defenses against herbivores, Sala et al., 2012 argue that reserves represent regulation, that they are actively regulated and not merely the surplus of photosynthesis.

Wiley and Helliker, 2012 provide a similar definition. Passive storage is a non-regulated process, reflecting only the balance of carbon, whereas active storage is regulated (Wiley & Helliker, 2012). Wiley and Helliker, 2012 introduce a notion of priorities between carbon demands, and they present the same general hypothesis that plants have evolved to be conservative regarding carbon allocation preferring storage to crowth to minimize the risk of a mortal deficit. At the same time, they provide an alternative explication to the observations analyzed by Körner, 2003 that the increase in carbohydrates due to low temperatures and to aridity is adaptive (Wiley & Helliker, 2012). To support it, Wiley and Helliker, 2012 cite the partial recovery of reserves with reduced growth following a depletion by defoliation (Li et al., 2002), which is consistent with a higher priority on storage than on growth.

While Sala et al., 2012 and Wiley and Helliker, 2012 take a whole-plant approach, A. M. Smith and Stitt, 2007 examines a similar set of questions but limited to studies on leaf starch in *Arabidopsis thaliana* and employing genomic and metabolic observations. The identification of biochemical mechanisms that generate active regulation would be important evidence for it. They conclude that photosynthesis, growth, and reserve formation of leaf starch are coordinated (A. M. Smith & Stitt, 2007). The principal observation

is that photoperiod variations affects total diurnal accumulation of leaf starch (Gibon, Bläsing, et al., 2004; A. M. Smith & Stitt, 2007). Yet, the synthesis and mobilization of starch appears to be regulated so that reserves run out only at the end of the nighttime period (A. M. Smith & Stitt, 2007). On the other hand, sugars vary little but in *pgm* mutants, which do not produce starch, sugars oscillate diurnally (Gibon, Bläsing, et al., 2004). While RNA transcripts vary throughout the day, enzymes associated with starch synthesis and mobilization do not vary diurnally (Y. Lu et al., 2005; A. M. Smith & Stitt, 2007; S. M. Smith et al., 2004). Carbon starvation caused by a prolonged night only leads to changes in enzyme concentrations after two days of darkness (Gibon, Blaesing, et al., 2004). To summarize, A. M. Smith and Stitt, 2007 posit that the responses to photoperiod changes splits into two categories, an acute and acclimatory response. If enzymes define what reactions are possible and their kinetics, a physiological response could be rather complex without requiring an enzyme change (Tyson et al., 2003).

In conclusion, there exist two interpretation of the same observations, and these interpretations seem to contradict each other, suggesting the utility of in-depth mathematical analysis to resolve the apparent contradiction. Our work, especially Chapter 2, is a small step in a this undertaking. While the analysis of Körner, 2003 contains a few, the reasoning of Sala et al., 2012 and Wiley and Helliker, 2012 is not without gaps. What they define as passive storage is just stoichiometry. As we noted above, a decrease in carbohydrates indicates a deficit and an increase indicates a surplus, but only in the sense that demand exceeds supply and vice versa. Changes in supply and demand affects the level of nonstructural carbohydrates if the balance is not maintained. Therefore a reduction in growth must yield an increase in storage given no other changes. However, there is a complication. We must interpret storage in preceding sentence as the rate of change in nonstructural carbohydrates, and storage becomes a positive flux if carbohydrates are increasing and a negative flux if decreasing. Therefore, an increase in storage could correspond to a negative flux that is less negative than before. In fact, this situation is the norm for chemical reactions. A chemical reaction converts a set of reactants into products (Angeli, 2009); a certain number of carbon atoms are necessary to synthesize starch, for example. However, these stoichiometric numbers do not determine the velocity of reactions nor the dependence of velocities on reactant concentrations, together termed reaction kinetics (Angeli, 2009). Even if an analysis of all chemical reactions responsible for nonstructural carbohydrate metabolism is not feasible, the mathematical structure must resemble that of chemical reaction systems. Regulation must arise from kinetics, and seen in this light, the analysis of Körner, 2003, 2015 may be reconciled with that of Sala et al., 2012; Wiley and Helliker, 2012.

1.6 The Current State

We have summarized the state of this science from the era when works which gave birth to the current work were begun. We note that ideas described above have not changed. They form conceptual basis for theoretical and experimental works. Recent reviews are based on it (Dietze et al., 2014; Fatichi et al., 2019; Hartmann & Trumbore, 2016). Source-sink relations are employed in models (Hayat et al., 2017; Schiestl-Aalto et al., 2015). The implicit opportunity cost between growth and storage is cited in the interpretation of observations (Blumstein et al., 2023; Blumstein et al., 2022; Hinman & Fridley, 2018; J. Huang et al.,

2021). Studies still investigate the question of whether carbohydrates are indicators of carbon balance (Weber et al., 2019; Wiley et al., 2019). Links to the vascular system still raises interest (Kannenberg et al., 2017; Kannenberg & Phillips, 2019) as much as seasonal variations (Davidson et al., 2021; Martínez-vilalta et al., 2016; Schoonmaker et al., 2021; Tixier et al., 2020) and diurnal variations (Gersony et al., 2020; Tixier et al., 2018). Despite this research, nonstructural carbohydrates seem to escape a neat or comprehensive description. However, the language and its implied conceptualization remains well entrenched.

In this milieu, we present this current work which consists of three distinct strokes. In Chapter 2, we describe a theoretical study on the relationship between carbon balance and nonstructural carbohydrates. While it does not fully explain several empirical phenomena of nonstructural carbohydrates, this chapter provides a mathematical viewpoint that resolve the apparent contradiction between the analysis of Körner, 2003, 2015 and Sala et al., 2012; Wiley and Helliker, 2012. It differs from other modeling studies by using mathematical tools to fill in gaps and therefore sharpen existing theories without being detailed numerical simulation. Such simulations exist but have not managed to resolve these theoretical debates. The main results are the recognition of the difference between kinetics and stoichiometry in terms of carbon allocation, the possibility of lag and other forms of hysteresis, and the interaction between seasonal variations of supply and demand.

We also present an experiment on the effect of drought on seasonal variations in nonstructural carbohydrates in Chapter 3. Even though we observed a reduction in growth, we did not observe a significant difference in nonstructural carbohydrates. With the aid of our mathematical analysis in Chapter 2, we provide a possible explanation and future studies that could more definitively answer this question.

In Chapter 4, we apply the analysis of Chapter 2 to ecosystem models. As an analysis of chemical reaction kinetics leads to an analysis of feedbacks in Chapter 2, we pursue this idea to argue that the essential mathematical structure of models depends on these feedbacks. By examining them closely, we might identify the necessary structure so that a model correctly predicts a ecosystem response to climatic changes without knowing the details of all involved processes and without simulating them explicitly. Such an analysis is necessary for the development of sub-models of nonstructural carbohydrates but it allows a comparison of models that are on the surface difficult to compare. While its importance is in its implications for the overall development of models, we use nonstructural carbohdyrates as a restricted example to explore these ideas.

At the end of this document (Chapter 5), we discuss several threads that could act as a guide in future works. We give a summary of our results, highlighting their utility in the current science of nonstructural carbohydrates and plant physiology. We hope this document presents an advance in this field.

Chapter 2

Modeling starch dynamics from seasonal variations of photosynthesis, growth, and respiration.

Oswald, S. W. and Aubrey, D. P. Accepted by *Tree Physiology*.

Abstract Nonstructural carbohydrates (NSCs) buffer differences in plant carbon supply (photosynthesis) and demand (respiration, growth, etc.) but the regulation of their dynamics remains unresolved. Seasonal variations in NSCs are well-documented, but differences in the time-average, amplitude, phase, and other characteristics across ecosystems and functional types lack explanation; furthermore, observed dynamics do not always match expectations. The failure to match observed and expected dynamics has stimulated debate on whether carbon supply or demand drives NSC dynamics. To gain insight into how carbon supply and demand drive seasonal NSC dynamics, we derive a simple model of NSC dynamics based on carbon mass balance and linearizing the NSC demand to determine how supply-driven and demand-driven seasonal NSC dynamics differ. We find that supply-driven and demand-driven dynamics yield distinct timings of seasonal extrema, and supply overrides demand when carbon supply is low in winter (e.g., at high latitudes). Our results also suggest that NSC dynamics often lag changes carbon mass balance. We also predict differences in NSC dynamics across mass, suggesting saplings are more dynamic and respond faster to the environment than mature trees. Our findings suggest substrate-dependent regulation with environmental variation is sufficient to generate complex NSC dynamics.

2.1 Introduction

Plants drive the terrestrial carbon cycle (Bonan, 2008). For terrestrial ecosystems, plant photosynthesis represents the principal source of carbon and free energy (Chapin et al., 2011). The study of plant physiological responses thus provides insights into how ecosystems will respond to climate change. Despite strong mechanistic descriptions of photosynthetic responses to its environmental drivers (Farquhar et al., 1980; von Caemmerer, 2013), obthe same for growth, carbon storage, or carbon allocation remains lacking (Fatichi et al., 2019; Hartmann & Trumbore, 2016). Uncertainty in plant physiological responses is a major source of uncertainty for terrestrial ecosystem carbon cycle models (Arora et al., 2013; Friedlingstein et al., 2014) appearing to result from differences in model structure (Lovenduski & Bonan, 2017; Quetin & Swann, 2018); these discrepancies suggest models fail to capture important feedbacks or regulatory mechanisms in long-term responses. For instance, free-air CO2 enrichment (FACE) studies find that these models correctly predict increased photosynthesis but not necessarily increased growth, typically because of nitrogen limitation (Norby & Zak, 2011; R. S. Nowak et al., 2004). NSCs mediate the decoupling of photosynthesis and the rest of plant metabolism (Aubrey et al., 2012; Aubrey & Teskey, 2018; Ruswick et al., 2021). Describing the dynamics of NSCs will elucidate the nature of this decoupling. Sugars and starch, collectively nonstructural carbohydrates (NSCs), are the stable products of photosynthesis, requiring no nutrients to synthesize, unlike biosynthesis for growth or secondary metabolites. Photosynthesis need not equal growth, respiration, and other aspects of plant metabolism at short-timescales because change in NSCs buffers the difference. Photosynthesis only determines the supply of NSCs but not the demand for NSCs in metabolism. Growth, respiration, and other processes together form the demand for NSCs and therefore only depend on photosynthesis indirectly through their combined effect on the amount of NSCs. NSC concentrations vary temporally in many observations. For instance, NSC concentrations oscillate over the course of each year in many species, but these seasonal variations differ in time-average,

maximum, minimum, and when the maximum and minimum occur across organs, species or functional groups, latitude, and climate (Davidson et al., 2021; Martínez-vilalta et al., 2016; Richardson et al., 2013). Seasonal variations in NSC concentrations likely reflect seasonal changes in plant carbon balance, that is asynchrony between supply and demand (Hartmann & Trumbore, 2016) but the exact nature of this relationship remains contested. Differences in the observed dynamics of sugars and starch, and differences in temporal dynamics across plant organs have also remained difficult to fully explain. In fact, sugars play many roles beyond storage (e.g., biosynthesis, osmoregulation, phloem transport), and their variations may not reflect carbon balance while starch dynamics do.

The nature of the regulation of NSC dynamics remains a major knowledge gap for plant carbon dynamics (Chapin et al., 1990; Hartmann et al., 2020; Körner, 2015; Kozlowski, 1992; Landsberg, 2003), and the exact nature of storage's role in plant carbon dynamics also remains contested (Dietze et al., 2014; Fatichi et al., 2019; Hartmann et al., 2020; Hartmann & Trumbore, 2016; Körner, 2015; Sala et al., 2012). See Sala et al., 2012; Dietze et al., 2014; or Hartmann and Trumbore, 2016 for recent reviews. The debate centers on whether NSC regulation is passive or active (Dietze et al., 2014; Wiley & Helliker, 2012) and whether plant growth is source or sink limited (Fatichi et al., 2019; Körner, 2015). The latter relates to the former because carbon supply minus demand (e.g., growth) equals the change in NSCs regardless of why supply or demand increased or decreased. Some authors interpret large stocks or seasonal increases in NSCs as evidence of non-photosynthetic controls on growth such as nitrogen limitation, water limitation, or temperature-dependent changes (Fatichi et al., 2014; Körner, 2003, 2015; Woodruff, 2014; Woodruff & Meinzer, 2011), and thus they interpret observed NSC dynamics as evidence of sink-limited growth. This interpretation explains the lack of consistent growth responses to CO_2 enrichment studies despite increased photosynthesis, contrary to source-limited growth (Ainsworth & Long, 2005). Other authors suggest that NSC demand may be regulated to maintain NSCs at a certain level, refilling NSC reserves preferentially over supporting growth when reserves are depleted (Dietze et al., 2014; Sala et al., 2012; Wiley & Helliker, 2012). These different frameworks for NSC regulation lead to differing interpretations of the same observed dynamics; while they have motivated many experiments, the basic questions posed by these previous works remain incompletely answered.

Although not formulated in mathematical terms, many researchers have studied these conceptualizations of NSC dynamics via mathematical modeling. NSC dynamics have long been present in plant physiological models (Thornley, 1970, 1971), but due to the recent interest in NSCs, new works have implemented versions of NSC regulation or sink-limited growth models (exploring the latter is more common than the former), often with an eye toward the improvement of dynamic global vegetation models (Hayat et al., 2017; Jones et al., 2020; Leuzinger et al., 2013; Potkay et al., 2022; Schiestl-Aalto et al., 2015; Schiestl-Aalto et al., 2019). Many carbon allocation models often also imply certain forms of NSC dynamics, even if not directly modeled (see reviews, e.g., Cannell and Dewar, 1994; Franklin et al., 2012; Le Roux et al., 2001). While such models contain useful insights into NSC dynamics, the complexity of their formulation, along with the difficulty of parameterization, hinders analyzing their structure and applying them to experiments.

Despite the accumulation of experiments and models, the basic science of NSC regulation has received few significant refinements in 30 years (cf. Chapin et al., 1990; Fatichi et al., 2019); this slow advance could indicate the need for a shift in perspective. Experiments and models of NSC dynamics have focused on the large number of environmental factors influencing these dynamics (Davidson et al., 2021; Dietze et al., 2014; Hartmann & Trumbore, 2016; Jones et al., 2020; Martínez-vilalta et al., 2016; Richardson et al., 2013; Schiestl-Aalto et al., 2015); however, this focus neglects the role of internal feedbacks, which may instead form the basis of regulation. As precedent, consider the classic idea that feedbacks between carbon and nitrogen substrate limitation ultimately drive carbon allocation (Thornley, 1972); while the environment influences allocation, the regulation results from the presence of feedbacks. The mathematical study of dynamical systems supports this viewpoint. The importance of substrate dependence by NSCs on NSC demands alone, especially on respiration, is also a classic idea (Thornley, 1970, 1971), and it has experimental support (Collins et al., 2021; Högberg et al., 2001; Sevanto et al., 2014). Many models of NSC dynamics make similar assumptions about how the amount of NSC stored affects its rate of change (Hayat et al., 2017; Jones et al., 2020; Schiestl-Aalto et al., 2015; Thornley, 2011); these assumptions are implicit statements about NSC regulation, but their consequences are underexplored. Examining these implications may yield a useful shift in perspective.

To gain insight into how variations in NSC supply and demand result in observed NSC dynamics and the role of NSC regulation, we formulate NSC carbon mass balance in terms of concentrations. We derive a simple model for its conceptual utility, applicable to the analysis of experiments and more sophisticated models; the novelty of our approach is not detailed descriptions of component processes (see instead Hayat et al., 2017; Jones et al., 2020; Potkay et al., 2022; Schiestl-Aalto et al., 2015; Thornley, 1991 but techniques for describing how feedbacks govern NSC dynamics. A simple substrate dependence of demand on the amount of stored NSC is sufficient to regulate NSC dynamics. This simple regulation, in turn, permits complex NSC dynamics when the environmental changes.

To obtain practical insights, we analyze how seasonal starch dynamics vary under changes in seasonal photosynthesis (supply-driven seasonal dynamics) or changes in demand such as temperature-dependent seasonal variation in growth and respiration (demand-driven seasonal dynamics); we focus on starch under the assumption that sugar concentrations are regulated to remain near-constant. We demonstrate that each scenario creates a distinct seasonal variation in starch concentrations. We also demonstrate that peaks and valleys in seasonal dynamics lag imbalances in supply and demand; peaks and valleys represent moments when supply momentarily equals demand. Our results suggest starch dynamics lag changes in carbon balance, but the degree of lag varies. Despite our focus on seasonal dynamics independent of plant size, our results suggest that more massive plants (mature trees) exhibit more lag and dampened starch dynamics when compared to less massive plants (saplings).

2.2 Description

2.2.1 Theoretical Framework

Three ideas form the basis of our approach. Beginning with a set of equations describing carbon mass balance, (1) expressing these equations in terms of concentrations scales NSC dynamics by plant size, approximately eliminating mass dynamics; (2) effective feedbacks yield a single stable steady state in a constant environment, which implies that NSC concentrations affect the rates appearing carbon mass balance; and (3) starch dynamics reflect changes in carbon balance while sugar dynamics do not.

To explain the intuition for the mathematical framework, we begin with an analogy between NSC dynamics and the dynamics of water filling and draining from a bucket (Fig. 2.1a). The change in NSC (change in water level) equals the rate of NSC supply (rate of inflow) minus the rate of NSC demand (rate of outflow) (Fig. 2.1a). Expressing NSC dynamics in concentrations (idea 1) rather than absolute mass is analogous to expressing the amount of water as a fraction of the bucket's total capacity rather than the absolute amount of water. Environmental conditions influence the supply and demand rate like adjustable valves whose changing aperture increases or decreases the conductance for flow in or out, modifying the flow rate but not necessarily determining it (Fig. 2.1a). How the amount of NSC affects its supply and demand rate is analogous to how the amount of water affects the water pressure and, in turn, the inflow and outflow rates. When the environment is constant, a negative feedback between water level and net flow creates a stable steady state (Fig. 2.1a) (idea 2). The nature of this feedback regulates the water level. As carbon mass balance applies to sugars, starch, and total NSC, the analogy is applicable to either sugar or starch dynamics by a shift in interpretation.

We define NSC concentration as $s = y/m$ for a plant (or tissue) with y kg carbon of NSC and a total carbon mass of m kg. Differentiating this definition and rearranging provides a relationship (2.1) between the change in NSC carbon concentrations $ds/dt = \dot{s}$ and changes in NSC carbon mass $\dot{y}$ and plant carbon mass $\dot{m}$ (see Appendix A.1). For ease of exposition, we will simply say NSC concentrations and palant biomass, rather than carbon biomass, because the resulting quantities have approximately the same value. Note that here again, y and s can be reinterpreted as the mass and concentration of either sugar or starch as the same definition applies to both.

$$\dot{s} = \frac{\dot{y}}{m} - s\frac{\dot{m}}{m} \tag{2.1}$$

Using our analogy (Fig. 2.1a), the second term of the right-hand side (2.1) corresponds to how changes in bucket size affect the relative water amount, even though only the inflow and outflow affect the absolute amount of water. Although experiments report NSC concentrations as the fraction of NSC mass per dry biomass, theoretical or modeling papers sometimes use the fraction of NSC carbon mass per total carbon mass. We use the latter definition, because the former yields equations where the mass of nutrients (e.g., nitrogen, phosphorous, etc.) affects the NSC concentration, complicating equations; however, we show that the two definitions yield roughly similar values and have the same dynamics (see Appendix A.1).

To obtain a useful description of dynamics, we insert rates of photosynthesis, respiration, growth, and so on into (2.1). We then assume that respiration and growth rates vary as a function of NSC concentration s and combine all demands into a single demand term. To simplify, we linearize the demand about $s = 0$ yielding (2.2). See supporting information Notes S3 for full derivation.

$$\dot{s} = A(1 - s) - Us \tag{2.2}$$

In (2.2), A is the specific rate of photosynthesis, or the mass C assimilated per mass C of plant mass per unit time, while we call U the usage rate, derived as the linear coefficient from linearizing NSC demand. In this form, supply and demand rates are relative to plant mass. If the only demands are respiration and growth, then the usage rate is the rate of respiration plus growth in mass per unit mass of NSC. The usage rate U is the aperture of outflow valve while demand is the rate of outflow (Fig. 2.1a); it serves to quantify all other effects on demand beyond the feedback due to substrate-dependence. This feedback is present virtually all models, past (Dewar, 1993; Thornley, 1970) and present (Hayat et al., 2017; Jones et al., 2020; Schiestl-Aalto et al., 2015; Thornley, 2011). For that reason, this linearization may be applied to those models to yield (2.2) with minor exceptions (e.g., Hayat et al., 2017 have respiration rates which do not depend on the amount of NSC stored). See additional discussion on the generality of this linearization in supporting information (see Appendix A.4).

While a natural analogy for mass balance, our physical analogy (Fig. 2.1a) goes beyond mass balance to include a feedback or regulation (water pressure regulates the net flow in and out). Mass balance is a simple and uncontroversial approach both for theoretical calculations or modeling (Jones et al., 2020; Lacointe & Minchin, 2008; Landsberg & Waring, 1997; Schiestl-Aalto et al., 2015; Thornley, 1991) or for experimental estimates (Furze et al., 2019; Klein & Hoch, 2015; Wiley et al., 2019). Mass balance does not preclude any dependence of NSC supply and demand on the amount of stored NSC, meaning it is compatible with active and passive regulation of NSC, or even no regulation. The nature of regulation must refer to how stored NSC affects its supply and demand rate (i.e., how the blue streamlines in Fig. 2.1c, 2.1d vary vertically) . Some feedback must be present as without any feedback, NSC can "overflow" or can become negative (i.e., some streamlines in Fig. 2.1d would leave the range $0 \leq s \leq 1$). As these outcomes do not correspond to reality, they indicate a breakdown of a model; so any good model must contain some feedback (i.e., all streamlines in Fig. 2.1d cannot be the same and also remain within $0 \leq s \leq 1$). A thought experiment demonstrates the problem: assume a constant environment in which supply and demand only vary due to the feedback (e.g., Fig. 2.1c rather than Fig. 2.1d); in other words, we assume the valve apertures do not change in time (but may be set to any value). In the analogy (Fig. 2.1a), no feedback means that the net flow of water (supply minus demand) does not depend on water level and therefore the rate of change is constant; in other words, all streamlines (Fig. 2.1c) are parallel lines. If positive, then the bucket fills forever (streamlines increase with time), and if negative, it drains forever (streamlines decrease with time). If zero, then no change occurs (horizontal streamlines). To exclude these possibilities, supply and demand must vary as a result of changes in NSC concentrations (i.e., the streamlines must vary vertically). Thus, at low NSC concentrations, supply exceeds demand, which prevents emptying, and at high NSC concentrations, demand exceeds supply, which prevents filling up (Fig. 2.1b, 2.1c). As NSC

concentrations increase or decrease (for each case respectively), the rate of supply and demand change until a balance point occurs; at this concentration, supply equals demand and no further change occurs (Fig. 2.1b, 2.1c). This balance point changes as the environment changes (Fig. 2.1d), but its presence prevents model breakdown. This argument demonstrates that the amount of stored NSC must affect its own dynamics, but it does not mean that the amount of NSC is the only internal control regulating NSC dynamics. In fact, the addition of other internal controls is similar to a coupled system of sugar and starch dynamics. Other internal controls may mediate this feedback, but ultimately steady states require a feedback between the amount of NSC and its supply and demand.

Although playing distinct roles in carbon dynamics, growth and respiration have approximately the same effect on NSC whenever they collectively yield the same U rate. This "lumping" approach to NSC demands is taken by other researchers, notably Thornley, 2011 in the context of modeling respiration response (demand is termed C substrate utilization), Jones et al., 2020 in a simple NSC model for climate models (demand termed plant carbon expenditure), and Sala et al., 2012 in reviewing the role of NSC in carbon dynamics (demand termed C demand strength or C sink activity). While these studies and many whole-plant NSC models do not distinguish starch and sugar dynamics, Schiestl-Aalto et al., 2019 do present a whole-plant model with explicit differences in sugar and starch dynamics. Several models of phloem transport also contain explicit sugar and starch dynamics (Daudet et al., 2002; De Schepper & Steppe, 2010; Lacointe & Minchin, 2008).

To consider explicit sugar and starch dynamics, the picture in Fig. 2.1a is modified to have two buckets, one for each pool. Instead of one, we have two mass balance equations (see details in Appendix A.5), which include all processes affecting the amount of total NSC as well as the conversion between sugars and starch (starch synthesis and hydrolysis). While the combined system describes the coupled sugar and starch dynamics, we postulate that sugar dynamics do not reflect carbon balances. Sugar concentrations affect the osmotic pressure and sap viscosity of cells and surrounding tissues, in turn influencing cell hydration and phloem translocation (Secchi & Zwieniecki, 2011; Stroock et al., 2014; Talbott & Zeiger, 1998; Woodruff, 2014; Woodruff & Meinzer, 2011). Starch is not osmotically active in plants and can vary without affecting water balance or phloem transport. When illuminated, *Arabidopsis* leaves show starch accumulation while sugar concentrations remain constant, while *pgm* mutants, which cannot synthesize starch, show sugar accumulation instead (Gibon, Bläsing, et al., 2004; A. M. Smith & Stitt, 2007). These observations suggest that starch synthesis and hydrolysis keep sugar concentrations near a constant value, despite changes in photosynthesis, respiration, growth, and transport affecting sugar concentrations, such that the overall effect is to pass carbon imbalance onto the starch pool. However, instead of assuming sugar concentrations never vary, we make the subtler assumption that two timescales exist: a short timescale on which the coupled sugar and starch dynamics arrive at a steady state independent of carbon balance, and a long timescale on which changes in carbon balance change the coupled steady states. In terms of the bucket (Fig. 2.1a), the sugar and starch buckets exchange water faster than water enters and exits the sugar bucket, so that the water level in either bucket is determined by the other at the long timescale due to the exchange in water between buckets. The relationship between the two depends on how they exchange water (namely, the steady state of these dynamics), and we assume that it keeps sugar concentrations near

a homeostatic value. If starch and sugar dynamics are so strongly coupled, then their dynamics may be expressed using only one of starch, sugar, or total NSC since each formulation only reflects a change of coordinates. The technical term for this assumption is reduction to an approximate center manifold. Equation (2.2) can then be formulated for any of the above and converted in between these; note that any feedbacks are also converted. Since we analyze seasonal dynamics below, we take the long timescale to be the same as seasonal dynamics ($\sim$ a year) and the short timescale to be much shorter than that. Note we assume this timescale separation holds for simplicity, but given a system of sugar and starch dynamics, both the timescale and the relationship between sugar and starch concentrations can be computed. If starch synthesis and hydrolysis keep sugar concentrations near a certain value, then the variation in starch and total NSC will be almost the same (differing by the almost constant sugar concentrations). The same logic may be applied to NSC dynamics across various organs (roots, stems, leaves, etc.). If NSC translocation is faster than changes in carbon balance, then an average whole-plant NSC concentration contains sufficient information for dynamics at the long-time scale, even if NSC concentrations are not uniform over the plant body. See supporting information A.5 & A.6 for additional discussion of these points. For the remainder of this article, we focus on starch dynamics for these reasons.

2.2.2 Analysis techniques

For NSC modeling, the novelty of our approach is not the detail of our model, but rather our mathematical analysis. We apply techniques from dynamical systems theory to describe the relationship between NSC regulation, dynamics, and responses to the environment. We do our best to explain the principles of these techniques but recommend an excellent introductory text for readers seeking to apply these techniques (Strogatz, 1994). See also Appendix A.4 for an extended introduction and additional references.

Starch dynamics in changing environments reflect the external forcing of a changing environment and the internal response of feedbacks. Streamplots (Fig. 2.1c, 2.1d) are a geometric illustration of the flow of dynamics for Equation (2); each blue curve shows the time evolution of starch concentrations from all possible starting conditions under the same time-series of A and U. Fig. 2.1c shows a streamplot for a constant A and U while Fig. 2.1d shows a streamplot for time-varying A and U. Models with similar geometry in the streamplot will generate similar responses, even if their details, equations, or parameterizations differ considerably; the geometry captures the essential properties of dynamics, the essential structure, and how supply and demand rates vary as function of starch concentration determines the geometry.

If environmental conditions are constant, then A and U are constant (valve apertures are held at a constant). As shown in the thought experiment from the previous section (Fig. 2.1b), all starch concentrations tend toward a balance point where supply equals demand (Fig. 2.1c). Instead of balance point, this starch concentration is normally called a fixed point, steady state, or equilibrium of (2.2). All trajectories or orbits from other initial starch concentrations converge on this value (Fig. 2.1c). When the environment is constant, this fixed point is the long-term starch response, independent of the initial amount (Fig. 2.1c). The fixed point is said to be stable, and in this case, the fixed point is the attractor for this system in a constant environment (Fig. 2.1c). The attractor is the set of starch concentration toward which the system

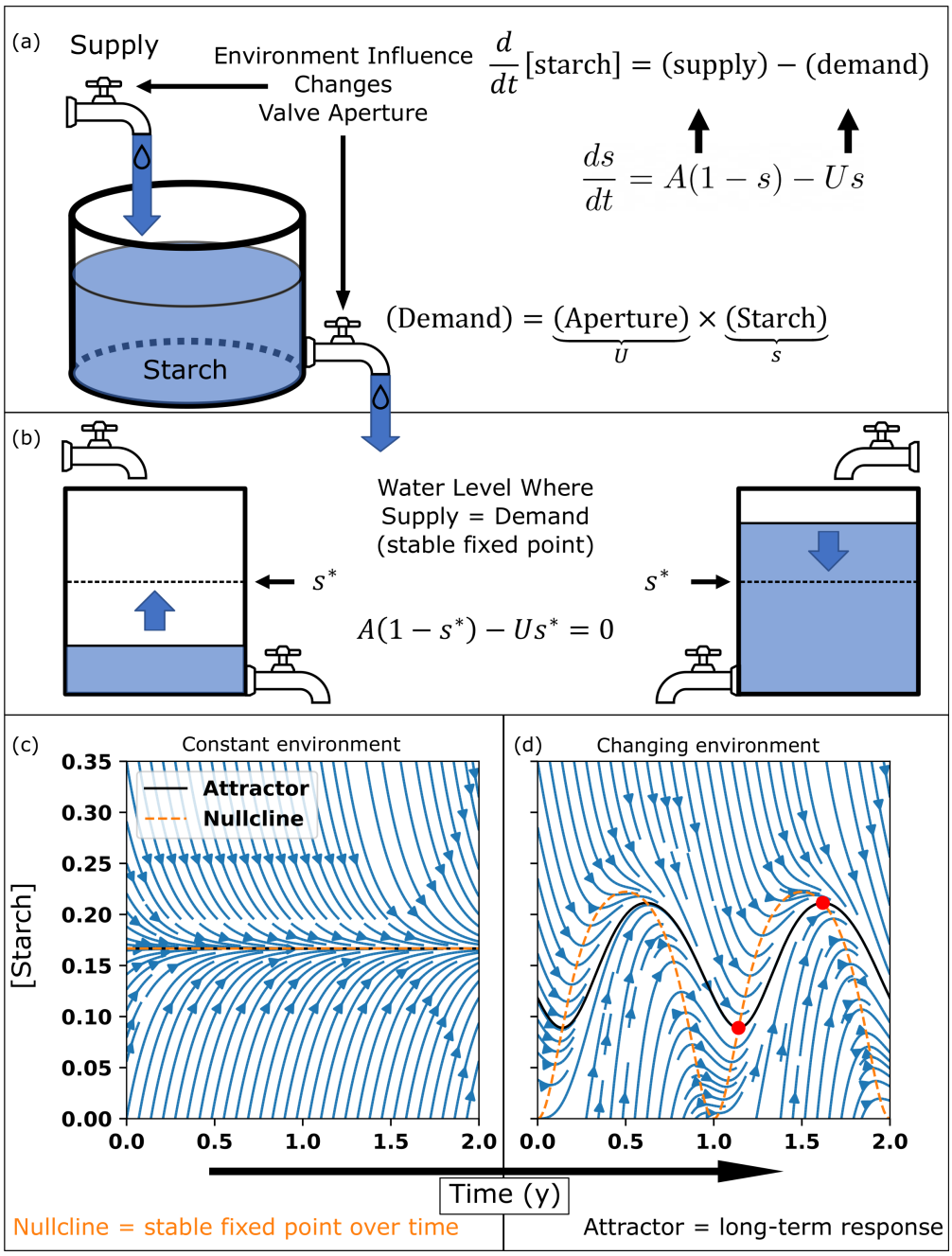

Figure 2.1: NSC starch dynamics graphical derivation: dynamics analogous to water flowing in and out of a bucket where water level = [starch]; inflow rate = supply; outflow rate = demand; outflow valve aperture = usage rate (demand per unit starch); environment influences supply and demand rate by changing valve aperture (**a**). In constant environment, starch tends toward its stable fixed point (AKA steady state, equilibrium) at which the supply rate balances the demand rate (**b**). Streamplots (blue curves) show how simulated time-series evolve from all starting positions under the same external drivers (**c**); the starch nullcline (dashed orange) is the path of the stable fixed point through time and indicates how the balance between supply and demand shift in time (**c**). All time-series quickly approach a long-term starch response called the attractor (solid black) (**c**); in a constant environment (left panel), the nullcline and attractor are constant in time and are equal, but in changing environments (right panel), the nullcline and attractor are no longer constant nor equal (**c**). Intersections (red points) between the nullcline and attractor always correspond to extrema (maxima or minima) of the attractor (**c**).

inevitably evolves at long time scales, independent of initial values. In a sense, the attractor is what one is most likely to measure in experiment. To calculate the fixed point s^* for a constant environment (Fig. 2.1c) solve for zeros of (2.2).

$$\dot{s} = f\left(t, s^*\right) = A\left(1 - s^*\right) - Us^* = 0 \tag{2.3}$$

Equation (2.2) has only one zero, hence a single fixed point. Equation (2)'s simplicity makes direct calculation of the fixed point easy (cf. Jones et al., 2020 in supporting information S3); the fixed point in a constant environment is given by (2.4).

$$s^* = \frac{A}{A + U} \tag{2.4}$$

Plotting how the fixed point s^* varies as A and U vary demonstrates that external influences on supply and demand has nonlinear effects due to the feedbacks present.

While the fixed point indicates where starch concentrations converge in a constant environment (Fig. 2.1c), the other important quantities is how quickly starch concentrations approach their fixed point. That rate of convergence can be estimated from the divergence of (2.2) ($\mathrm{div}\ \dot{s} = \partial\dot{s}/\partial s$) as the quantity r in (2.5).

$$r = A + U = -\frac{\partial \dot{s}}{\partial s} \tag{2.5}$$

For brevity, we call r the response rate (also known as a Lyapunov exponent). Note that the response rate has unit dimension$1/\mathrm{time}$; alternatively, $\log(2)/r$ is a halving time (the approximate time needed to starch concentrations to half the distance to the fixed point). Higher rates of photosynthesis, respiration, and growth imply higher response rates, lower halving times, and thus faster convergence to the fixed point. Interesting time-scale separations are possible when $r \ll 1$ (time-average methods) or$r \gg 1$ (quasi-steady state approximations).

The constant environment, with constant A and U, describes the feedback (Fig. 2.1c), but changes in the environment change photosynthesis, respiration, growth, and other processes causing the balance between supply and demand to shift (Fig. 2.1d). As A or U change with time, no true fixed points exist; however, the existence of a stable fixed point for all possible environments implies that a stable long-term response exists. Solving (2.3) at each moment in time traces a curve in the starch-time plane (orange dashed curve in Fig. 2.1c, 2.1d; black dashed curve in Fig. 2.3-2.7) where the change in starch is momentarily zero; the slope is zero, and thus we call this curve the starch null isocline (nullcline for short). As the environment changes, starch concentrations do not remain on the nullcline unlike a true fixed point; however, while it is not the actual starch response, the nullcline still represents the balance between supply and demand. Starch concentrations will tend toward a long-term response, an attractor (black curve in Fig. 2.1d) determined by temporal variation in supply and demand and independent of the initial value, but not necessarily the nullcline (orange dashed curve in Fig. 2.1d). As intuition, the nullcline indicates the direction in which NSC mass fractions will change (reflecting imbalances in supply and demand), the response rate measures the strength or time-scale of those changes, and the attractor is the long-term

response. Short-term, transient responses quickly decay so the attractor represents the system's dynamics at long time-scales and represents the cumulative recent history of supply and demand imbalances.

Effectively, changes in starch concentrations lag changes in the starch nullcline; the blue and black curves in the streamplot, which represent possible observable time-series, lag the nullcline (Fig. 2.1d). The response may be dampened (smaller in magnitude). The lags and dampening occur because while nullcline reflects immediate changes in environmental conditions, these changes only become apparent in the starch time-series once sufficient accumulation or depletion has occurred. The relative difference between the response rate and the rate of change in the nullcline thus determines the degree of lag and dampening. Faster rates reduce the lag while slower rates increase the lag; this phenomenon is explored in simulations (Fig. 2.1d, 2.3-2.7). The nullcline is a useful intermediate step in describing how variations in A and U push starch dynamics. Intersections between the nullcline and the attractor (or any time-series; both black and blue curves in Fig. 2.1c, 2.1d, 2.3-2.7) indicate whenever the imbalance in supply and demand switches sign; at this moment, supply and demand momentarily equal each other and this intersection always coincides with a local maximum or minimum (depending on the direction of intersection) of starch concentrations (e.g. red dots in Fig. 2.1d; visible in Fig. 2.3-2.7); by definition, the nullcline corresponds to starch concentration, where the slope (in starch-time plane) is zero. Even without any model, detecting maxima and minima in observed time-series indicates when starch dynamics switch between accumulation and depletion.

2.2.3 Application to seasonal NSC dynamics

Practical insight results from the application of these ideas to specific phenomena. To illustrate how starch dynamics respond to variations in A and U, we analyze possible seasonal starch dynamics using hypothetical seasonal variations in A and U in this article. We consider several scenarios: (1) seasonal variation in A drives starch dynamics, and U is constant (supply-driven dynamics); (2) A is constant, and seasonal variation in U drives starch dynamics (demand-driven dynamics); (3) A and U are synchronized (same timing of maximum; i.e., in phase); (4) A and U are anti-synchronized ($\max U$ occurs six months before $\max A$; i.e., 180° phase difference); (5) U leads A ($\max U$ occurs three months before $max A$; i.e., 90° phase difference). Note that in supply-driven dynamics, only supply is affected by external conditions but demand still varies, as demand depends on starch. Supply and demand both vary in all scenarios; we only change how the external environment influences the supply and demand rate. In analyzing seasonal dynamics, all simulations presented are based on (2.2) where the specific photosynthetic A and usage rate U is varied with time to simulate seasonal variation in photosynthesis and metabolic demand independent of NSC availability; the valves are constantly changed to modify the inflow and outflow rate (Fig. 2.1a). Note we focus on the response of starch dynamics rather than accurate simulation of photosynthetic, growth, or respiration, for simplicity. Our goal is to describe how the starch dynamics respond to variation in photosynthetic, growth, or respiration; and how feedbacks influence this response.

For periodic variations in A and U (i.e., seasonal variations), the nullcline and resulting attractor will also be periodic while the transient responses are not periodic (Fig. 2.1d); the streamlines (blue curves) are not periodic as they contain a transient response, while the attractor is periodic (black; Fig. 2.1d), forming

a closed loop in lower rows of Fig. 2.4, 2.5. Any idealization of seasonal dynamics must be periodic; otherwise, interannual feedbacks exist and the seasonal dynamics are transient. Likewise, the average seasonal dynamics will be periodic. For these reasons, we refer to the attractor as the starch concentrations one observes in the following unless otherwise noted. In Fig. 2.3-2.7, we compute the nullcline and attractor, and compare it to seasonal variations in A and U (direct computation method of the attractor in Appendix A.7, but a numerical integration method works as well). We suppress the transient responses (the blue curves in Fig. 2.1d) for Fig. 2.3-2.7 to avoid overcrowding.

For all scenarios, we assume that A and U have at most one annual maximum and one annual minimum (unless constant). Observations of gross primary production (GPP) (i.e., photosynthesis at ecosystem scale, proportional to A) are consistent with this assumption (Xiao et al., 2010) as are many starch time-series (Martínez-vilalta et al., 2016). Similarly, we assume that variations in A and U on time-scales much shorter than a year (i.e., daily variations) are averaged out and that variations are periodic, meaning that interannual variations at longer timescales are neglected. Our analysis of seasonal dynamics is simplified if starch dynamics are decoupled from plant mass dynamics; this approximation is valid if changes in plant biomass are small enough that seasonal A and U only change due to the environment; this assumption should be accurate for sufficiently short timescales and for larger trees (see Appendix A.8). When valid, our analysis is mass-independent; the starch dynamics will be the same for plants of any size along if the specific photosynthetic and usage rates are the same.

To identity realistic seasonal variations in A for supply-driven dynamics, we simulated the variation in A by biome and by latitude. Biome seasonal variation in A was based on GPP observations, while latitude variations were based on light variation from solar position (more below). For demand-driven dynamics, we simulated seasonal changes in U to mimic the effect of seasonal temperature variation on growth and respiration. For synchronized and asynchronized dynamics, a combination was used. Our goal was to determine how A and U determine starch, rather than accurately model A or U responses (cf. Schiestl-Aalto et al., 2015). Specific biomes and latitudes illustrate, rather than predict, how A varies to aid interpretation of how starch dynamics respond to variation in A. We describe calculation details of specific seasonal variations in A and U in Appendix A.9 and only provide a brief overview here; however, the relevant variation in A and U is present when needed (Fig. 2.3-2.7).

To determine reasonable magnitudes of A, we estimated average annual A using annual GPP and standing biomass estimates from Saugier et al., 2001 and Chapin et al., 2011 (see Table 6.6). We then determined reasonable seasonal variations of A using the observed seasonal variation in GPP across several different biomes in the continental United States based on satellite data (Xiao et al., 2010) and rescaled those observed GPP rates to match the average annual specific photosynthetic rate estimated for that biome. The values we use for specific photosynthetic rates are order-of-magnitude estimates. Estimating U independently is more difficult, requiring estimates of specific growth, respiration, and litter production rates. Instead, we simply adjusted the magnitude of U so that the resulting starch concentrations would vary around 5 to 10%, a value consistent with measurements of starch. For demand-driven dynamics, the seasonal variation of U is designed to mimic a temperature-dependent enhancement (i.e., U increases as temperature increases) based on a Q10 exponential temperature response; the timing assumes a maximum

Table 2.1: Ecosystem scale estimates of average annual specific photosynthetic rate (A; y^{-1}).

Biome	A
Tropical Forest	0.1238
Temperate Forest	0.1124
Boreal Forest	0.0855
Mediterranean Shrubland	0.1563
Tropical Savanna	0.3638
Temperate Savanna	1.8403
Desert	0.7639
Tundra	0.2508
Cropland	2.0313

near the summer solstice. For comparing asynchonized and synchronized dynamics, U switches smoothly between a high and low value to facilitate adjusting the amplitude and phase of U. Exact simulation details are provided in Appendix A.9.

Table 2.1 shows estimated annual average A for US biomes while Fig. 2.3 (in blue) shows the observed seasonal variation in A (scaled to have the same average as the corresponding biome in Table 2.1). Specific photosynthetic rates A range plausibly 0–2 y^{-1}; $A = 0.2\,y^{-1}$ indicates the amount of carbon assimilated per year is 20% of total carbon biomass. Based on observations of starch concentrations, Equation (2.2) implies U typically will be greater than A with a ratio $U/A \approx (1-s)/s$. To match observed starch concentrations ranging from 5–25%, U must range approximately 3–19 times greater than A.

2.3 Results

As it forms a foundation for understanding simulation results, we begin our analysis by discussing how the starch fixed point or nullcline, as in (2.4), varies as specific photosynthetic rates A and usage rates U vary (Fig. 2.2). Variations in the nullcline describes changes in the balance between A and U. As expected, increasing A increases supply pushing the fixed point toward higher starch concentrations (Fig. 2.2a) while increasing U decreases demand pushing the fixed point toward lower starch concentrations (Fig. 2.2b), assuming no other changes. In terms of concentrations, increases in NSC supply or demand have diminishing returns; for instance, doubling A would not quite double the fixed point of starch concentrations, and starch concentrations may be maintained under variations of A if U changes appropriately. Feedback creates the diminishing returns; changes in A instantaneously change supply but also indirectly change demand once sufficient time passes for starch to deplete or accumulate. The steady state respiration and growth rates are functions of photosynthesis (e.g., steady state demand is $Us^* = UA/(A+U)$), while they are unrelated for instantaneous changes. How source or sink limitations on growth affect NSC dynamics depends on whether limitations are transient or long-term.

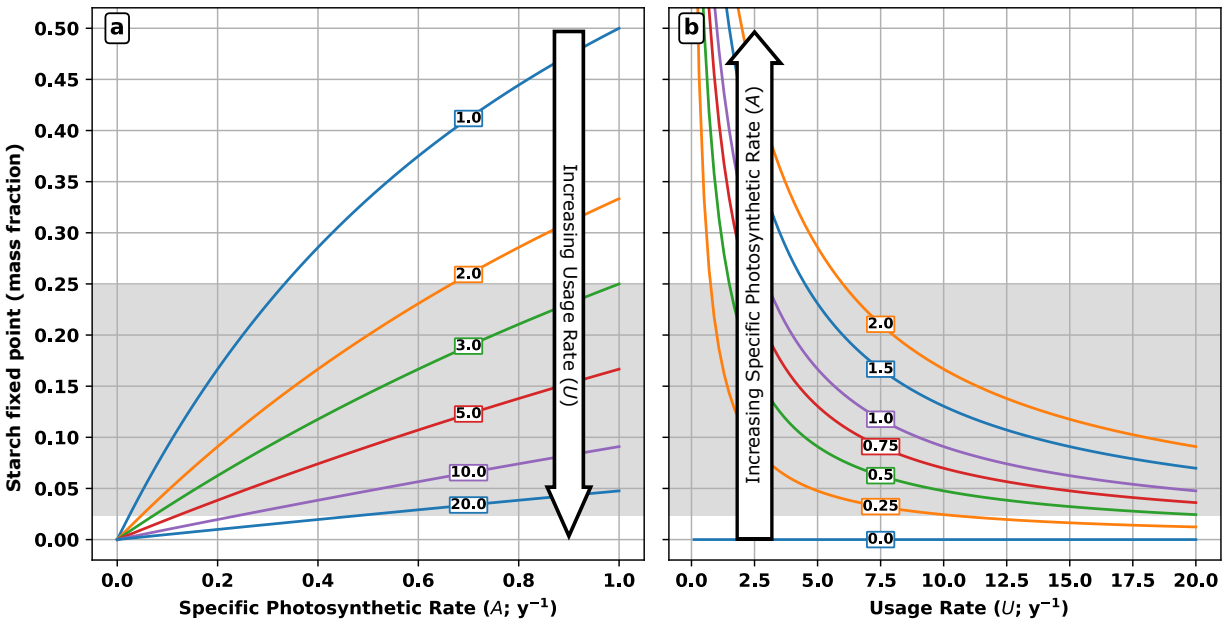

Figure 2.2: The starch fixed point (value of nullcline) increases with increasing specific photosynthetic rates A with constant usage rate U (**a**) but decreases with increasing usage rates U with constant specific photosynthetic rates A (**b**); numbers on each curve indicate the value of U in (**a**) or of A in (**b**) held constant along the curve. Shaded range indicates typical values for NSCs.

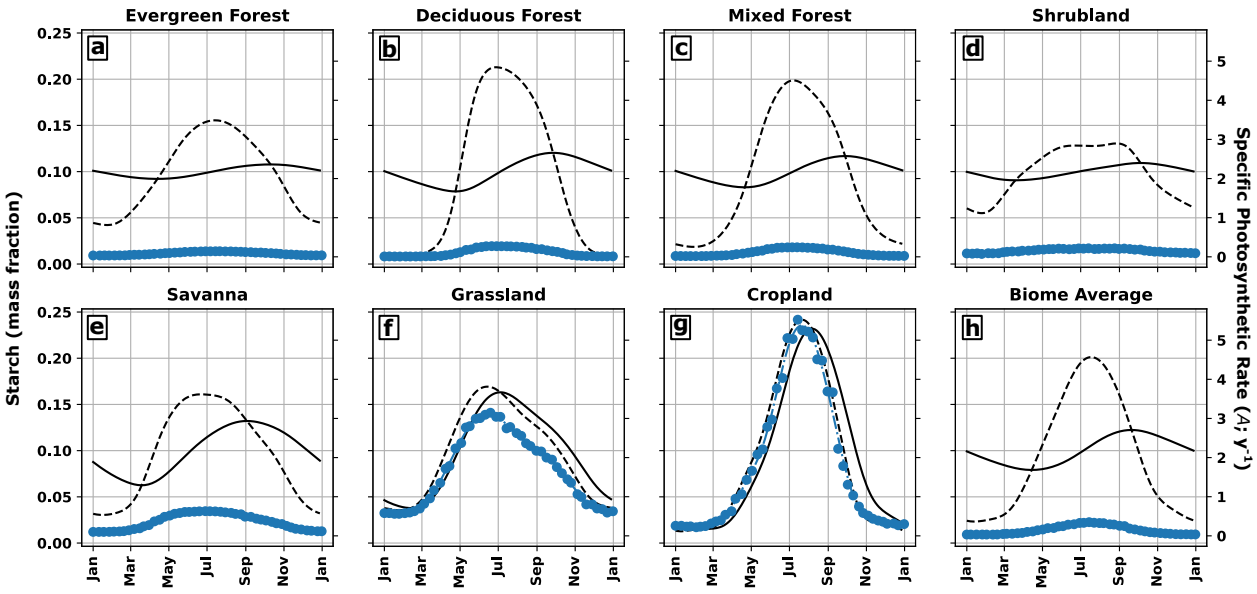

Figure 2.3: Seasonal variation in starch concentrations (solid black) and the starch nullcline (dashed black) assuming seasonal variation in specific photosynthetic rates (A, dash-dotted blue) only (supply-driven dynamics); the seasonal variation of A is based on gross primary production reported in Xiao et al., 2010 and ecosystem biomass reported by Saugier et al., 2001, dots indicate the data.

Changes in starch concentration time-series will lag those in the starch nullcline as demonstrated in each simulation (Fig. 2.2-2.7). Starch concentrations reach their seasonal maximum and minimum at intersections with the nullcline, indicating a switch in the net imbalance of supply and demand; therefore, starch concentrations do not necessarily reach their seasonal maximum and minimum during the summer and winter when the nullcline is high and low (high and low imbalance), but instead during the spring and fall when the nullcline switches between its high and low value (imbalance switches sign). This phenomenon is present in all simulations (Fig. 2.2-2.7), although the degree of lag depends on the response rate.

2.3.1 Scenario 1: supply driven seasonal starch dynamics

If seasonal variation in A drives seasonal starch dynamics (supply-driven seasonal dynamics), then the resulting attractor of starch concentrations has one seasonal maximum (peak) and one seasonal minimum (valley) per year (Fig. 2.3 & 2.4). Longer days in summer lead to higher average daily specific photosynthetic rates. High summertime photosynthesis corresponds to high starch nullcline. Starch concentrations increase in summer and decrease in winter. The seasonal maximum occurs in late summer or fall while

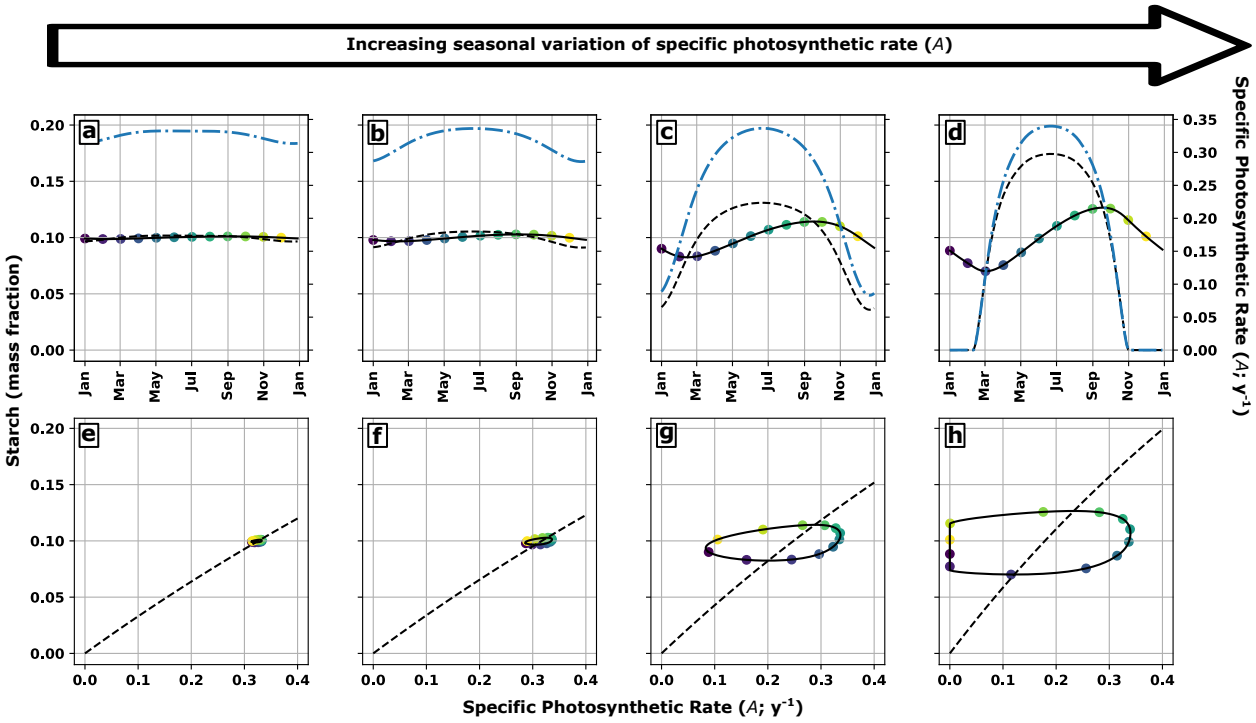

Figure 2.4: Seasonal variation in starch concentrations (solid black) and the starch nullcline (dashed black) assuming seasonal variation in specific photosynthetic rates (A, dash-dotted blue) only (supply-driven dynamics) by time-series (a-d) and bifurcation diagram (e-h); points on solid black curves indicate same time points; specific photosynthetic rates based on clear-sky seasonal light variation at latitudes 15°, 30°, 60°, and 75° for (a-d) and (e-h) respectively.

seasonal minimum occurs in spring or early summer when the net imbalance in supply and demand switches from positive to negative and vice versa (nullcline intersects attractor). The timing of these switches is the same across most biomes and latitudes because A oscillates between a high and low value (i.e., summer and winter) in these biomes and latitudes (Fig. 2.3 & 2.4). The degree of lag varies from virtually no lag (croplands, Fig. 2.3g) to about three months (deciduous forests, Fig. 2.3b); the magnitude of A explains the degree of lag as the response rate $r = A + U$. Recall that U is constrained to give the same average starch concentrations. Changes in demand also lag supply as demand is proportional to starch concentrations.

As seasonal variation in annual A increase with latitude, seasonal variation in starch concentration increases (Fig. 2.4). Increasing latitude increases the degree of variation in seasonal A but also reduces the overall average annual A (Fig. 2.4). To keep average starch concentrations around 10%, U also decreases with latitude (but is still held constant); assuming the same U by latitude implies a decrease in average starch concentrations with latitude. In both cases, the decrease in specific photosynthetic rates results in a lower response rate indicating greater lag (Fig. 2.4).

2.3.2 Scenario 2: demand driven seasonal starch dynamics

Even if photosynthesis is constant, seasonal variation in growth and respiration (i.e., in U) also creates seasonal variation in NSC dynamics (demand-driven dynamics, scenario 2). If seasonal variation in U is highest in summer and lowest winter (to simulate temperature-dependent variation in sink activity), then the resulting attractor also has one seasonal maximum (peak) and one seasonal minimum (valley) per year but the timing is inverted (Fig. 2.5). Demand is upregulated in summer, meaning the nullcline is downregulated so that the nullcline's maximum occurs in winter (when U is lowest) rather than summer. Likewise, starch concentrations reach their maximum in spring or early summer rather than winter when the net imbalance in supply and demand switches from positive to negative and vice versa (nullcline intersects the attractor). Demand exceeds supply throughout summer. Although shifted in time, the timing of these maxima and minima is determined by the maxima and minima of the nullcline and the response rate; both of which depend on changes in U (cf. Fig. 2.6b). For instance, if high summertime temperatures or low summertime water availability inhibited growth so that U was low in summer, then the maxima could be shifted forward by six months to be in late summer or fall as under supply-driven seasonal starch dynamics. Starch concentrations fall faster in summer than they increase in winter despite nullcline's symmetry because the response rate r is much higher in summer than winter (Fig. 2.5). While the same phenomenon is present in supply-driven seasonal dynamics (Fig. 2.4), to have the same amplitude in starch concentrations requires greater seasonal variation in U than seasonal A, making it more visible in demand-driven seasonal dynamics (Fig. 2.5).

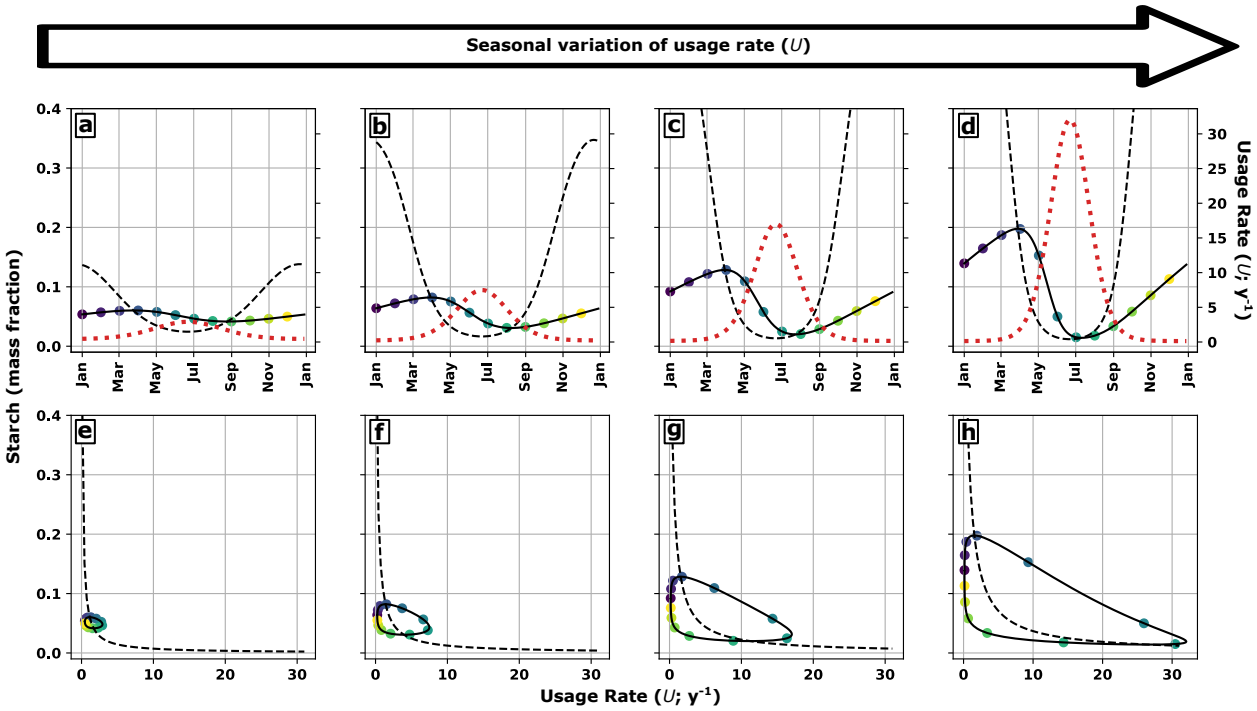

Figure 2.5: Seasonal variation in starch concentrations (solid black) and the starch nullcline (dashed black) assuming seasonal variation in usage rates (U, dotted red) only (demand-driven dynamics) by time-series (a-d) and bifurcation diagram (e-h); points on solid black curves indicate same time points.

2.3.3 Scenarios 3-5: synchrony vs. asynchrony in supply and demand driven starch dynamics

Outside of controlled experimental conditions, plants in most ecosystems would simultaneously experience changes in both A and U. Although the interaction of supply and demand driven dynamics could create many different seasonal patterns, we compare the effect of different degrees of synchrony (phase differences) between the seasonal variation of U and of A (Fig. 2.6). Varying the amplitude changes the relative strength of A and U (Fig. 2.6). When the environment influences both supply and demand, the resulting starch dynamics (Fig. 2.6) fall between the general patterns of supply-driven (Fig. 2.3, 2.4) and demand-driven dynamics (Fig. 2.5). When A varies little (simulating low latitudes), U (simulating sink activity) drives seasonal variation in starch concentrations which resemble demand-driven dynamics (Fig. 2.5) but shifted in time depending on the timing of U (Fig. 2.6a-d). Strong seasonal variation in A, especially zero wintertime A, can dominate seasonal variation in NSC mass fractions regardless of seasonal variation in growth and respiration; seasonal starch concentrations begin to resemble supply-driven seasonal dynamics (Fig. 2.6j-l). Namely, even if reduced, demand still exceeds supply in winter because photosynthesis ceases in winter so any demand exceeds supply (Fig. 2.6j-l). As a result, demand-driven dynamics may be more common at low latitudes while supply-driven dynamics are typical at high latitudes, even within the same species (if its range is sufficiently large) or functional group (e.g., low latitude conifers vs. high latitude conifers). Asynchrony in A and U strengthens the degree of seasonal variation in starch concentrations (Fig. 2.6b,f,j), while synchrony weakens the seasonal variation (Fig. 2.6d,h,l). High synchrony in A and U is likely in ecosystems with strong seasonality, but high synchrony dampens seasonal variation in starch dynamics. In many ecosystems, demand may be upregulated in spring before supply (e.g., growth onset leads leaf flush), suggesting some asynchrony.

Maxima and minima (peaks and valleys) in starch concentrations time-series indicate switches in the net imbalance between supply and demand; therefore, their timing provides a crude classification scheme for comparing synchronized and asynchronized supply and demand. Spring maxima and fall minima indicate demand exceeds supply in summer which can only occur when A remains high in winter relative to summertime with significant seasonal variation in U (sink activity) (Fig. 2.6d,h). Fall maxima and spring minima indicate supply exceeds demand in summer which occurs when either A in winter is zero or very low (Fig. 2.6l) or A (source activity) and U (sink activity) are especially asynchronous (Fig. 2.6b,f,j).

2.4 Discussion

In summary, we derived a simple dynamical system describing whole-plant starch dynamics, and we have demonstrated different patterns of seasonal starch dynamics result from variations in photosynthesis A and sink activity U. We demonstrate several techniques for conceptualizing and analyzing NSC dynamics. Our simulations also illustrate that simple regulation may generate complex dynamics; while starch concentrations tend to a constant in a constant environment, an ever-changing environment causes starch

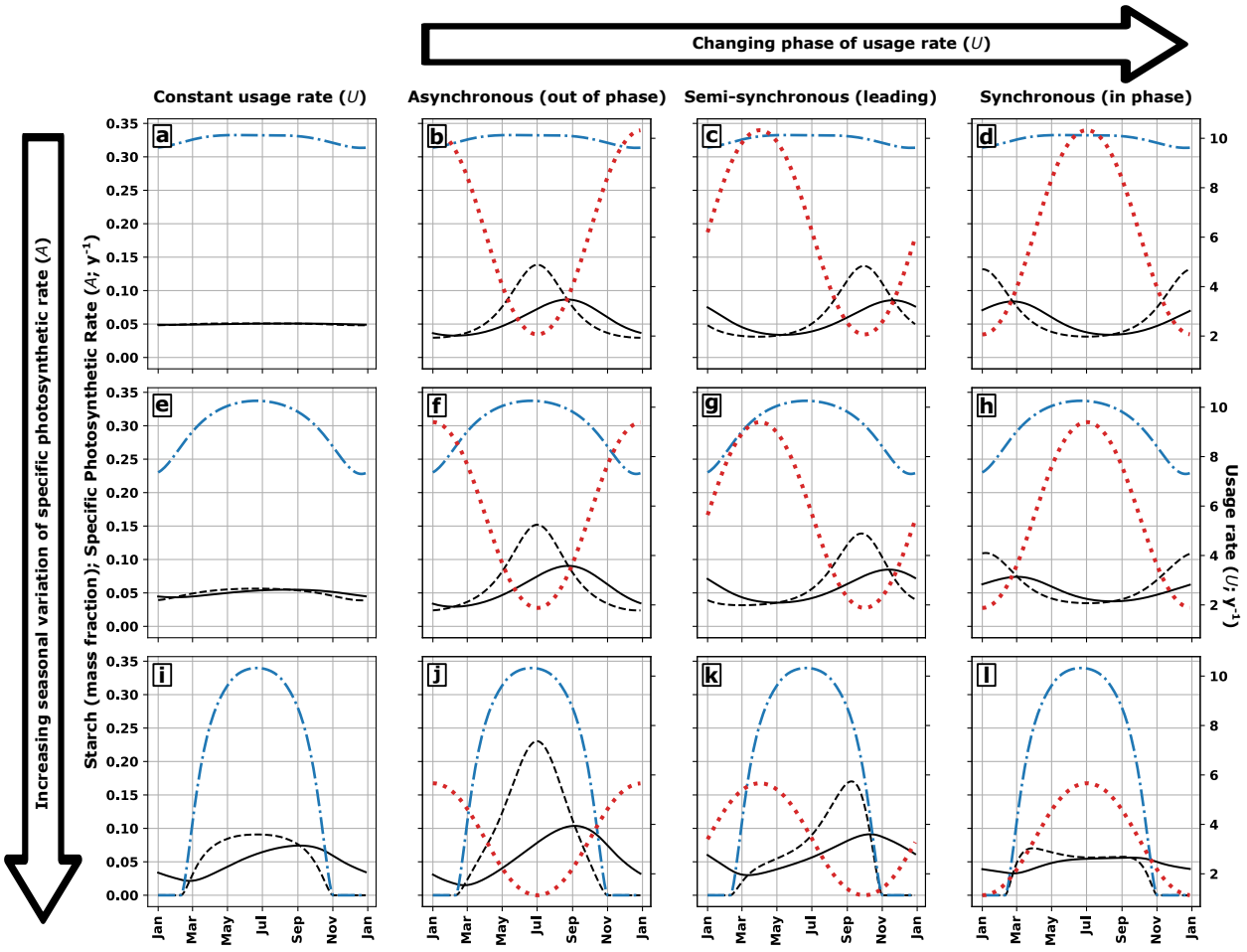

Figure 2.6: Seasonal variation in starch concentrations (solid black) and the starch nullcline (dashed black) when specific photosynthetic rates (A, dash-dotted blue) and usage rates (U, dotted red) are asynchronized with A and U out of phase (b,f,j), semi-synchronized with U leading A by 0.25 y (c,g,k), or synchronized with A and U in phase (d,h,l); seasonal variation with constant usage rate shown for comparison (a,e,i).

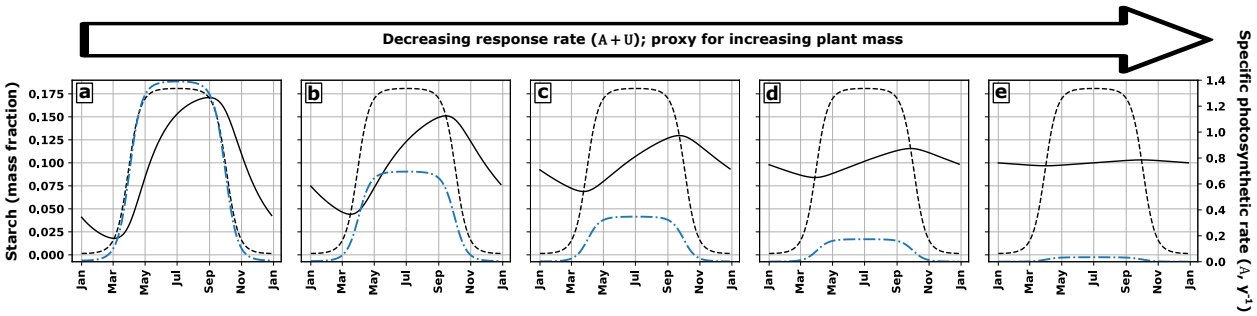

Figure 2.7: Seasonal variation in starch concentrations (solid black) with decreasing response rates $r = A + U$ (specific photosynthetic rate plus usage rate) but with the same starch nullcline (dashed black); variation in specific photosynthetic rates (dash-dotted blue) shown for comparison but a similar response is possible under variation in usage rate. Decreasing response rate corresponds to increasing plant mass (see text for explanation).

concentrations to reflect the recent variations in that environment. We conclude with several relevant implications for NSC research.

First, our results provide insight into seasonal starch dynamics. Seasonal maxima and minima in starch concentrations indicate switches in the imbalance of supply and demand (Fig. 2.2-2.7). Starch accumulates when supply exceeds demand and depletes when demand exceeds supply. As a result, peaks and valleys in starch concentration lags the maximum imbalance in supply and demand (i.e., the nullcline reflecting the balance point of supply and demand) and the degree of lag depends on the response rate (overall magnitude of supply and demand). Plants in latitudes and ecosystems without seasonal variations in photosynthesis, respiration, and growth will not have seasonal variations in starch, a prediction consistent with Martínez-vilalta et al., 2016 (cf. their Fig. 6). Our results provide further theoretical support for the importance of detecting the timing of NSC minima and maxima, as suggested by Martínez-vilalta et al., 2016; unfortunately, experimental observation of maxima and minima requires high frequency measurements in addition to adequate sample sizes. The timing of extrema in supply-driven starch dynamics (minimum in spring, maximum in fall) appears typical for winter deciduous (cf. Fig. 5 in Martínez-vilalta et al., 2016) (Tixier et al., 2020) while the timing of extrema in demand-driven dynamics (maximum in spring, minimum in fall) appears typical for conifers and evergreen angiosperms (cf. Fig. 5 in Martínez-vilalta et al., 2016) (Aubrey & Teskey, 2018; Oswald & Aubrey, 2020); however, our simulations suggest that the typical timing of demand-driven dynamics will shift toward that of supply-driven dynamics as latitude increases (Fig. 2.6d,l). High response rates (high photosynthesis and growth) lead to lower lag in starch concentrations, meaning a spring minimum and fall maximum shift toward a winter minimum and summer maximum in supply-driven dynamics. Thus, conifers at high latitudes (where photosynthesis is low or zero in winter) have summer or fall maxima in starch concentrations consistent with supply-driven

dynamics (cf. Schoonmaker et al., 2021) rather than winter or spring minima in conifers at low latitudes exhibit demand-driven dynamics (cf. Aubrey and Teskey, 2018) (Oswald & Aubrey, 2020)). This switch suggests that photosynthesis can hide the influence of sink-limited growth and demand-related environmental influences; Blumstein and Hopkins, 2021 make a similar observation: they find a growth-storage tradeoff is only apparent after variation in photosynthesis is removed. While greater asynchrony in supply and demand would generate greater seasonal variation in starch dynamics, observations of photosynthesis, respiration, and growth suggest these processes are synchronized with a growing season at high latitudes; half-synchrony is equally plausible as growth rates may reach their maximum in spring, preceding the summertime high of photosynthesis and respiration, especially xylogenic growth precedes canopy leaf out. Our results suggest that seasonal dynamics may not reflect large seasonal asynchronies. Note that we have not made any assumptions regarding phenology beyond seasonal variations in photosynthesis, respiration, and growth. Our analysis of seasonal starch dynamics complements the discussion by Piper, 2021 in which a conceptual framework of how average non-structural carbon compound (NCC) concentrations and its seasonal amplitude vary with growth rates. Independent measurements of respiration and growth rates would help constrain simulations, as U is harder to estimate in practice; models of sink-limited growth (e.g., Schiestl-Aalto et al., 2015) would also benefit from additional respiration and growth measurements.

Second, although our focus was seasonal dynamics, our framework is applicable to dynamics at other scales. For instance, a similar analysis of diurnal starch dynamics would complement our analysis of seasonal dynamics and provide insight into diurnal starch dynamics (Gersony et al., 2020; A. M. Smith & Stitt, 2007; Tixier et al., 2018). Constant environment experiments simplify the application of our framework as A and U are constant. Constant light, shading, or on-off photoperiod experiments are particularly amenable, especially when other factors such as temperature are held constant. To illustrate, suppose a complete shading experiment by assuming $A = 0$ and constant U; thus Equation (2.2) becomes $\dot{s} = -Us$ implying starch concentrations decay exponentially $s = s_0 e^{-Ut}$; Weber et al., 2018 observed this decay in whole-plant starch and sugar concentrations for *Acer pseudoplatanus*, *Quercus petraea*, *Picea abies*, and *Pinus sylvestris* in complete darkness. This result offers an the alternate interpretation to their experiment, suggesting demands decreased exponentially as NSC ran out. When re-illuminated, starch concentrations then increase to the fixed point $A/(A+U)$ with the difference decaying exponentially at the response rate $r = A + U$. Weber et al., 2018 also observed this response, meaning Equation (2.2) describes the data using few parameters. Furthermore, comparing concentrations between different constant environments (i.e., controlled conditions of a growth chamber) would directly test the utility of Equation (2.2).

Third, our calculations clarify the quantitative relationship between the dynamics of NSC mass and its concentration. Several authors have questioned if NSC concentrations indicate the degree of NSC "storage" (Hartmann & Trumbore, 2016; Hoch, 2015); NSC mass and concentrations are equivalent—one can be converted to the other given total biomass—but while NSC mass tracks the absolute amount of NSC available for remobilization, concentrations measure remobilization relative to total mass. Photosynthesis and growth must also be expressed in relative terms; experimental observations confirm this relationship (Wiley et al., 2019).

Our calculations suggest that observed NSC dynamics on seedlings or saplings do not necessarily scale to mature canopy trees (Hartmann et al., 2018), as their response rates differ. To see why, we consider how seasonal starch dynamics change with plant mass. First, photosynthetic rates do not scale proportionally with plant mass and therefore specific photosynthetic rates vary with plant size. While photosynthesis and respiration rates increase in absolute size as plants grow larger, the rate relative to biomass shrinks; saplings might photosynthesize 1–3 times their total mass per (order-of-magnitude calculations) while mature canopy trees might only photosynthesize 0.1–0.5 times their total mass per year (Table 2.1). Self-shading decreases the marginal photosynthetic gain for new leaf area while overall mass needed to support new leaf area increases faster than linearly; this decrease agrees with estimates based on allometric scaling (e.g., Enquist and Niklas, 2002) and is present in process models such as the 3-PG model (Landsberg, 2011; Landsberg & Waring, 1997) where the specific photosynthetic rate scales as $A \propto \left(1 - e^{-km}\right)/m$, tending to zero as mass increases (cf. Hayat et al., 2017). With constant U, one expects decreasing starch concentrations; however, observations (Woodruff et al., 2004; Woodruff & Meinzer, 2011) and several models (Hayat et al., 2017; Potkay et al., 2022) suggest that sink activity (measured by the usage rate U) also declines with increasing size. Thus, typical magnitudes of A, U, or both likely decrease as plant mass increases, leading to lower response rates for larger trees even if the nullcline is not affected.

To illustrate the effect on starch dynamics, consider the response rate $r = A + U$ changing with the same seasonal variation in the starch nullcline (Fig. 2.7). High response rates mean supply and demand quickly come into balance with each other, due to high turnover of starch (Fig. 2.7a,b) while low response rates mean supply and demand slowly come into balance with each other, due to low turnover (Fig. 2.7d,e). As $r \to \infty$, starch concentrations become indistinguishable from the nullcline while when $r \to 0$, starch concentrations do not respond to seasonal variations the nullcline because these variations are much too fast relative to the response rate. More massive trees would have smaller response rates than less massive ones and therefore have smaller seasonal amplitudes of starch as well as greater lag and dampening of responses. Alternatively, plants in poor, harsh environments having low photosynthetic and growth rates relative to total mass would also have smaller seasonal amplitudes and greater lag than fast-photosynthesizing, fast-growing counterparts. This argument suggests tree mass is an important factor in analyzing of NSC dynamics, especially cross-study comparisons (cf. Martínez-vilalta et al., 2016), and complements growth-storage tradeoff discussions (Piper, 2021). Note many studies on NSC dynamics do not report plant mass measurements (or estimates) at all; these measurements are not only necessary for determining whole-plant pool size but also response rates.

Our approach is limited in scope but we believe it contains promise for NSC research. Simply put, our simple model does not address dynamics that require multiple pools such as partitioning and spatial dynamics across the plant body. Typical observations reflect these dynamics in addition to seasonal carbon balance (e.g., Davidson et al., 2021; Tixier et al., 2020). Although often constant relative starch dynamics, sugars do vary seasonally (Richardson et al., 2013; Schoonmaker et al., 2021); leaves, stems, and roots often exhibit differences in NSC dynamics (Tixier et al., 2018; but see Schoonmaker et al., 2021). Our simple model and others (Hayat et al., 2017; Jones et al., 2020; Schiestl-Aalto et al., 2015) help identify what dynamics to expect by whole-plant carbon balance which in turn helps identify when measurements

indicate other drivers. Furthermore, without modification, our derivation works for the mass balance of individual tissues. For instance, the bucket represents just leaf starch; supply becomes leaf photosynthesis; and demand then reflects leaf carbon export in addition to growth and respiration. The interpretation shifts but the main ideas of our derivation, carbon mass balance and feedbacks generating a steady state, apply immediately. For instance, leaf starch concentrations should lag photosynthesis, and Gersony et al., 2020 observe maximum daily leaf starch concentration around 18:00 in *Quercus*; they observe a lagging starch time-series to daily photosynthesis, similar to the supply-driven seasonal dynamics but at a daily time-scale. *Arabidopsis* leaves also show the same pattern (A. M. Smith & Stitt, 2007).

As discussed above, our analogy (Fig. 2.1) extends to multiple NSC pools (including other compounds and individual organs). The theoretical difficulty is not adding pools or processes, but rather specifying the necessary feedbacks or regulation of all processes (and their parameterization) and then analyzing how the individual pieces fit together. For instance, observed changes in sugar concentrations require assumptions beyond carbon dynamics to describe and are most likely related to xylem and phloem function (Jensen, 2018; Sapés et al., 2021; Sapés et al., 2019; Sevanto, 2018). Spatial dynamics also depend heavily on phloem dynamics, not solely on whole-plant carbon balance. To improve models of NSC dynamics, detailed experimentation of phloem dynamics and the chemical kinetics of starch synthesis and hydrolysis would prove useful; however, the concepts of attractor, nullcline, and response rate are applicable in models with more NSC pools and may prove useful for identifying the feedbacks (see Appendix A.5, A.6). Here we use such concepts to identify conditions under which more sophisticated models with explicit partitioning and spatial dynamics would simplify to our simple model, especially when certain timescale separations are present (see Appendix A.5, A.6). Equation (2.2) and other whole-plant models (e.g., Hayat et al., 2017; Jones et al., 2020; Schiestl-Aalto et al., 2015) remain valid approximations of whole-plant starch dynamics. Additional investigation is required to verify validity.

Lastly, our theoretical framework provides a new perspective on active and passive regulation as well as source and sink-limited plant growth. Regulation of NSC dynamics is a matter of feedback, of how photosynthesis, growth, and respiration depend on the amount of NSC and not how they affect the rate of change in NSC, which is determined by mass balance. Whether photosynthesis, NSC, or nutrients limit growth depends on the timescale; transient responses may differ from long-term responses (the attractor). For instance, at least one FACE experiment observed a transient growth increase that vanished at long-time scales due to nitrogen limitation (Norby & Zak, 2011). The consequences of this shift in perspective merit further investigation in future works.

Chapter 3

Season of drought affects growth, but not nonstructural carbohydrates dynamics, in *Pinus taeda* saplings

Oswald, S. W. and Aubrey, D. P. Submitted to *Tree Physiology*, 3/1/2023.

Abstract The degree to which nonstructural carbohydrate concentrations are actively regulated in plants remains an open question. Furthermore, numerous studies have linked them to drought resilience. Supposing active regulation, this link suggests that plants may modify their carbon allocation after a drought to anticipate future water stress. To study this possibility, we performed an experiment in which six-month droughts were simulated on potted *Pinus taeda* saplings inside a greenhouse. One treatment experienced the six-month simulated drought during summer (Mar-Sep), while a second experienced it during winter (Sep-Mar). Both treatment groups were compared to a control. Plants were harvested at monthly intervals following simulated droughts to measure dry biomass and nonstructural carbohydrates. To assess growth, height and diameter measurements were recorded at monthly intervals before harvest, and a number of other physiological measurements were also collected. We analyzed the resulting nonstructural carbohydrates to determine if the timing of drought affected the seasonal variation of nonstructural carbohydrates following the drought. We found the summer drought caused greatly growth reduction than the winter drought. Drought in either season reduced growth rates relative the control, but we did not observe any changes in nonstructural carbohydrate variation in drought treatments relative to control. However, our results suggest temperature and overall mass might explain temporal variations in whole-plant starch. We also discuss a number of explanations for the lack of treatment effect on nonstructural carbohydrate concentrations.

3.1 Introduction

Plants store energy and carbon harvested during photosynthesis within the chemical bonds of sugars and starch. These nonstructural carbohydrates (NSCs) decouple the plant's carbon supply from its demands (Dietze et al., 2014; Hartmann & Trumbore, 2016; Sala et al., 2012; Wiley & Helliker, 2012). Storage of NSCs allows growth and respiration rates to exceed to photosynthetic rates for short periods of time; thus, changes in NSCs dynamics indicate changes in the balance between these processes. Seasonal variation in NSC concentrations has been widely documented in temperate and boreal plant species (Davidson et al., 2021; Martínez-vilalta et al., 2016; Richardson et al., 2013; Schoonmaker et al., 2021). The magnitude and other characteristics of seasonal variations differ between sugars and starch as well as across organs, biomes, and functional groups (Martínez-vilalta et al., 2016). Seasonality in NSC dynamics results from seasonality in photosynthesis, respiration, growth, and other processes (Hartmann & Trumbore, 2016), which complicates the investigation of the role of NSCs in plant responses to disturbances. Many environmental changes may modify plant carbon dynamics. Photosynthesis alone responds to changes in carbon dioxide, light, temperature, and water (via stomatal conductance and xylem conductance), while growth and respiration rates respond to temperature, water, and nutrient availability (Körner, 2015; Sevanto et al., 2014). Changes in NSC concentrations also have been observed after some environmental changes affecting carbon supply and demand. For instance, starch and sugars (primarily sucrose) decrease in shaded plants (Weber et al., 2018; Wiley et al., 2019) while increasing after carbon dioxide fertilization (Ainsworth & Long, 2005). Regrowth after defoliation or loss of the shoot leads to depletion of NSCs, followed by

reaccumulation of NSCs (Ruswick et al., 2021; Weber et al., 2019). Changes in NSC concentrations after temperature increases (Collins et al., 2021) have also been observed.

While NSC concentrations exhibit little seasonal variation in tropical ecosystems (Martínez-vilalta et al., 2016), seasonality in NSCs might reflect both environmental variation and adaptation to this variation. Active regulation of NSC dynamics requires that growth (and other demands) are downregulated to refill or maintain carbon reserves (Wiley & Helliker, 2012). Several authors have investigated NSCs from the perspective of a growth-storage tradeoff (Blumstein et al., 2022; Schoonmaker et al., 2021). Piper, 2021 discusses hypothetical relationships between overall growth rate and NSCs. A growth-storage tradeoff suggests that slow-growing, stress-tolerant species will maintain a higher level of NSC than fast-growing, stress-intolerant species on average over time; however, the degree of seasonal variations in NSCs could also vary with the overall growth rate with fast growing, stress-intolerant species consuming a greater fraction of their NSC reserves each year(Piper, 2021). If NSC dynamics are actively-regulated, then individual plants of the same species might exhibit a similar shifts after stress events reflecting the same growth-storage tradeoff. To acclimatize to stress, individuals would maintain higher NSC concentrations on average or reduce the amount of seasonal depletion of NSCs compared to unacclimated individuals. In otherwise favorable conditions, individuals might grow or respire less to maintain higher NSC reserves or modify their growth phenology to modify the seasonal variation in NSCs.

Drought, a widely studied disturbance, affects NSC dynamics in several ways. First, drought often reduces photosynthesis via stomatal closure to maintain xylem conductance and tissue hydration (Sperry & Love, 2015; Talbott & Zeiger, 1993, 1998). Second, drought reduces growth because cell expansion requires sufficient turgor pressure, and drought reduces turgor pressures across the plant (Hsiao et al., 1976; Körner, 2003; Sperry & Love, 2015). Third, drought increases the osmotic pressure required to maintain cell hydration (Martínez-Vilalta et al., 2019; Sapés et al., 2020; Sapés et al., 2019) and phloem translocation (Jensen, 2018; Sevanto, 2018), presumably affecting the concentration of sugars in cytosol and phloem sap. This effect is compounded by changes in phloem sap composition leading to changes in viscosity (Jensen, 2018). Lastly, these effects and other changes in metabolism during drought may affect respiration rates. However, the effects of drought on photosynthesis, respiration, and growth should, in turn, influence how NSC concentrations varies across studies. Some studies have observed decreases in NSC concentrations after drought (Galiano et al., 2011; Hartmann et al., 2013; Sapés et al., 2020), while others have detected increases (Galvez et al., 2011; Galvez et al., 2013), and yet others have observed little change (Anderegg & Anderegg, 2013; Schönbeck et al., 2018), or a combination thereof (Piper, 2011; Sevanto et al., 2014). Furthermore, a meta analysis of drought-induced mortality experiments found both increases and decreases in NSC concentrations associated with mortality, while loss of xylem conductance was more consistently associated with mortality (Adams et al., 2017). The duration and intensity of the drought may explain these differences (Sevanto et al., 2014). Acclimation over longer time periods could also explain varying results to droughts (Oswald & Aubrey, 2020; Schönbeck et al., 2018). Despite the direct link between sugars and plant water balance, stronger drought effects are observed in starch (e.g. Sapés et al. (2020)). The stronger effect on starch may result from tighter controls on sugar concentrations regarding omroregulation and phloem translocation. Large swings in sugar concentrations would mean large swings

in osmotic potentials, affecting cell hydration as well as xylem and phloem function. Seasonality of NSC is also typically stronger in starch (Martínez-vilalta et al., 2016), suggesting that starch acts like a capacitor to buffer swings in sugar concentrations (Daudet et al., 2002).

The usual seasonal dynamics of NSCs mean that NSC concentrations change over the course of several months, even without drought-related changes. The timing of drought events would interact with the seasonal dynamics of NSCs, with the season of occurrence in part determining the drought's effect. For example, starch accumulates during winter in conifer species (e.g., *Pinus taeda*, *Pinus palustris*) in the southeastern US while it depletes during summer, especially in roots and stems. While these species grow during a summer growing season, they photosynthesize year-around, suggesting that wintertime photosynthesis supports springtime growth. Therefore, a drought during winter that reduces photosynthesis would disrupt this accumulation even if no immediate effect on growth occurred, but could reduce growth in the following year due to the loss in winter photosynthesis. A summertime drought would disrupt growth rates immediately, moreso than photosynthesis (Fatichi et al., 2014), leading to NSC concentrations. In addition, if plants acclimate to stressful environments by slowing growth and increasing NSC reserves, then these changes will persist after a drought when water availability increases.

To test these ideas and investigate these phenomena further, we conducted a greenhouse experiment with *Pinus taeda* L. (loblolly pine) to observe how the timing of drought interacts with the seasonality of NSC dynamics. We sought to test whether a summer drougth (in phase with the growing season) or a winter drought (out of phase with the growing season) affects NSC dynamics immediately post-drought and whether changes in growth rates explain those changes.

3.2 Materials and Methods

Overview of experiment To observe the effect of drought timing and to test whether changes in growth explain changes in the seasonal variation of NSCs, we grew a population of 300 *Pinus taeda* in 20 L pots inside a greenhouse at the Savannah River Ecology Lab (33.3429° N, 81.7345° W), located on the US Department of Energy's Savannah River Site, a National Environmental Research Park. Using an automatic irrigation system (see below), plants were assigned to 21 irrigation lines; we simulated drought by reducing the soil moisture. Plants on the same line received the same irrigation. Irrigation lines were divided into three treatments, each with seven irrigation lines: a simulated winter drought, a simulated summer drought, and a control group (well-watered). Each winter and summer drought line started with 12 individuals, while the control lines started with 16 individuals. We simulated drought by reducing irrigation to maintain a lower soil moisture during a six month period. The winter drought ran from September 9, 2019 to March 25, 2020; while the summer drought ran from March 25, 2020 to September 8, 2020. After drought, soil moisture was increased to match control conditions. We potted saplings six months before the beginning of the winter drought to permit acclimation to the greenhouse environment. To minimize genetic differences, all individuals were clones from Arborgen's (Selma, AL, USA) varietal AGV 123. To measure changes in NSC dynamics, we harvested one individual per line before and after each drought, then subsequently harvested at roughly monthly intervals for 10 months post-drought.

We sampled the control population any time we sampled the other treatment populations. A number of environmental and physiological measurements were taken before, during, and after droughts. See relevant paragraphs for details below.

Simulating drought, irrigation system parameters, soil Following (Nemali & van Iersel, 2006), we built an automatic irrigation system to maintain soil moisture at a given setpoint. Drought was simulated by reducing soil moisture to a setpoint below a threshold at which reduced soil water potentials significantly. To choose a threshold, we empirically determined a soil moisture release curve to relate VWC and soil water potential. A control system irrigated all plants on an irrigation line for 30 s at a maximum frequency of once per 30 min. After irrigation, soil moisture was allowed to equilibrate for 15 min before the control system would irrigate again. Pots were irrigated by four drip emitters (2 $\mathrm{gal\,h^{-1}}$, about 3.8 $\mathrm{L\,h^{-1}}$), arranged roughly in a square (spacing 15–25 cm) to distribute water evenly over the soil surface. The control system irrigated if the average of soil moisture measurements taken at 2 $\mathrm{min^{-1}}$ for 15 min (30 measurements per sensor) was less than the set point. Each irrigation line had two soil moisture sensors (Decagon ECHO-5 VWC; now Meter Group EC-5) inserted 3 cm from the bottom of two different pots. Soil moisture sensors were arranged to minimize the distance between all plants on a line and a sensor. Sensors were moved after harvested to a neighboring plant on the same line. Sensors failed and were replaced throughout the study. The control system irrigated based on the average of the two sensors, except when sensors reported values less than -10% or more than 60%, in which case the control system would exclude a sensor to prevent using measurements from a failed sensor. The soil mositure release curve suggested that soil water potentials drop significantly below 10% VWC; the original setpoint was 7.5% VWC, corresponding to a soil water potential of -0.5 MPa. This setpoint caused some mortality within the first two months of the winter drought, suggesting that the setpoint was too low and that induced water stress was too intense. The setpoint was increased to 12% for drought treatments and this threshold was used for the rest of the study. To apply drought, the set point was lowered below 12% VWC. Water potential measurements of soil samples suggested that water potential greatly declined for VWC $< 10\%$ but plants exhibited water stress and some mortality for VWC $< 15\%$. We used a Campbell Scientific (Logan, UT, USA) CR1000: Measurement and Control Datalogger as a controller and the Decagon ECHO-5 VWC[1] (Meter Group, Pullman, WA, USA) sensor to measure soil moisture. We used two Campbell Scientific (Logan, UT, USA) AM16/32 Multiplexers as relays for the soil moisture sensors and two switch relays to control the solenoid valves.

Biomass measurement and NSC sample preparation For each harvest, we removed one plant at random from each irrigation line for a total of six plants per treatment group. We thoroughly washed roots to remove soil. To reduce metabolic activity which might shift NSC concentrations after harvest, we microwaved plant material at 600 W for 90 s (Landhäusser et al., 2018). To avoid sampling bias, we microwaved all plant material, in batches if necessary. We dried each harvested plant at 50°C for at least a week. We separated harvested plant material into leaves, stems, and roots, and then weighed each

[1] Predecessor to Meter Group's EC-5

individually. We coarsely ground all plant material (size $\approx 1\,\mathrm{mm}$) using a Thomas Scientific (Sweedesboro, NJ, USA) Mill, then mixed the coarsely ground material to homogenize. We took a subsample of the homogenized material and then ground it further to pass through a 0.5 mm mesh using a Wiley Ball Mill.

Growth & environmental measurements To estimate growth rates, we measured the height and stem diameter at ground height for all plants monthly as long as the individual plant was alive in the study. We measured heights using a meter stick and measured diameters using calipers (diameters $< 1\,\mathrm{cm}$) or a measuring tape (diameters $> 1\,\mathrm{cm}$) depending on size. We measured specific leaf area using LI-COR Biosciences (Lincoln, NE, USA) LI-3100C leaf area meter to measure the leaf area of needles and a mass balance. To characterize environmental conditions, we measured greenhouse CO_2 concentration using a Vaisala (Helsinki, Finland) GMP 221 CO_2 sensor, temperature and vapor pressure using a Campbell Scientific (Logan, UT, USA) EE181-L air temperature and relative humidity probe, and photosynthetically active radiation (PAR) photon flux density using an Apogee instruments (Logan, UT, USA) SQ-215-SS PAR light sensor. The CR1000 datalogger recorded the average of measurements taken at 30 s intervals over 15 min.

NSC Chemical Analysis Following the protocol in (Landhäusser et al., 2018) (See Supplemental 1), we extracted solubles sugars by washing samples with 1.5 mL of ethanol-water solution (80% by volume or 13.7 M) per mg 30 of sample at 90°C for 10 min. An ethanol-water solution was used to prevent gelatinization of starch or hemi-celluloses (Landhäusser et al., 2018). After sugar extraction, we washed the samples twice more to remove any residual sugar. The remaining material was dried then digested using α-amylase incubated at 85°C for 30 min and γ-amylase (amyloglucidase) at 55 °C for 30 min. We measured the concentration of extracted sugar using the sulfuric acid-phenol assay using 18.6 M sulfuric acid and 0.213 M phenol (Buysse & Merckx, 1993; Chow & Landhausser, 2004; Dubois et al., 1956; Landhäusser et al., 2018). For quality control, we analyzed synthetic controls of cellulose, starch, glucose, sucrose, and fructose with known concentrations. We repeated the extractions if the error as estimated by synthetic control in extraction exceeded 10%.

Other physiological measurements During the simulated droughts, we measured leaf water potentials at monthly intervals. We selected three to five plants per irrigation line and determined the leaf water potential of a random mature needle for each plant, using a PMS (Corvallis, OR, USA) instruments pressure chamber. We estimated maximum photosynthetic rates using LI-COR Biosciences (Lincoln, NE, USA) LI-6400XT portable photosynthesis system to perform gas exchange measurements. We surveyed light-saturated photosynthetic rates at five intervals (roughly once per season beginning winter 2019–2020 with the first drought treatment; see Fig. 3.3) using one plant per line; measurements were made using photosynthetically active photon flux density of 2000 $\mu\mathrm{mol\,m^{-2}\,s^{-1}}$, a reference CO_2 concentration of 450 $\mu\mathrm{mol\,mol^{-1}}$, a flow rate of 500 $\mu\mathrm{mol\,m^{-2}\,s^{-1}}$. Reference H_2O and air temperature were similar to greenhouse conditions around 10 $\mathrm{mmol\,mol^{-1}}$ and 20 °C.

3.2.1 Data Analysis

Our analysis had two global goals: (1) to estimate the effect of drought on nonstructural carbohydrates, height, diameter, and other measurements through time; and (2) to determine whether estimated temporal variation in photosynthesis, growth, and respiration explains observed temporal variation in nonstructural carbohydrates. To this end, we employed different statistical methods, and as shorthand, we refer to the former as our empirical analysis and the latter as our explanatory analysis.

Empirical Analysis To characterize observed dynamics for NSCs and other measurements, and to estimate the differences resulting from drought treatments, we employed linear regression models. In general, the experimental design contains a multi-level or hierarchical structure. Individual plants are grouped within irrigation lines which are then grouped into treatments and arranged into spatially complete blocks. Outcomes vary considerably by irrigation line. Not accounting for this variation yields over-confident estimates of drought treatment effects. To account for this variation, we allow for the true effect to vary by irrigation line, and where relevant by individual plant. We employ a Bayesian data analysis (Gelman et al., 2014), but the likelihood is identical to a linear mixed effect model in which time, treatment, and organ-related parameters are the fixed effects while deviations in these parameters by irrigation line and by individual plant are the random effects. The principal difference is that instead of estimating the average drought effect across blocks with point estimates from each irrigation line using restricted maximum likelihood (REML), we estimate the average using a distribution (Chung et al., 2015); doing so corrects for the overcertainty in REML estimation.

For readers unfamiliar with Bayesian methods, the model assigns probabilities to parameter values to express uncertainty in the true value of the parameters. In figures and in the text, we report posterior means as point estimates (the expected value under the posterior probability distribution) and a 95% credible interval (which indicates a range that has 95% probability of containing the true value). The credible interval therefore indicates a range of probable values for the true value. All estimates of time-varying quantities (e.g., height, mass, NSC concentrations) are conditional on time, but marginalized by irrigation line and individual plants (meaning these effects are averaged out) unless otherwise indicated.

Graphical predictive posterior checks were used to verify model representativeness; comparisons of posterior and prior distributions were used to ensure priors were sufficiently weak. For computations, we used the Markov Chain Monte Carlo method to sample the posterior. Specifically, we used the No-U-Turn Sampler (NUTS) to sample via Hamiltonian Monte Carlo with code provided by `rstanarm` package (version 2.21.3) in R (Goodrich et al., 2022), built on the Stan Modeling Language (Stan Development Team, 2022) (`rstan` version 2.21.7). We used four markov chains, with 2000 total iterations and a warmup of 1000 iterations, yielding a total post-warmup sample size of 4000. Markov chain convergence was checked using standard diagnostics (e.g., lack of divergent transitions, split $\hat{R}$, low autocorrelation) and graphical outputs provided by `shinystan` (version 2.6.0) (Gabry & Veen, 2022).

We provide a brief description of model structure and differences for each data set as well as any data preprocessing. For leaf water potentials and light-saturated photosynthetic rate measurements, time was treated as a categorical variable and was crossed with treatments. The intercept was allowed to vary by

irrigation line. We assumed a negative lognormal distribution for leaf water potentials (i.e., if y is leaf water potential, we assumed $\log(-y)|x$ was normally distributed) whereas light-saturated photosynthetic rate measurements were not transformed.

We assumed a lognormal distribution for height and diameter measurements, conditional on time and treatment. Based on a logistic growth model with sinusoidal relative growth rates, we assumed that the linear predictor μ for height and diameter had the following relationship with time Eq 3.1 where $\omega = 2\pi$ if time is measured in years. Seasonal growth patterns must have this frequency, so ω was not estimated by the model.

$$\mu = \beta_0 + \beta_1 t + \beta_2 \cos(\omega t) + \beta_3 \sin(\omega t) \tag{3.1}$$

which corresponds to a relative growth rate (RGR) for height and diameter measurements (by differentiating Eq (3.1)).

$$\mathrm{RGR} = \beta_1 - \omega\beta_2 \sin(\omega t) + \omega\beta_3 \cos(\omega t) \tag{3.2}$$

To calculate the amplitude α and phase t_0 of relative growth rates, $A = \omega^2\sqrt{\beta_2^2 + \beta_3^2}$ and $t_0 = \frac{1}{2} + \frac{1}{2\pi}\tan^{-1}\left(-\frac{\beta_2}{\beta_3}\right)$. All four time-parameters were allowed to vary by treatment. The intercept β_0 and time-average parameter β_1 were allowed to vary by irrigation line (and correlations were permitted), and the intercept was allowed to vary by individual plant within an irrigation line (the same plants were measured multiple times for height and diameter). We assumed that seasonality was the same within a treatment to avoid the additional complexity; this hierarchical structure was sufficient to reproduce representative replicates of the data set. A logistic growth model was considered, but the resulting nonlinear model was more difficult to sample without large improvement so the linear model was chosen (which is a time-local approximation) instead. For each plant with more than three measurements, the height and diameter measurements were smoothed to identify and remove data entry errors (e.g., drops by an order of magnitude from one month to the next) before analysis.

Conditional on time, organ, and treatment, we assumed dry biomass measurements were lognormally distributed. We allowed the intercept and time effect to vary by irrigation line. To analyze total mass, we added individual organ mass measurements per plant and used a separate model for the total mass data. This model had the same covariates except for organ, which was removed by aggregation. The time coefficient corresponds to a time-average relative mass growth rate.

Nonstructural carbohydrates were analyzed both by organ and by whole-plant concentration (average weighted by organ mass fractions) using a generalized additive model (GAM) or smoothed splines for the temporal dynamics. Logit-transformed nonstructural carbohydrate concentrations were assumed to be normally distributed after conditioning on covariates. Because a number of starch concentrations were recorded as exactly zero (even without those less than zero), we used a perturbed logit transformation $y \mapsto \mathrm{logit}(\varepsilon + (1 - \varepsilon y))$ with $\varepsilon = 5 \times 10^{-4}$ rather than a true logit-transformation. Only variation in the intercept by irrigation line was sufficient to reproduce the data. Other than smoothness, a GAM makes minimal assumptions about temporal dynamics. This structure is useful for characterizing differences in temporal dynamics but not the physiological causes. To estimate the effect of photosynthesis, growth, and respiration on observed NSC dynamics, we used a simple process model based on Oswald and

Aubrey, 2023 to determine covariates for seasonal variations in photosynthesis, respiration, and growth rates suitable for use in a regression model. We explain these methods in the following section

Explanatory Analysis To analyze how changes in photosynthesis, growth, and respiration rates affect NSC dynamics, we applied a simple model of starch dynamics based on a mass balance equation. We only examined starch dynamics because temporal variation consistent with seasonality was only observed in starch concentrations. Let s denote starch concentration in mass fraction (kg/kg), we assume that its dynamics are given by (3.3) where A is the specific photosynthetic rate (rate of mass photosynthesized per biomass) and U is the specific usage rate; here it is defined as $\frac{1}{m}\left(\frac{\partial R}{\partial s}+\frac{\partial G}{\partial s}\right)_{s=0}$ for a respiration rate R and a growth rate G. The derivation is discussed at length in (Oswald & Aubrey, 2023).

$$\frac{ds}{dt} = A(1-s) - Us \tag{3.3}$$

Given the observed starch concentrations were low and the specific photosynthetic rates were high (see below), the relaxation time $1/(A+U)$ was short and therefore the deviation from the steady state (3.4) was small, on the order of 10^{-4} for our data. While starch dynamics can lag environmental conditions, a short relaxation time means that little hysteresis was present in this dataset.

$$s^* = \frac{A}{A+U} \tag{3.4}$$

Therefore, covaraties for carbon supply A and demand U can be substituted. A logit transformation linearizes many possible relationships, facilitating the application of linear regression models.

$$\operatorname{logit}(s^*) = \log\left(\frac{s^*}{1-s^*}\right) = \log\left(\frac{A}{U}\right) \tag{3.5}$$

Note that the starch concentration data only identifies the ratio A/U; ulterior estimates of A identify the magnitude of U.

To determine the relaxation time (response rate), we estimated the magnitude of A in our experiment using photosynthetic and mass measuremets; the magnitude U is then inferred from observed values using (3.4). Let P be the leaf-level photosynthetic rate (CO_2 $\mathrm{mol\,m^{-2}\,year^{-1}}$), we converted P to A using estimates of the leaf mass fraction (LMF), the specific leaf area (SLA; $\mathrm{m^2\,g^{-1}}$), and the molar mass of carbon (12 $\mathrm{g\,mol^{-1}}$).

$$A = (\mathrm{LMF})(\mathrm{SLA})(\mathrm{C\ Molar\ Mass})P \tag{3.6}$$

Variation in LMF and SLA values leads to uncertainty. To determine a possible range of LMF and SLA, we use a normal distribution for SLA (mean = 1.78, sd = 0.18 $\mathrm{m^2\,kg^{-1}}$) and a beta distribution for leaf mass fraction ($\alpha = 12.57, \beta = 18.11$, mean=0.4098). Using the Farquhar, von-Caemmerer, and Berry (FvCB) model of leaf gas exchange (Farquhar et al., 1980; von Caemmerer, 2013; Yin & Struik, 2009), we calculated the leaf-level photosynthetic rate from the measured greenhouse PAR, temperature, RH,

and CO_2 . Daily variation greatly exceeds seasonal variation; we found that variation in daylength alone explains most of seasonal variation in photosynthetic rates. Using daylength allows the calculation of seasonal photosynthetic rates during times without CO_2 measurements. We estimate that A_0 was about $2.34\,[1.34, 3.57]\,\text{year}^{-1}$.

Seasonal variation in photosynthesis is driven by changes in daylength (Fig. 3.1e), therefore, we assumed that for a daylength $D(t)$ at time t, $A = A_0 D(t)$ where A_0 is a constant. To account for possible changes in photosynthesis A and NSC usage U, we assumed $A/U \propto m^\gamma$. We estimated temperature-dependent seasonal variation in specific respiration rates using a Q10 temperature response $R \propto e^{\tau T}$ for temperature T. We used the average temperature over 5-day periods to reduce the subseasonal variation (although these were correlated with temperatures at time of harvest), given the large difference temporal resolution between the NSC and temperature measurements. To estimate the effect of seasonal growth rates from relative height and diameter growth rates, we used the estimated relative height and diameter growth rates per individual plant. Relative height and diameter rates were closely correlated, so we only included relative height rates to avoid overfitting. Letting H denote the relative height growth rate, we have the following combined model.

$$\operatorname{logit}(s^*) \sim \mathrm{N}\left(\log \frac{A_0}{U_0} + \log D(t) + \gamma \log m - \tau T - \alpha H, \sigma^2\right) \tag{3.7}$$

Note that U should the sum of growth and respiration, whereas the combined model (3.7) assumes a product; however, this simplification is approximately correct if the parameters γ, τ, α are small enough, and in that case, a first-order Taylor series expansion about zero yields the above model. We considered an additional model with a smooth spline term for time to account for any additional variation.

Results

For conciseness, we use the notation $x\ [a, b]$ to indicate a posterior mean as the point estimate and a 95% credible interval under the posterior distribution of the appropriate model. Unless otherwise indicated, estimated indicates a posterior mean.

Although not identical to field conditions, environmental conditions inside the greenhouse exhibited similar seasonal variation (Fig. 1). While photosynthetically active radiation (PAR) mirrors seasonal variations observed in field conditions, temperature does not quite follow a sinusoidal pattern more typical of the seasonal variation in daily average, maximum, and minimum temperatures due differences in greenhouse heating and cooling. Concentrations of CO_2 increased slightly through the study and followed a strong day-night pattern, with low concentrations during the day. Seasonal decreases in daily minimum CO_2 concentrations correspond approximately with seasonal variation in photosynthesis (Fig. 3.1). Although temperature, VPD, and CO_2 concentrations are important factors in photosynthesis, changes in day-length drive seasonal variation in leaf-level photosynthesis (Fig. 3.1e). These observations cannot explain any observed differences in height, diameter, or biomass as they do not contain any information on spatial variation; however, fans continually mixed the air inside the greenhouse, minimizing spatial

variation in air temperature, CO_2, and vapor pressure. Light variation is possible but unlikely since irrigation lines of each treatment were distributed throughout the greenhouse; allowing effects to vary by irrigation within a treatment group accounts for this variation.

Typical weekly averages of soil volumetric water content were about 5 $\mathrm{cL\ L^{-1}}$ VWC lower on drought irrigation lines than control lines during drought, although the first two months of the winter drought, the weekly average was about 10 $\mathrm{cL\ L^{-1}}$ lower in the winter drought relative to the control (Fig. 3.2). The signal is noisy due to a high degree of variability in measurements along the same irrigation line (Fig. 3.2 displays one standard error of the pointwise weekly average). Pointwise t-tests do not yield significant differences due to the high variability (e.g., for the seven-day period after 2019–10–02, control VWC was 11.2 $\mathrm{cL\ L^{-1}}$ higher than winter VWC, but with a t-statistic $t = 3.93$ on 11 degrees of freedom, $p = 0.073$); however, pointwise comparisons do not capture the consistent differences through time.

Estimated averages of daytime needle water potentials in drought treatments were within 0.25 MPa of the control (Fig. 3.3a); however, during the second month of the winter drought treatment (2019–10–07), the estimated average leaf water potentials of the winter drought was $-0.39\ [-0.74, -0.04]\ \mathrm{MPa}$ relative to control. The magnitude of this difference co-occurs with lowest weekly average VWC (Fig. 3.2), consistent with higher water stress during that time. The credible intervals of all other differences span zero, indicating high probability of small, near-zero differences; although consistent with little reduction in needle water potentials due to treatments, the the typical width of the credible intervals is about 0.5 MPa. This uncertainty reflects the greater variability within lines at each time point rather than across time.

Typical estimated average light-saturated leaf photosynthetic rates of winter and summer drought treatments were between -1 and -2 $\mu\mathrm{mol\ m^{-2}\ s^{-1}}$ relative to control. While the regression model indicates a high probability that averages were lower in winter drought treatment (> 80% for all time points) and in the summer drought treatment (>90% except for 2020–04–28, which was 80%), the model also indicates these differences are probably small (most credible intervals span zero) (Fig 3.3b). Furthermore, summer drought treatment shows these differences before the simulated drought began, suggesting that these differences do not indicate responses to simulated drought.

Overall, the estimated average height of control plants increased more than drought treatments, suggesting the simulated droughts reduced growth rates (Fig. 3.4a-d). Over the entire study period, the average relative height growth rates were $0.93\ [0.75, 1.10]\ \mathrm{year^{-1}}$, $0.67\ [0.50, 0.84]\ \mathrm{year^{-1}}$, and $0.60\ [0.43, 0.77]\ \mathrm{year^{-1}}$ for the control, winter, and summer drought groups, respectively; that is, winter and summer drought groups had estimated average relative height growth rates 27% and 35% lower than control, respectively (Tab. 3.2). While the expected differences are relatively large near the end of the study (2021–02–07; Tab 3.1)—roughly 29% and 39% lower than control for winter and summer drought groups, respectively—the uncertainty is quite high due to different outcomes across irrigation lines. For instance, irrigation lines 4, 5, and 6 (winter, summer, and control) had estimated average height of $122\ [109, 136]\ \mathrm{cm}$, $74\ [67, 74]\ \mathrm{cm}$, and $179\ [164, 195]\ \mathrm{cm}$, respectively, which corresponds to 32% and 59% lower than control for winter and summer drought groups. This difference was much larger than irrigation lines 13, 14, and 15 (winter, summer, and control) which had estimated average height of $107\ [95.8, 118]\ \mathrm{cm}$, $74.9\ [67.3, 60.6]$

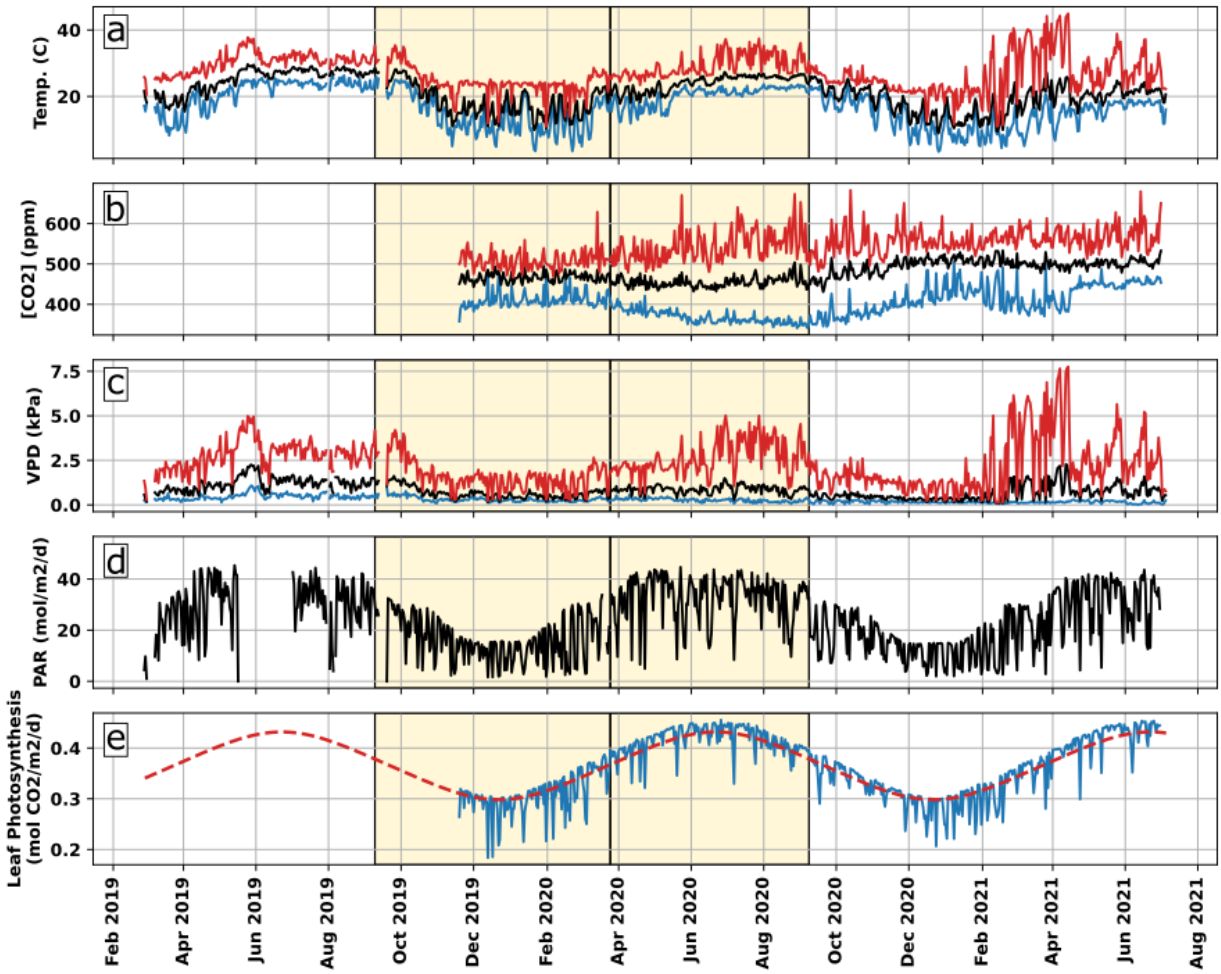

Figure 3.1: Daily mean (black), daily max (red), and daily min (blue) of greenhouse air temperature (a), carbon dioxide air concentration (b), vapor pressure deficit (c); daily light integral (d) and daily average leaf photosynthetic rate estimated from the Farquhar-von-Caemmerer-Berry model (e, solid blue) daily average leaf photosynthetic rate estimated from daylength (e, dashed red).

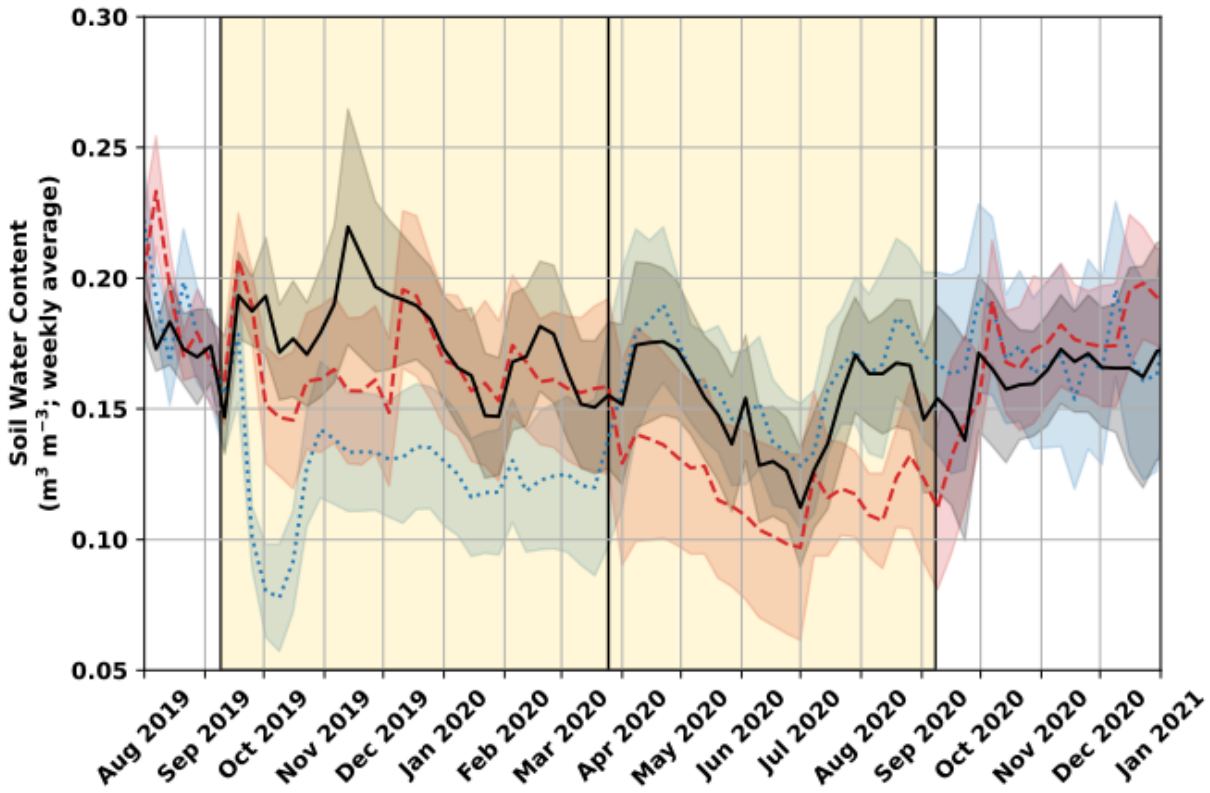

Figure 3.2: Weekly average volumetric soil water content ± pointwise standard error for control (solid black), winter (dotted blue), and summer (dashed red) group. Yellow shading indicates simulated drought dates for respective treatment.

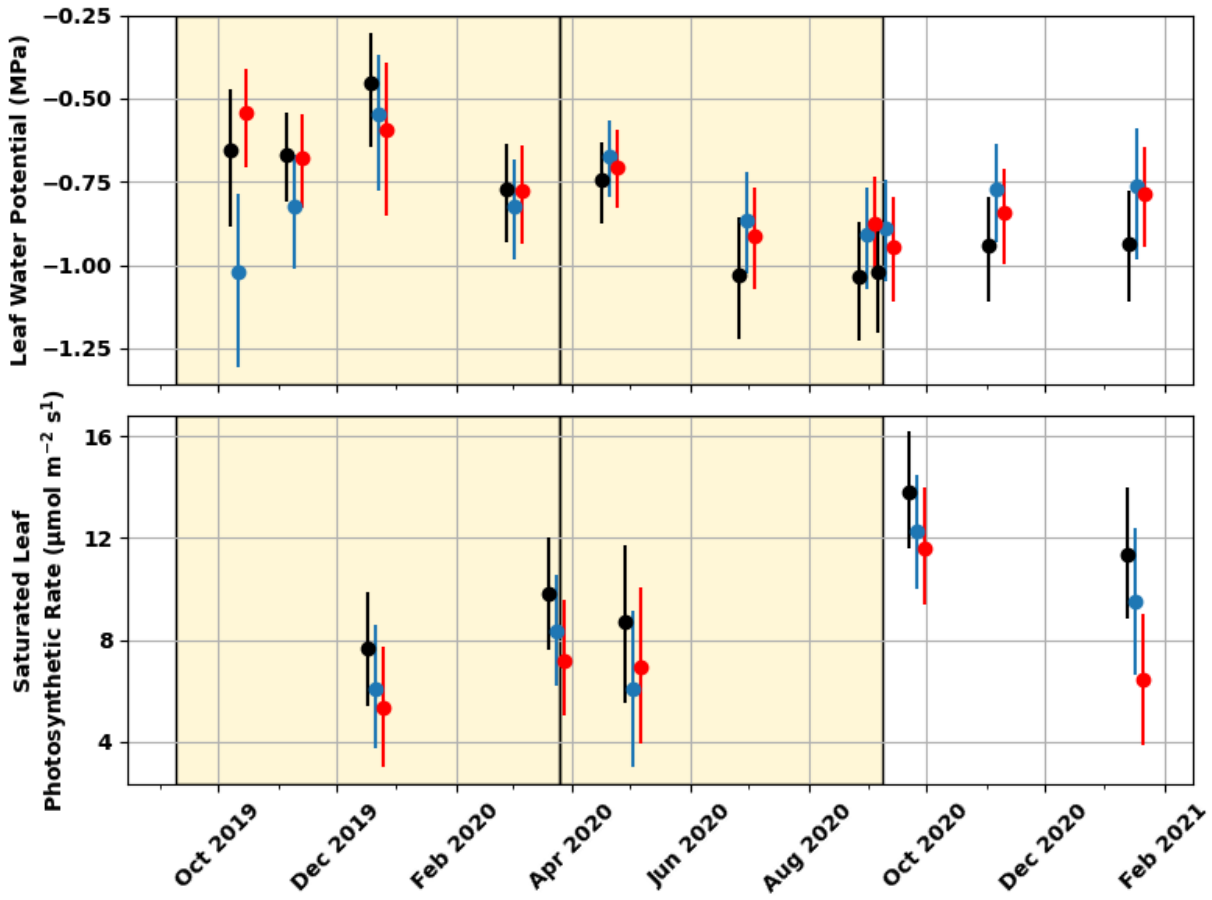

Figure 3.3: Leaf physiological measurements
Estimated mean and 95% credible interval leaf water potentials (measured by pressure chamber) and light-saturated leaf photosynthetic rate (measured by gas exchange) by control (black), winter drought (blue), summer drought (red) treatments. Yellow shading indicates simulated drought dates for respective treatment.

Table 3.1: Comparison of height (cm) estimates at selected times. The notation $x\ [a, b]$ indicates posterior mean as point estimate and a 95% credible interval. Differences are relative to control.

Time	Treatment	Estimate	Difference	$P(x < 0)$
2019–04–26	Control	$27.7\ [25.1, 30.6]$		
	Winter	$30.0\ [26.5, 33.5]$	$2.0\ [-2.2, 6.3]$	0.17
	Summer	$29.6\ [26.5, 33.0]$	$1.9\ [-2.2, 6.1]$	0.17
2019–08–31	Control	$48.0\ [42.4, 53.5]$		
(before treatments)	Winter	$44.0\ [39.0, 49.4]$	$-3.9\ [-11.4, 3.73]$	0.86
	Summer	$41.1\ [36.3, 46.4]$	$-6.9\ [-14.3, 0.37]$	0.97
2021–02–07	Control	$134\ [94.3, 180]$		
(after treatments)	Winter	$95.2\ [68.8, 129]$	$-39\ [-94, 12]$	0.94
	Summer	$82.1\ [59.7, 111]$	$-52\ [-104, -3.5]$	0.98

cm, and $123\ [113, 135]\ \mathrm{cm}$, respectively, about 14% and 50% lower than control for winter and summer drought groups; however, the average height of control line 15 was about 31% lower than control line 6. This variation explains the uncertainty in relative height growth rate parameters (Tab. 3.2). Height measurements show seasonal growth (highest slope in May–June) (Fig. 3.4a-d; Tab. 3.2). We summarize this seasonality using the amplitude and phase of sine function, which indicate the maximum deviation from the temporal average and the time of year of maximum growth rates, respectively (Tab. 3.2). Note that the temporal average and amplitude are almost the same because relative growth rates are effectively zero in winter. A reduction in summertime growth rates lowers both the temporal average and the amplitude. Estimated amplitudes of the relative height growth rates were 56% and 69% lower relative to control for the winter and summer drought groups (Tab. 3.2), also indicating a reduction in growth rates. Estimated phases were approximately the same (Tab. 3.2) indicating that the maximum of growth rates occurs at about the same time.

Overall, the estimated average diameter of control plants increase more than those in drought treatments, suggesting the simulated droughts reduced growth rates (Fig. 3.4e-h). Over the entire study period, the average relative diameter growth rates were $1.03\ [0.88, 1.19]\ \mathrm{year}^{-1}$, $0.85\ [0.70, 1.01]\ \mathrm{year}^{-1}$, and $0.75\ [0.60, 0.90]\ \mathrm{year}^{-1}$ for the control, winter, and summer groups, respectively; that is, winter and summer drought groups had estimated average relative diameter growth rates 17% and 27% lower than control, respectively (Tab. 3.4). The evidence of a strong treatment effect is weaker for diameters than heights given the higher probability of small differences. Thus, while the estimated differences are large near the end of study (2021–02–07; Tab. 3.3), 26% and 34% lower than control for winter and summer drought groups, respectively; the uncertainty is driven by high variability in irrigation lines, similar to the height data. Diameter measurements also show seasonal growth (Fig. 3.4e-h; Tab. 3.4). We summarize this seasonality using the amplitude and phase of sine function, which indicate the maximum deviation from

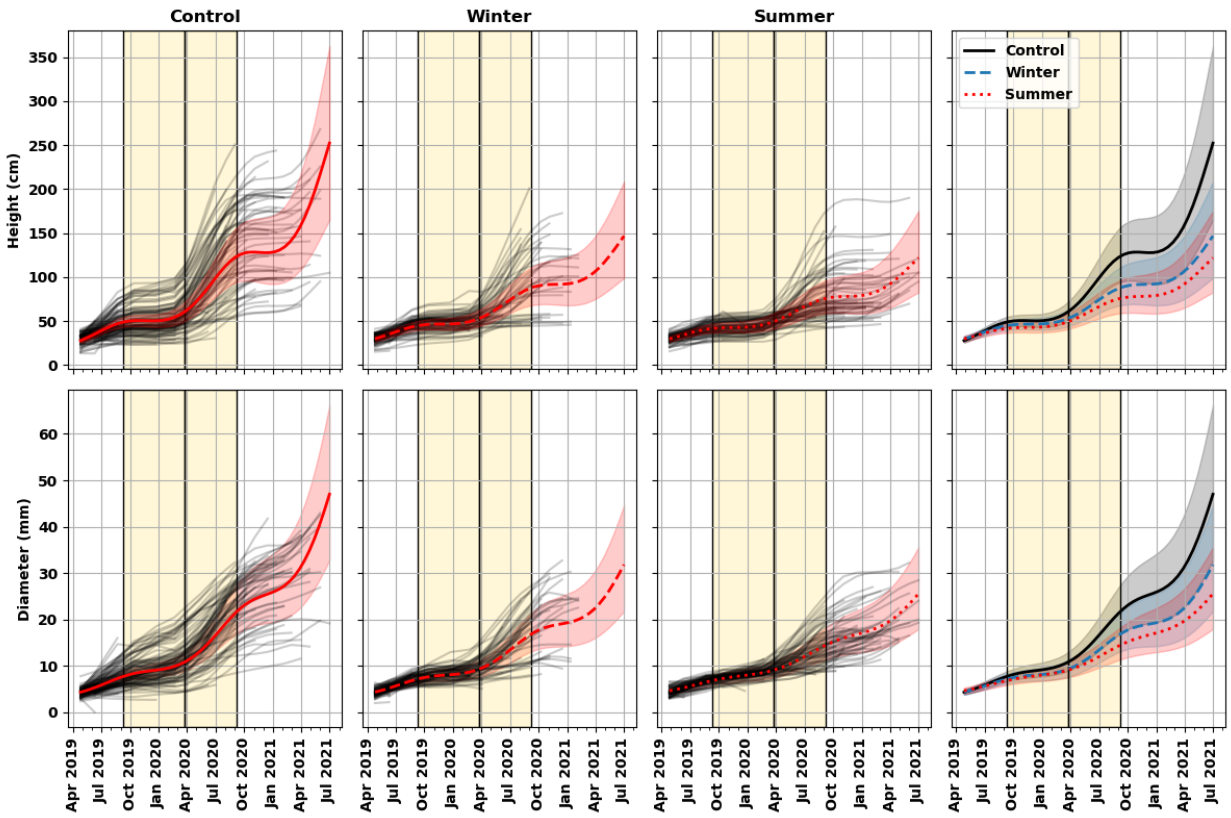

Figure 3.4: Height and ground diameters with estimated average and 95% credible band by treatments: no drought control, winter drought, and summer drought, from left to right; last column compares estimated average for control (black solid), winter (blue dashed), and summer (red dotted) side-by-side. Yellow shading indicates simulated drought dates for respective treatment;

Table 3.2: Comparison of relative height growth rate parameters. The notation $x\ [a, b]$ indicates posterior mean as point estimate and a 95% credible interval. Differences are relative to control. Time-average and amplitude have units y^{-1}.

Parameter	Treatment	Estimate	Difference
Time average	Control	$0.93\ [0.75, 1.10]$	
	Winter	$0.67\ [0.50, 0.84]$	$-0.25\ [-0.49, -0.01]$
	Summer	$0.60\ [0.43, 0.77]$	$-0.33\ [-0.57, -0.08]$
Amplitude	Control	$1.02\ [0.88, 1.17]$	
	Winter	$0.45\ [0.33, 0.57]$	$-0.57\ [-0.76, -0.39]$
	Summer	$0.33\ [0.24, 0.41]$	$-0.70\ [-0.86, -0.53]$
Phase	Control	May 21 [May 17, May 25]	
	Winter	May 27 [May 19, Jun 3]	$5\ [-2.9, 14]$ d
	Summer	May 16 [May 9, May 23]	$-5\ [-14, 3]$ d

Table 3.3: Comparison of diameter (mm) estimates. The notation $x\ [a, b]$ indicates posterior mean as point estimate and a 95% credible interval. Differences are relative to control.

Time	Treatment	Estimate	Difference	$P(x < 0)$
2019–04–26	Control	$4.3\ [3.8, 4.9]$		
(before treatments)	Winter	$4.4\ [3.8, 5.0]$	$0.04\ [-0.80, 0.89]$	0.47
	Summer	$4.6\ [4.0, 5.3]$	$0.30\ [-0.54, 1.19]$	0.24
2019–08–31	Control	$7.5\ [6.8, 8.6]$		
	Winter	$7.0\ [6.1, 8.1]$	$-0.51\ [-1.95, 0.98]$	0.76
	Summer	$6.7\ [5.8, 7.7]$	$-0.82\ [-2.26, 0.65]$	0.88
2021–02–07	Control	$27\ [20, 37]$		
(after treatments)	Winter	$20\ [15, 27]$	$-7.2\ [-18.0, 2.87]$	0.93
	Summer	$18\ [13, 24]$	$-9.4\ [-19.9, 0.19]$	0.97

the temporal average and the time of year of maximum growth rates, respectively (Tab. 3.4). Estimated amplitudes of the relative diameter growth rates were 17% and 70% lower relative to control for the winter and summer drought groups (Tab. 3.4), also indicating a reduction in growth (especially for the summer drought group). Estimated phases were approximately the same (Tab. 3.4) indicating that the maximum in growth rates occurs at about the same time.

The estimated average total biomass of control plants increased more than drought treatments, suggesting some evidence of reduced net primary production rates (Fig. 3.5); the estimated effect was similar across all organs (Fig. 3.5; Tab. 3.5). However, the strength of the effect is uncertain and the model indicates relatively high probabilities that winter biomass growth rates exceeded controls (at least 10%, depending on organ), meaning that these differences may be small and not reliably linked to drought treatment. As with the height and diameter data, variation among irrigation lines greatly increases uncertainty.

Estimated average whole-plant sugar concentrations appear to have increased and then decreased during the study (Fig. 3.6); however, it is unclear that this variation reflects any seasonal pattern. While estimated average sugar concentrations are not the same across treatments through time, the largest difference was the summer leaf sugar concentrations *before* the summer drought (2020-03-25), when summer leaf sugar concentrations were $-1.7\ [-3.9, -0.2]\ \mathrm{cg\,g^{-1}}$ relative to control. Furthermore, during most of the study period, differences in the estimated averages are typically less than $2\ \mathrm{cg\,g^{-1}}$. In fact, the model indicates at least a 96% probability that the absolute difference in winter sugar concentrations and the control is less than $2\ \mathrm{cg\,g^{-1}}$ and a 86% probability that the absolute difference is less than $2\ \mathrm{cg\,g^{-1}}$ for summer sugar concentrations relative to control. Visually, the credible intervals of any two treatments overlap during most the study (Fig. 3.6). Therefore, we observed little evidence of large differences in sugar concentration dynamics due to drought treatments.

Table 3.4: Comparison of relative diameter growth rate parameters. The notation $x\ [a, b]$ indicates posterior mean as point estimate and a 95% credible interval. Differences are relative to control. Time-average and amplitude have units y^{-1}.

Parameter	Treatment	Estimate	Difference
Time average	Control	$1.03\ [0.88, 1.19]$	
	Winter	$0.85\ [0.70, 1.01]$	$-0.18\ [-0.40, 0.040]$
	Summer	$0.75\ [0.60, 0.90]$	$-0.28\ [-0.50, -0.067]$
Amplitude	Control	$0.50\ [0.40, 0.60]$	
	Winter	$0.41\ [0.30, 0.53]$	$-0.084\ [-0.24, 0.072]$
	Summer	$0.15\ [0.095, 0.20]$	$-0.35\ [-0.46, -0.24]$
Phase	Control	Jun 11 [Jun 5, Jun 17]	
	Winter	Jun 11 [Jun 3, Jun 20]	$0\ [-10, 11]$ d
	Summer	Jun 20 [Jun 8, Jul 1]	$9\ [-4, 22]$ d

Table 3.5: Comparison of estimated time-average relative dry biomass growth rate (y^{-1}). The notation $x\ [a, b]$ indicates posterior mean as point estimate and a 95% credible interval. Differences are relative to control.

Organ	Treatment	Estimate	Difference
Total	Control	$1.97\ [1.64, 2.31]$	
	Winter	$1.71\ [1.32, 2.10]$	$-0.26\ [-0.78, 0.24]$
	Summer	$1.50\ [1.04, 1.92]$	$-0.48\ [-1.02, 0.09]$
Root	Control	$2.15\ [1.73, 2.57]$	
	Winter	$1.88\ [1.42, 2.33]$	$-0.27\ [-0.88, 0.32]$
	Summer	$1.60\ [1.07, 2.13]$	$-0.55\ [-1.21, 0.12]$
Stem	Control	$2.22\ [1.80, 2.63]$	
	Winter	$1.82\ [1.34, 2.28]$	$-0.4\ [-1.06, 0.22]$
	Summer	$1.58\ [1.05, 2.12]$	$-0.65\ [-1.35, 0.03]$
Leaf	Control	$1.69\ [1.27, 2.10]$	
	Winter	$1.44\ [0.97, 1.91]$	$-0.25\ [-0.88, 0.36]$
	Summer	$1.32\ [0.83, 1.85]$	$-0.37\ [-1.04, 0.28]$

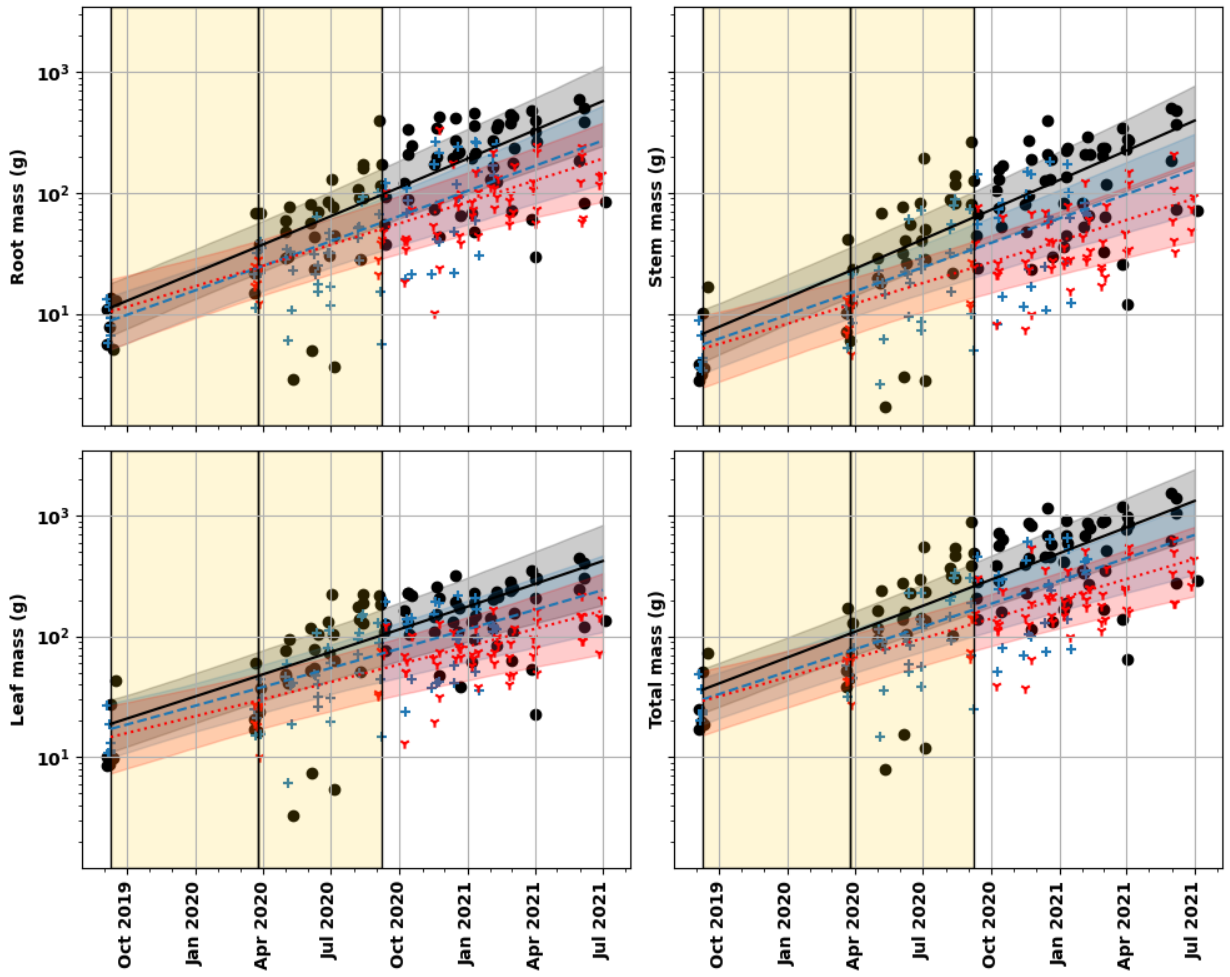

Figure 3.5: Dry biomass (log scale) with estimated average and 95% credible band by no drought control (black solid, •), winter drought (blue dashed, +), and summer drought (red dotted, Y). Yellow shading indicates simulated drought dates for respective treatment. Points jittered by ± 5 days.

Estimated average starch concentrations show springtime maxima, consistent with seasonal variation (Fig. 3.7). Temporal dynamics were similar across all organs (Fig. 3.7). Differences between drought treatments and the control were very small; the model indicates a 93% and 83% probability that the difference from zero is less than 2 $\mathrm{cg\,g^{-1}}$ for winter and summer drought treatments, respectively, relative to control. Note that the credible intervals of any two treatments overlap during most of the study, even more so than for sugar concentrations. Any differences due to the drought treatments were smaller than experimental error or variation among individuals. Therefore, timing of drought did not affect NSC dynamics sufficiently to produce detectable differences in our experiment, even though reductions in growth rates associated with drought were observed. However, variation in temperature and mass explained some but not all the observed variation in whole-plant starch dynamics (Fig. 3.8). Using relative height or diameter growth rates as estimates of whole-plant growth rates provided little explanatory power (based on differences in expected log pointwise predictive density (ELPD) relative to their standard errors), and our model with relative height rates indicates its effect is near zero (in fact, the probability that the effect has the correct sign is only 66%) (Fig. 3.8). Both metrics suggest growth rates do not explain observed starch dynamics.

Discussion

Within the precision of our experiments, we observed little change in NSC dynamics across drought treatments, and the timing of drought did not have any apparent effect on NSCs. Despite large variation in individual outcomes, we did observe small differences in average mass, height and diameter increment across treatments. In summary, the small difference in average mass is consistent with a reduction (about 13% and 24% for winter and summer relative to control) in net primary production on average, and differences in height and diameter are consistent with reductions in growth rates (about 27% and 35% for winter and summer relative to control) due to water stress, as expected (Hsiao, 1973; Hsiao et al., 1976). Based on our experiment, the season of drought neither affects the magnitude or duration of the post-drought accumulation and depletion of NSC as we observed no changes in NSC dynamics by treatment. Differences in growth do not explain observed changes in NSC concentrations. These conclusions would contradict standard theory about the relationship of NSCs to growth (Dietze et al., 2014; Mcdowell, 2011). To deepen our analysis, we examine possible explanations for this negative result consistent with standard theory and discuss their implications for future studies on nonstructural carbohydrates.

First, we consider the expected size of NSC response given a hypothetical change in photosynthetic or usage rates. To estimate the potential magnitude and duration of an NSC response, we use Equations (3.3) and (3.4) substituting in hypothetical reductions in usage rates due to growth reduction. Estimated specific photosynthetic rates A were quite high, ranging 1-4 $\mathrm{y^{-1}}$while NSC concentrations were typically 0.5-5%; therefore the NSC usage rate U was quite high, roughly 18-100$\times$ greater than A (the estimated range in our model was [89, 638] $\mathrm{y^{-1}}$). Following (Fatichi et al., 2014), suppose a 50% in the growth rate during drought, and no change in photosynthesis or respiration. Setting $U \mapsto U/2$ in equation (3.4), the maximum change in starch concentrations would approximately double under drought; however,

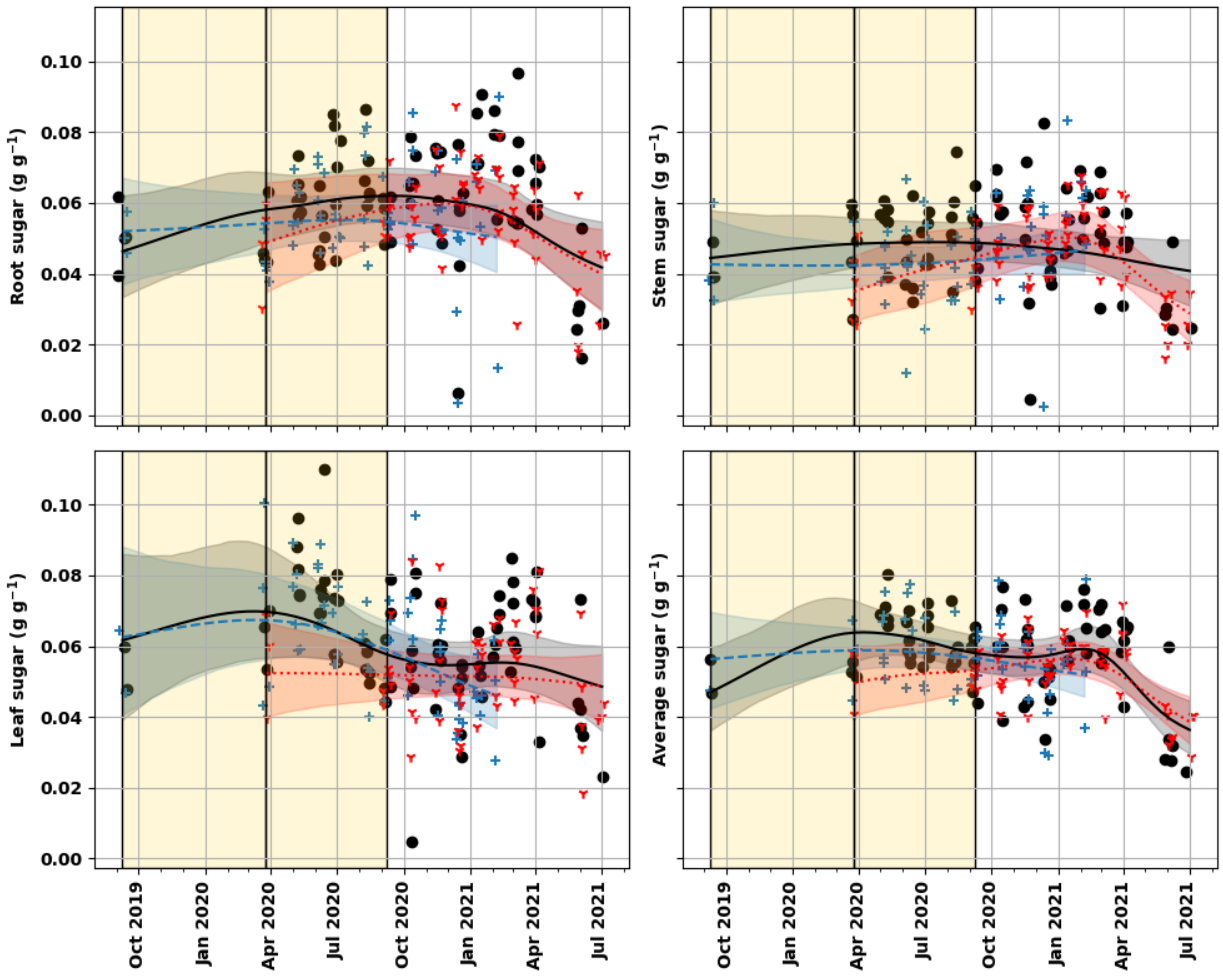

Figure 3.6: Sugar concentrations with estimated average and 95% credible band by treatment: control (black solid, •), winter drought (blue dashed, +), and summer drought (red dotted, Y). Points jittered by ± 5 days.

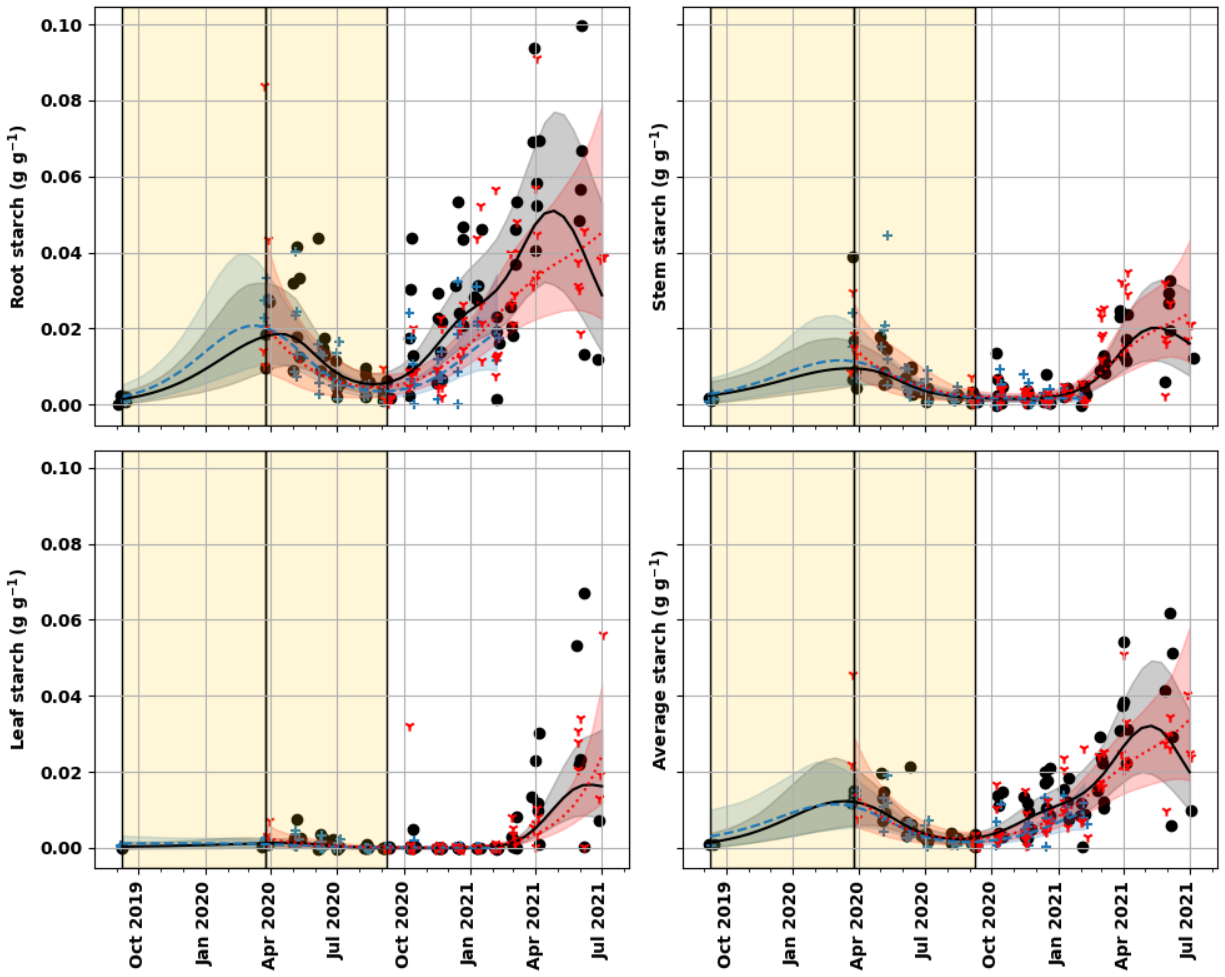

Figure 3.7: Starch concentrations with estimated average and 95% credible band by treatment: control (black solid, •), winter drought (blue dashed, +), and summer drought (red dotted, Y). Points jittered by ± 5 days.

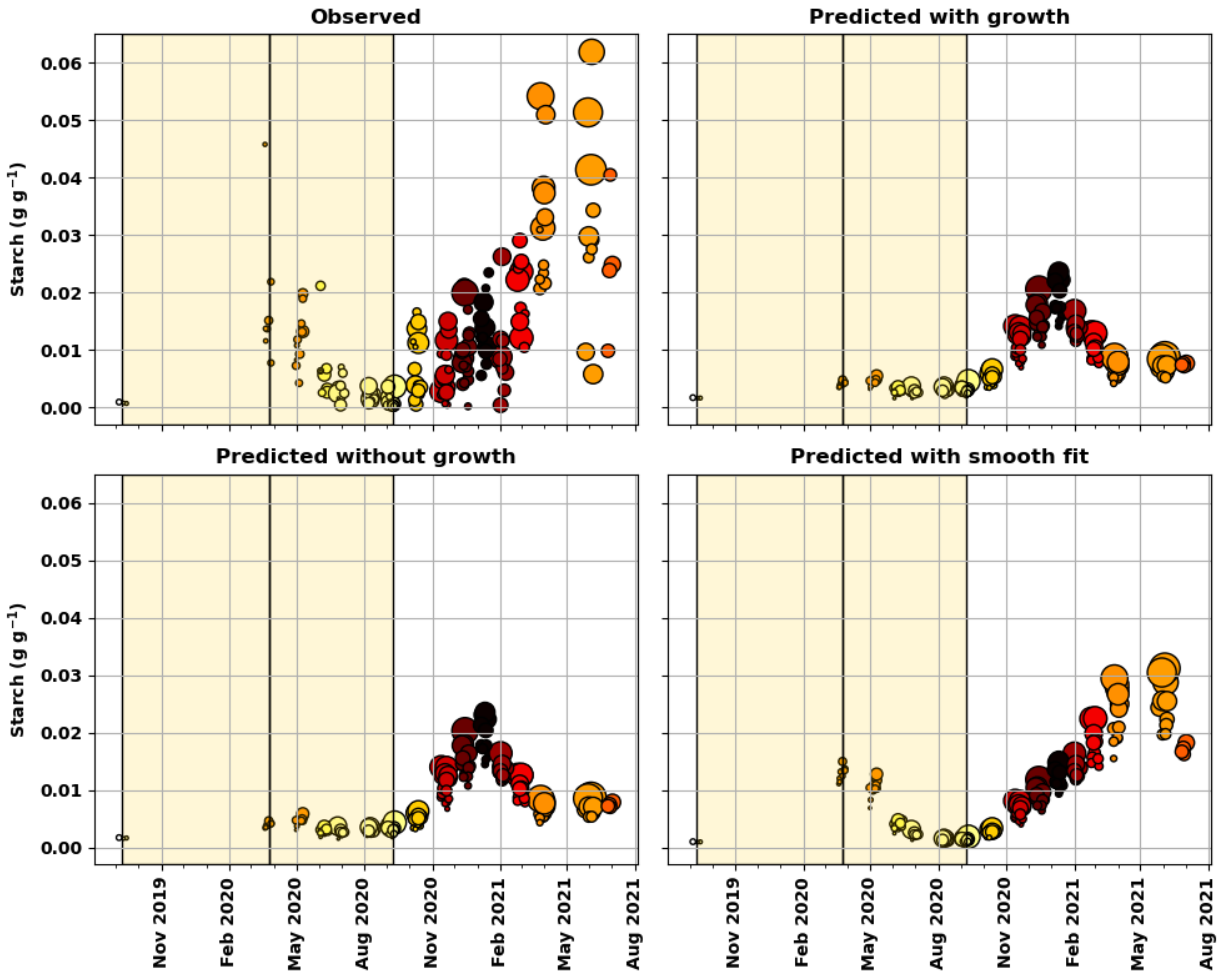

Figure 3.8: Observed whole-plant starch concentrations (upper left) by temperature (color, lighter = warmer) and by mass (point size) to model predicted estimates using estimates of photosynthesis (i.e., daylength), respiration (i.e., temperature, Q10 response), and mass-dependent changes; one model (with growth) included relative height rate as an estimate of growth rate, another contained an additional smooth time effect (cubic basis spline). Points jittered by ± 5 days.

because starch concentrations were low during the study, that doubling corresponds to an small absolute difference in starch concentrations, typically less than 2 $\mathrm{cg\,g^{-1}}$ which is about the level of precision for the NSC chemical analysis (Landhäusser et al., 2018). In other words, assuming a hypothetical drought of greater intensity than our actual simulated drought, and overestimating its effect by neglecting changes in photosynthesis and respiration, still might not produce an effect large enough to detect reliably with NSC chemical analysis methods. Note that other sources of variation (such as individual and irrigation line variation) would further decrease measurement precision of average effects. For this reason, our lack of response need not contradict the standard theory relating growth and nonstructural carbohydrate dynamics.

Second, suppose that NSC dynamics in water stressed plants return to their baseline (i.e, the control's dynamics), would drought effects persist long enough to be detected? The relaxation halving time ($\log(2)/(A+U)$), estimated using (3.3) and (3.4), provides an estimate of how long such transient differences might persist. For our data, the relaxation halving time is quite short, 2–14 days, meaning that transient differences persist on the order of days rather than months. Under the hypothetical drought in which starch concentrations double, only 4–28 days are required for starch concentrations return to pre-drought baseline during post-drought recovery. For our experiment, any transient responses could then quickly disappear at a rate not detectable by our sampling frequency. Such fast changes have been observed in other experiments with saplings and seedlings such as in a shading experiment with saplings (Weber et al., 2018). Weber et al., 2018 observed NSC responses to shading and re-illumination with relaxation halving times of about 10 days. To have a higher sampling frequency while maintaining the study duration would have required a prohibitive number of plants, given the destructive nature of NSC measurements.

Third, some of the observed variation in NSC concentrations could reflect daily or weekly dynamics rather than seasonal dynamics. The short relaxation times supports this conclusion. Large diurnal changes in starch concentrations have been observed in the leaves of mature *Quercus rubra* (Gersony et al., 2020) and in most tissues of seven-year-old *Prunus dulcis* (Tixier et al., 2018); and similar dynamics have been observed in *Arabidopsis* leaves (Gibon, Bläsing, et al., 2004; A. M. Smith & Stitt, 2007). Some observations of the seasonal dynamics of whole-plant starch concentrations in several mature trees indicate the seasonal variation might be less dramatic for whole-plant averages rather than individual tissues (Furze et al., 2019). Our experiment was not designed to detect changes in diurnal dynamics, although harvest time of day did not appear to explain any variation in NSC concentrations.

Fourth, individuals in our study increased in mass 16–33-fold in about two years. Several authors have proposed the possibility ontogenetic changes in NSC dynamics (Hartmann & Trumbore, 2016), which is consistent with mass-dependent changes. Mass-dependent or other ontogenetic changes in photosynthesis, respiration, growth could wash out other drought related effects. In fact, our data suggests that the upward shift the starch concentrations through time is mass-dependent change after controlling for seasonal shifts (Fig. 3.8). The largest plants had become root-bound and had probably begun to experience the effects of pot-size limitation; the upward shift in starch with total mass is consistent with this. Note that only the largest plants had non zero leaf starch (Fig. 3.7). This result agrees with the prediction of mass-dependent changes suggested in (Oswald & Aubrey, 2023) and supports the assertion that

experiments on saplings in greenhouse experiments do not transfer to canopy trees in the field without modification (even with otherwise similar conditions) (Hartmann et al., 2018). However, our experiment was not designed to detect such mass-dependent effects, so this possibility also merits further investigation. While low relative to other species, sugar and starch measurements were not low relative to other observations in *Pinus taeda*, especially in potted saplings (Aspinwall et al., 2011; Griffin et al., 1996; Luedtke, 2013; Rowe et al., 2002).

Fifth, the high variability of measured soil water content suggests that the irrigation system had difficulty maintaining the correct thresholds. It is possible that plants within the same irrigation line experience a range of water availabilities leading to a wide range of outcomes, especially for control plants as variability in the growth and biomass data is higher among the control irrigation lines than the treatments. Better control of the soil water content could have reduced the variability and possibly allowed for the observation of a smaller effect; however, the large number of plants limited the ability of the irrigation system to control soil water content for each individual plant. Changes in experimental parameters could overcome these issues.

Observed starch dynamics are consistent with observations for *Pinus palustris* (another pine species in the southeastern United States), increasing in winter and decreasing in summer (Aubrey & Teskey, 2018; Oswald & Aubrey, 2020). This variation is theoretically consistent with seasonal starch dynamics driven by changes in respiration and growth rates (Oswald & Aubrey, 2023), and we observed covariation with whole-plant starch concentrations and temperature (a proxy for variation in respiration rates) (Fig. 3.8). Note this seasonal dynamic differs from other evergreen conifers at higher latitudes (Schoonmaker et al., 2021) (i.e., *Pinus sylvestris* and *Picea glauca*), for which starch increases in spring and decrease in fall. It may be that variation in respiration is a bigger factor in seasonal variation of starch than growth, but confirmation would require experiments to directly measure whole-plant respiration. Moreover, greenhouse temperatures decrease slightly on average over time, so the observed relationship between temperature and starch concentrations may not be causal; an experiment comparing plants grown under several temperatures constant in time would provide a more thorough test as constant temperatures should eliminate temporal variation and starch variation would then vary by temperature only. Alternatively, if seasonal variations in growth persist even under constant temperatures, variations due to growth may be easier to detect.

Our experiment suggests that while winter drought affected the growth rate in the following growing season, summer drought had a greater impact on growth rates. As evergreen conifers, *P. taeda* saplings still photosynthesize through winter and may continue to grow belowground if not aboveground, so a winter drought still reduces the overall growth and biomass accumulation of the trees. Our observations may be an example of a short-term "legacy effect". Dendrochronological studies have also found the effect of drought depends on its timing relative to growth phenology (Foster et al., 2014; Gao et al., 2018; Granda et al., 2013; M. Huang et al., 2018). It is unclear whether NSC dynamics mediated this effect. If only small changes in NSC concentrations are needed to generate the effect, then our results remain consistent with NSCs mediating drought legacy effects; however, it may be that the effect was mediated by some other aspect of physiology.

Relative to similar studies, our experiment contains a large number of NSC measurements. For instance, Sevanto et al., 2014 present a similar greenhouse drought study but their experiment only examines the acute response during water stress. Furthermore, they only had four plants per group and while they collected more physiological measurements, they were unable to sample their NSC dynamics repeatedly through time (Sevanto et al., 2014). Ruswick et al., 2021 present a similar experiment examining the effect of fire and its timing on seasonal NSC dynamics in *Liquidambar styraciflua* during resprouting instead of drought. While limited in time resolution, they found evidence that timing of fire interacts with seasonal NSC dynamics (Ruswick et al., 2021). Finally, Blumstein et al., 2022 found evidence of a growth-storage tradeoff in a common garden experiment with a large number of NSC measurements but only after controlling for the effect of photosynthesis. Their experiment did not attempt to measure seasonal NSC dynamics and in fact, they attempted to minimize its presence in their data (Blumstein et al., 2022). Our experiment was conducted with clonal plants, so genetic variation among individuals was low relative to natural populations.

As a final thought, several limitations of our experiment ultimately result from the destructive nature of NSC sampling. Our experiment cannot resolve individual variation in NSC dynamics or mass. Furthermore, high sampling rates provides better resolution of temporal variation in NSCs but also requires large numbers of plants making both other physiological measurements and experimental control of the environment more difficult. Methods allowing repeated non-destructive, *in vivo* measurement of whole-plant NSC concentrations would permit a similar study with better control for sources of variation and therefore could detect smaller effects on NSC dynamics than achievable in our setup. The search for such methods holds much potential for advancing the science of NSC physiology.

Chapter 4

Implementing dynamic nonstructural carbohydrates in earth system models: Insights on essential model structure

4.1 Introduction

The dynamics of plant physiology are a keystone to describing how ecosystems will respond to changing climatic conditions. Every year, via photosynthesis, terrestrial plants collectively absorb 121.7×10^{15} grams of carbon per year worldwide from the Earth's atmosphere, and they return approximately half of this amount each year to the atmosphere in respiration (Beer et al., 2010; Field et al., 1998), meaning that plants represent the largest factor in determining net ecosystem exchange of carbon. The ultimate climate effect of anthropogenic release of carbon dioxide depends on how plants respond to increases in carbon dioxide and temperature. Increasing atmospheric carbon dioxide concentrations increases terrestrial photosynthesis because plants with the ancestral C_3-photosynthetic pathway increases in leaf carbon dioxide increase carboxylation rates and decrease oxygenation (photorespiration) rates. While short-term photosynthetic responses are easily determined and observed, long-term changes in ecosystems due to increasing carbon dioxide or temperature are more difficult to predict; free air carbon dioxide enrichment (FACE) studies suggest that elevated carbon dioxide may not translate to increased net ecosystem exchange, despite increases in photosynthesis (Norby et al., 2022; Walker et al., 2021).

Vegetation models greatly vary in their predicted responses to elevated atmospheric carbon dioxide, and in particular how carbon allocation responds (De Kauwe et al., 2014). The inability to properly simulate complex carbon allocation responses contributes to the divergent predictions within ecosystem models (Merganičová et al., 2019); it likely explains why FACE or atmospheric warming experiments do not observe consistent growth responses, despite predictable photosynthetic responses (Ainsworth & Long, 2005; Norby et al., 2010; Norby & Zak, 2011). This difficulty is not new and has been the focus

of much previous modeling, theoretical, and experimental studies (Franklin et al., 2012; Hartmann & Trumbore, 2016); however, this problem is not limited to vegetation models. In simulations of future Earth climate, ecosystem models—computer simulations to approximate the effect of the biosphere on biogeochemistry—are an significant source of uncertainty. Ecosystem models agree in simulations of historical observations but differ in their predictions under climate change scenarios, and the suspected cause is that models fail to simulate important processes or other phenomena critical to their long-term climate responses. Carbon allocation in plants is one such problem, but it raises an important question: how much detail is required to simulate accurate long-term climate responses?

While carbon allocation traditionally refers to differential growth responses (e.g., changes in root growth relative to shoot growth), research over the past two decades has recognized the importance of allocation to storage, rather than growth, as an important physiological adaptation in plants (Chapin et al., 1990; Körner, 2003). The immediate chemical products of photosynthesis are sugars, and these compounds are the principal carbon substrates for plant growth (growth requires nitrogen and other nutrients) (Hartmann & Trumbore, 2016). Starch is synthesized from these sugars and together, these nonstructural carbohydrates (NSCs) form an intermediary between photosynthesis (carbon supply) and metabolism (carbon demand); however, these pools of carbon decouple photosynthesis from metabolism, acting like a battery to supply metabolism when photosynthesis cannot or acting like a capacitor to dampen variations in photosynthesis from their effect on carbon supply available for metabolism (Dietze et al., 2014). While starch only serves as storage, sugars also serve as transport molecules and solutes. While vegetation models often simplify carbon allocation, many do not simulate NSC dynamics at all. Several models of NSC dynamics suitable for ecosystem models have been published in recent years (Cho et al., 2022; Hayat et al., 2017; Jones et al., 2020; Potkay et al., 2022; Schiestl-Aalto et al., 2015), and several have been coupled to ecosystem models (Cho et al., 2022; Jones et al., 2020). However, inserting models of NSC dynamics into ecosystem models conflicts with existing structures, requiring significant work to rebuild the existing model. Although all are rather simple, these models also contain numerous structural and parametric differences from each other, hindering the analysis of their essential similarities and differences.

While likely necessary for accurate simulation, the complexity of ecosystem models makes understanding their behavior harder and hides essential features. Ecosystem models may several dozen state variables, hundreds of parameters, and any number of variable external forcings. Furthermore, many different functions could plausibly describe many ecosystem processes, within the resolution of available data, and ecosystem models often lack explicit representation of certain processes. The ignorance of process details resulting from limited data has been discussed *ad nauseum* (Babst et al., 2021; Merganičová et al., 2019). Model development requires identifying the ways in which models fail to reproduce reality. Models are necessarily simplifications of reality, therefore lack of detail in itself is not a model failure. Instead, failure to reproduce important feedbacks and other dynamical responses leads to model failure in that predicted responses of quantities of interest do not mirror reality. Small changes in models can lead to large differences in modeled outcomes; in fact, model structure has been suggested as a culprit for the wide divergence in modeled outcomes to climate change. Despite this complexity, many small changes in models effectively produce the same results. In the former case, a change in model changed some critical

aspect of model structure, whereas changes in latter case did not. Thus, we consider how to identify and describe this essential structure and since its properties are critical for producing accurate simulation of ecosystem dynamics.

Rather than propose another ecosystem NSC model, we examine the structural differences present in existing models and analyze what features are necessary for NSC dynamics. To do so, we briefly describe a theoretical framework, based on the topological analysis of dynamical systems. We apply this framework to identify structural features which prevent dynamic NSC within existing ecosystem models without NSC. We argue that this structural features also describe differences in responses to environmental forcings and the hysteresis of those responses. We also illustrate how investigating the essential dynamics yields simplified models with certain properties. In particular, the interaction of an NSC reserve pool and a nitrogen reserve pool can generate transient growth responses to CO_2 enrichment. The spatial interaction of NSC and nitrogen reserves across plant organs can generate dynamic plant carbon allocation responses. While we focus on developing specific insights for nonstructural carbohydrates, our results serve as an example for a wider investigation of the essential dynamics in ecosystem models.

4.2 Theoretical Framework

In this work, we consider broadly, ecosystem, vegetation, and biogeochemical models. These names are partly synonymous but emphasize different processes and therefore goals. Modeling the Earth's climate depends on specifying the flux of various gases such as water vapor and carbon dioxide between the terrestrial biosphere and the atmosphere. At their core, climate models simulate atmospheric processes, requiring a "land surface model" to specify such fluxes as boundary condition to the climate model. The study of terrestrial ecosystem processes in its own right has led to models of ecological processes (population dynamics, community assemblage, etc.), biogeochemistry (nitrogen deposition, soil redox reactions), and vegetation. Plant physiological processes such as photosynthesis have an enormous impact on ecosystem biogeochemistry, and since biogeochemical fluxes are the focus for climate modeling, plant physiology forms a significant part of land surface models. Here, we discuss models of mass flows or biogeochemical reactions. While we focus on plant physiology, much of what we say will generalize to models of ecological processes. In other words, the model specifies a set of mass flows or reactions, visualized as a set of boxes (mass pools / chemical species) and arrows (mass flows / reactions) (Fig. 4.1a). Even if not so strictly speaking, many biogeochemical reactions are mathematically chemical reactions (and often are large systems of reactions) and may be treated using techniques developed to analyze chemical reaction systems (Angeli, 2009). For instance, photosynthesis is clearly like a chemical reaction, converting atmospheric CO_2 to carbohydrates, because it is a system of biochemical reactions; however, processes such as the movement of water from deep soil horizons to shallow ones are reaction-like in which deep and shallow soil water acts like a reactant and product in a reaction moving water. As reactions conserve the total number of elements, only transforming chemical species, movement conserves the total amount of chemical species.

Ecosystem models do not specify possible reactions or processes (Fig. 4.1a) but also specify the rates (for arrows) at which they occur and the quantity of each pool (boxes), and how these quantities change

in time. This change in time is specified using a system of differential equations $\dot{x} = V(t, x)$ or as iterated maps $x_{n+1} = f(t_n, x_n)$ where x is the state, the quantities for each box. The latter is somewhat more common as numerical integration of differential equations converts the former into the latter; however, we will employ the former for conceptual simplicity as the choice makes little difference for many practical concerns. The rate of change in pool substrate, denoted $\dot{x}_i$ for substrate i, depends on a linear combination of reaction or flow rates, denoted r_j for reaction j, and may be written using a stoichiometric matrix Γ_{ij} such that $\dot{x}_i = \sum_j \Gamma_{ij} r_j$ (Angeli, 2009). Much of chemical reaction theory analyzes how stoichiometric relationships contained in Γ constrain the possible outcomes. Ecosystem models specify what rates r are as a function of the environment η, which may vary in time, and the current state so that $\dot{x} = \Gamma r(x, \eta)$. Following standard terminology in Chemistry, we call the nature of this dependence, the reaction's rate kinetics. Fig. 4.1b shows a hypothetical growth rate kinetics for nonstructural carbohydrates and nonstructural amino acids in Fig. 4.1a.

To illustrate by an explicit example, suppose in Fig. 4.1a we label each rate as photosynthesis A, respiration R, growth G, nitrogen uptake U, and exudation/export E. Let x, y, and z denote the pool size (in mass) of each box. The box and arrow diagram is equivalent to the following equations.

$$\dot{x} = G - L \tag{4.1}$$
$$\dot{y} = A - R - G - E \tag{4.2}$$
$$\dot{z} = U - \gamma G \tag{4.3}$$

Here γ converts G measured in units carbon mass into units nitrogen mass; in general, linear combinations of reaction rates include stoichiometric numbers (when tracking moles) and/or molar masses (when tracking mass). Since carbon is the focus, we normalize all quantities relative to carbon mass for simplicity of exposition. Models may have the same stoichiometric relationships but differ in kinetics. For instance, growth could follow mass action-like kinetics $G = G_0 yz$ or a saturating function $G = G_0 yz/(1 + k_1 y + k_2 z)$. A convenient simplification is to lump together processes with the same sign in (4.1)-(4.3) into a box's supply rate (positive sign) and demand rate (negative sign); Fig. 4.1c shows hypothetical rate kinetics for nonstructural carbohydrate supply and demand. Given these specifications, the goal of the model is to determine the long-term responses to climatic changes, the responses observed in experiments, and the processes that drive those responses. To this end, the model behavior is typically examined by simulation, comparing integral curves $x = \theta(t)$ (time-series) under different situations (Fig. 4.2a-c, upper row). Of particular interest is the long-term or asymptotic behavior of the model: is it the case that states tend toward to the same constant values (Fig. 4.2 left column), oscillate periodically (Fig. 4.2 mid column), or tend to different constant values (Fig. 4.2 right column)?

A streamplot (or phase portrait) offers an alternative to simulations in which one visualizes the dynamics like the flow of a stream (Fig. 4.1d; Fig. 4.2d-f, lower row); each column in Fig. 4.2 illustrates the same system. Points correspond to all possible states—plant mass and nonstructural carbohydrate concentration, for instance. Models specify how states change in time, assigning a vector V at each point x which indicates the speed and direction of flow. We can write flow as a function $\psi(t, x)$ sending point x to

another after time t. Shown in this manner, the asymptotic behavior—that is the set of points (or dynamical behavior) to which the model converges, $\lim_{t\to\infty} \psi(t, x)$—of the model is easy to see. Although not obvious from a single simulation, the streamplot clarifies whether a simulation tends to the same point, meaning a single value of nonstructural carbohydrates and amino acids (Fig. 4.2 left column), to a stable limit cycle, meaning both variables oscillate indefinitely in the absence of environmental oscillation (Fig. 4.2 middle column), or to one of two stable points, meaning each variable converges to a high or low value depending on its initial condition (Fig. 4.2 right column). Models often have states with far more than one or two variables, meaning a 2D streamplot cannot cleanly show the dynamical behavior; however, the intuition gained at low dimension leads to analytic techniques applicable in higher dimensions.

Many details of models do not affect the qualitative asymptotic behavior of the flow, because local variations in the speed and direction of flow do not create changes in the overall behavior. Unlike box and arrow diagram, kinetics plot, or equations (Fig. 4.1a-b; Eq 4.2), this behavior is easier to see in streamplots. When models generate streamplots that "look the same", they have the same asymptotic behavior. Formally, "looking the same" becomes topological conjugacy/equivalence. In brief, if the orbits of one flow are mapped to orbits of another flow by a homeomorphism then flows are topologically equivalent. If time-parameterization of the orbits is also preserved, then the flows are said to be topologically conjugate (Fig. 4.4 upper row). Graphically, topological equivalence means the flowlines of one model can be deformed into another without tearing, splitting, gluing, or merging them (stronger versions require the preservation of some degree of smoothness). It also implies a correspondence between the states in the two models (Fig. 4.4 lower row). This correspondence provides a precise notion of "wrong but useful" model. A useful model must be at least topologically equivalent to the true dynamics. Thus, we can compare the streamplots of models and hypothesize what the correct streamplot looks like, and this process corresponds to determining the conjugacy or equivalence class of the dynamics.

Omitting many subtleties (consult Guckenheimer and Holmes, 1983 or Wiggins, 1996 for details), the idea behind geometric methods is that the set of fixed points (or singular points) where $V(x, \eta) = 0$ and the local behavior around these points determines all interesting behavior, that is its conjugacy or equivalence class. Fixed points correspond to configurations in which supply and demand are balanced (also called steady states). The intersection of the supply and demand curves (Fig. 4.1c) corresponds to a fixed point in the streamplot (Fig. 4.1d). Derivatives of the vector field at a fixed point provide all qualitative information (and often quantitatively good approximations) for the behavior in a neighborhood around the point. For instance, eigenvalues and corresponding eigenvectors of the Jacobian matrix $J = dV_{x_0}$ at a fixed point x_0 provides information about the local flow around the fixed point. The flow contracts along the eigenvector for eigenvalues with negative real parts and expands for positive real parts (Fig. 4.3). Zero (or near zero) real parts indicate that contraction or expansion is much slower along one set of directions than others; this set of slow direction is called a center manifold (or approximate center manifold) (Fig. 4.3). Fig. 4.3 illustrates the case of stable fixed point (both eigenvalues are negative), saddle fixed point (one negative and positive eigenvalue), and a stable center manifold with a stable subspace (one zero eigenvalue and one negative one). While quantitatively the Jacobian is a local approximation (the approximation improves as one approaches the fixed point), the qualitative behavior remains the same even far away

from the fixed point until its "basin of influence" intersects of another fixed point. While more complex behavior is possible, describing the local behavior around each fixed point effectively describes the global behavior.

The fixed points and derivatives of a model provide tools for identifying essential model structure because these features describe the overall behavior, and because the number of fixed points and the signs of their associated eigenvalues are insensitive to changes in the model which do not change the topological equivalence or conjugacy class (even as the positions and magnitudes change). This insensitivity is called structural stability. Analyzing the stable, unstable, and center subspaces of a fixed point is also useful because it provides information about how certain model components interact with others. It is typical that eigenvalues span several orders of magnitude indicating that certain subsystems contract or expand from a fixed point much faster than others. Thus, if short term responses are of interest, the slow subsystems may be held constant to eliminate them from consideration. If long term responses are of interest, the fast subsystems may be replaced with their fixed points (or other asymptotic behavior). In this manner, we isolate a certain subsystem to examine it, effectively treating other parts of the model as an external environment.

4.2.1 Time-varying external environments

A subtlety we must address is that Fig. 4.2 shows how the system evolves in a constant environment (for instance, in a constant light environment). As the environment changes, the flowlines themselves change through time. Thus, the environment is not a set of parameters, but a set of time-varying functions $\eta = g(t)$ (for instance, temperature varies in some specified way), and the global behavior of the model is conditional on how η varies in time; that is $\dot{x} = V(t, x)$. In other words, we must treat the external environment as part of the system, and this is especially true when studying an isolated subsystem where other subsystems are treated as an environment. To separate the model's intrinsic structure from the extrinsic forcing of the environment, we need to identify how the model's long-term behavior follows from the temporal variation of the environment. For example, periodic oscillation is an constant environment (Fig. 4.2 middle column) is distinct from periodic behavior generated by a periodic environment (time-dependent field in Fig. 4.5).

We can treat the time-varying model as a streamplot by adding time t as an additional state variable with $\dot{t} = 1$ (time-dependent field in Fig. 4.5)[1]. Note that the streamlines in Fig. 4.5 differ only by starting value, and all trajectories experience the same environmental forcing (e.g., temperature varies in the same manner). Because $\dot{t} = 1$, this time-dependent vector field has no true fixed points so analyzing the local behavior of fixed points does not immediately apply, but the flowlines still converge inward to an attractor (black curve in Fig. 4.5), but this attractor is not necessarily the fixed point through time. Instead We call this curve (or surface) defined by $V(t, x) = 0$ the nullcline (black dashed curve in Fig. 4.5); this nullcline still represents balance point between supply and demand, but the system only observed at this balance point when at steady state. Instead, the system exhibits transient hysteresis, with a difference

[1] Time-independent models are symmetric under time-translation; but time-dependent models are not.

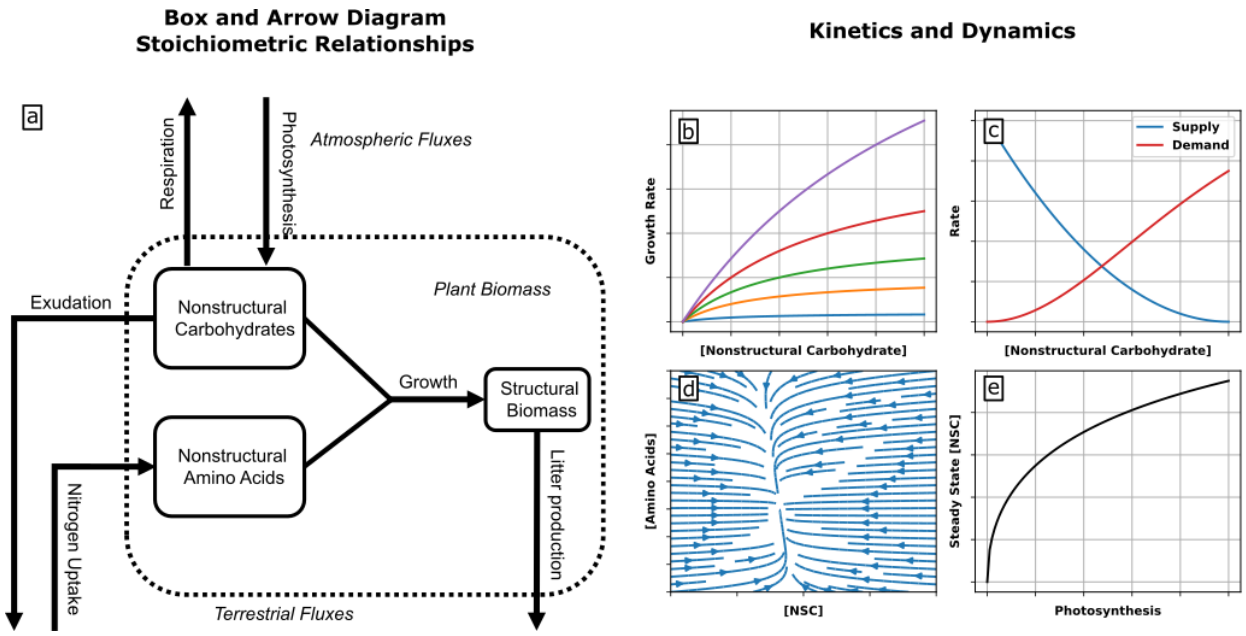

Figure 4.1: Visual summary of model framework. Like a set of chemical reactions, the set of mass pools and flows form a graph (a) along with their kinetics—how flow rates depend on reactants—completes a process model; example of growth rate kinetics by nonstructural carbohydrates and nonstructural amino acids (different colored curves) (b). Rather individual processes, one can examine dynamical properties such as the intersection of supply (input rate) and demand (output rate) by nonstructural carbohydrates determines the fixed points (c), how feedbacks generate a streamplot or phase portrait (d), or how changes in external parameters (like the environment / photosynthesis) change fixed points (e).

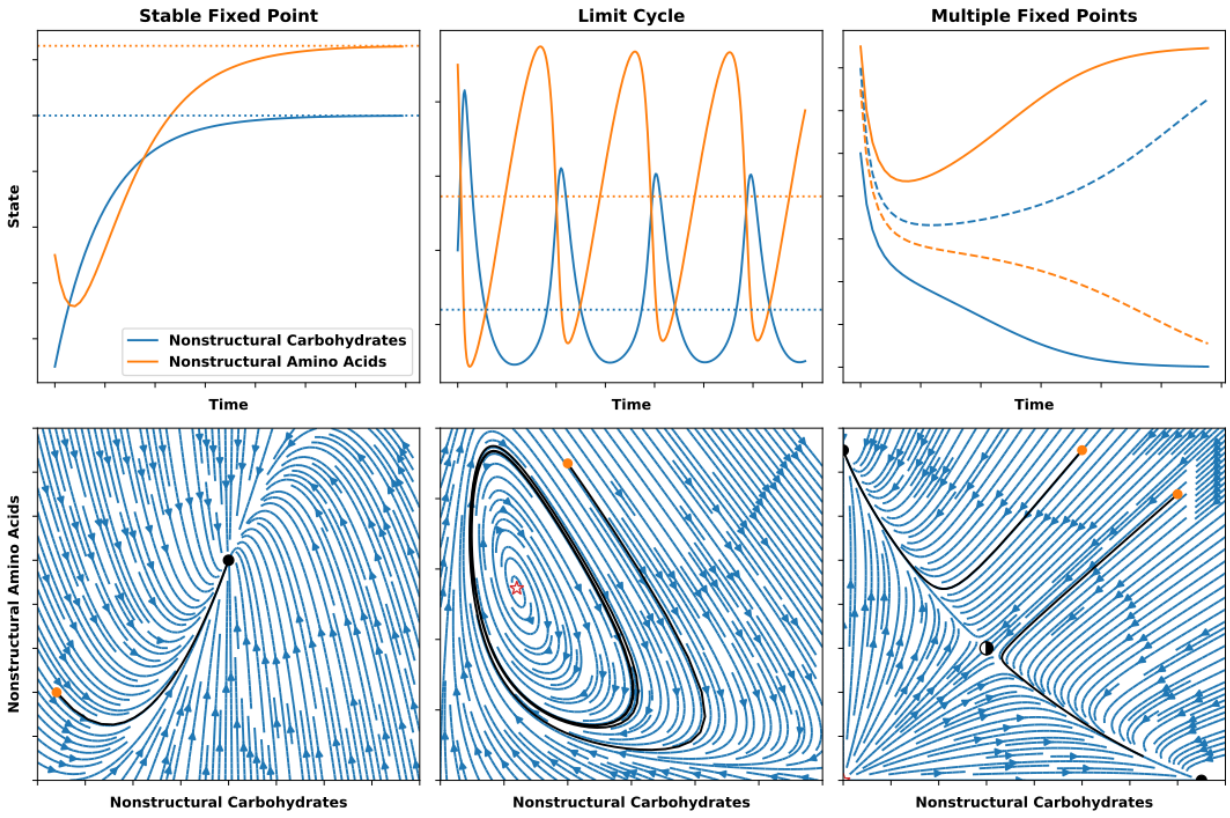

Figure 4.2: Models visualized by time-series of specific simulation beginning at a given initial condition and with constant forcing (top row) versus by streamplot (bottom row). How model feedbacks create certain long-run behaviors are easier to detect in geometric viewpoint. Models shown have a single stable fixed point (left column); a unstable fixed point and limit cycle (middle column); and four fixed points, two stable, one unstable, and one stable point (right column). The black trajectory is shown in the top row. Fixed points shown as black circles when stable, red-bordered stars when unstable, and half-filled circles when saddle points. Initial values shown in orange.

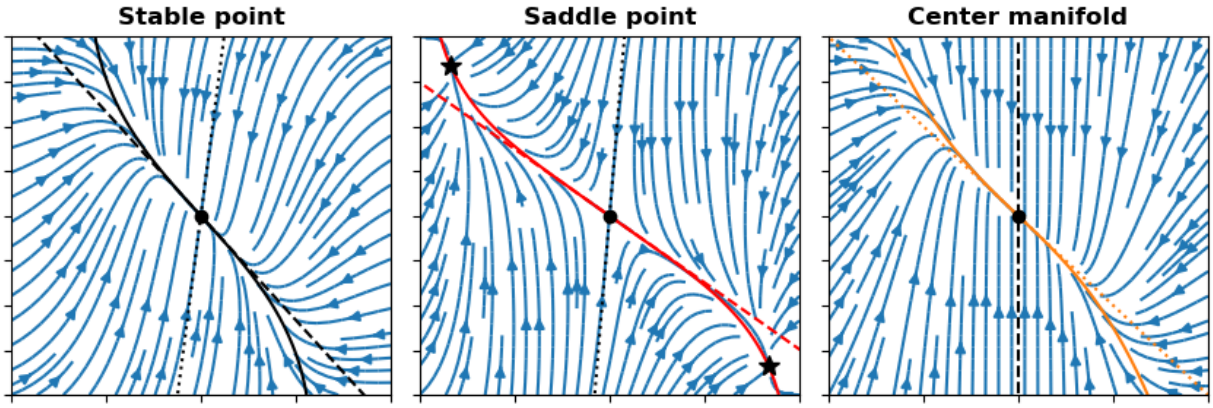

Figure 4.3: Eigendecomposition of the Jacobian matrix at a fixed point (black point) describes qualitative behavior around the point. Subspaces for each eigenvector drawn as dashed and dotted line, colored black when stable/contracting (real part of eigenvalue < zero), red when unstable/expanding (real part > zero), and orange for a center manifold (real part = zero). These subspaces are tangent to stable, unstable, and center manifolds (solid line with same color scheme). A fixed point is stable (resp. unstable) when all eigenvalues have negative real part (resp. positive); saddle points have both stable and unstable eigenvalues. When eigenvalues are zero (i.e., a nonhyperbolic point), the flow quickly reduces to the corresponding center manifold; eigenvalues close to zero relative to others correspond to an approximate center manifold. Note that the unstable manifold of the fixed point (mid) passes through two stable fixed points (black stars) and is a stable manifold for those fixed points. Stability on center manifolds requires higher order terms to determine (stable center manifold shown here).

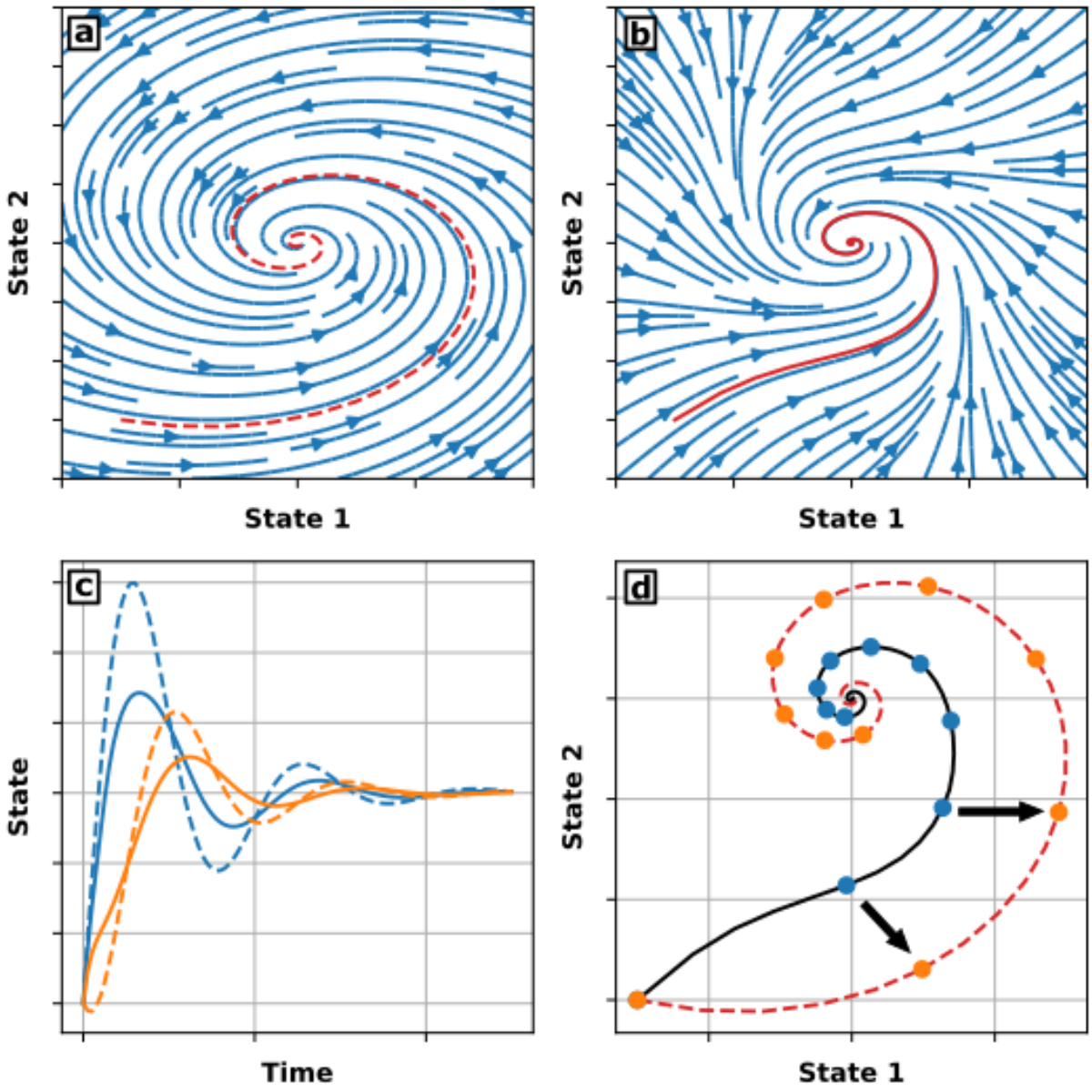

Figure 4.4: Illustration of topological conjugacy (via the Hartman Grobman theorem). The model depicted in (a) is conjugate to the model in (b); comparing a trajectory of model (a) (dashed) to model (b) (solid) shows the qualitatively similar behavior (c). Note trajectories are traversed at the rate in time (d), dots show equally spaced moments in time (arrows indicate correspondence).

between the fixed point in each environment and the longterm behavior. Under certain circumstances, the time-dependent vector field may be analyzed directly, but a more fruitful approach is to calculate time-independent vector fields with true fixed points that correspond to features of the time-dependent vector field. We discuss two different methods for reducing time-dependent dynamics to time-independent features: time-averaging and time-slicing (Fig. 4.5).

For time-averaging, average the vectors for point x (e.g., for each NSC; horizontal slices in Fig. 4.5), then analyze the resulting time-averaged vector field. The asymptotic behavior, like stability, matches the time-dependent vector field. This method is often invoked without explicit derivation and is also employed in parameter estimation (Jones et al., 2020). Time-averaging describes why models may not be stable at all times but are cumulatively stable over time (i.e., stable on average), but time-averaging requires certain assumptions about how the environment varies, and it is only when system responds sufficiently slowly to the environment that we may replace time-varying environmental parameters by constant time-averages and that fixed points of the time-averaged vector field correspond to time-averages (via the averaging theorem).

Alternately, consider the model within a time slice in Fig. 4.5 (vertical slice). Each time slice corresponds to a time-independent vector field, in which the environment is fixed and the fixed point of this vector field is the nullcline. As the environment varies, the nullcline moves and instead of analyzing the time-dependence directly, one can analyze how varying the environment as a constant parameter affects the vector field (inset right panel streamplot in Fig. 4.5). In this case, all time slices in Fig. 4.5 contain a stable fixed point (shown by the nullcline), because this model contains a single fixed point in all environments (inset shows this for light environments). The time-variation changes the environment, which in turn changes the location and strength of the fixed point, but not its overall existence or stability. The behavior of the model in any time-slice "looks the same" as—it is topologically conjugate to—the model in any other time-slice, because it is conjugate for each constant environment. The bifurcation diagram in Fig. 4.5 (inset right panel) shows this split with horizontal motion representing extrinsic change due to the environment and vertical flowlines representing intrinsic response. As intuition, this technique is like a thought experiment in which one holds the environment constant to eliminate external sources of variation to study the system's intrinsic responses. Given a plant's physiological response in any constant environment, the response in a time-varying environment may be calculated, but the former describes the intrinsic response. The system's response to the time-varying environment may be understood as the combination of a change in the fixed points and how fast the system converges to its fixed points.

As shown in Fig. 4.6, the distance between the attractor and the nullcline (the degree of hysteresis) depends on how fast the system contracts to (or expands away from) its fixed points relative to how fast the nullcline changes. The eigenvalues of J (for a given environment) measure the rate of contraction (or expansion) along the corresponding the eigenvectors (Fig. 4.3). We distinguish three cases: slow relaxation (Fig. 4.6 left), fast relaxation (Fig. 4.6 right), and resonance (Fig. 4.6 middle). At one extreme, the environment changes faster than system responds (Fig. 4.6 left) so the attractor tends toward an constant average value, and thus responds little to the environment. At the other extreme, the system responds much faster than the environment changes (Fig. 4.6 right) so the attractor is close to the nullcline. The

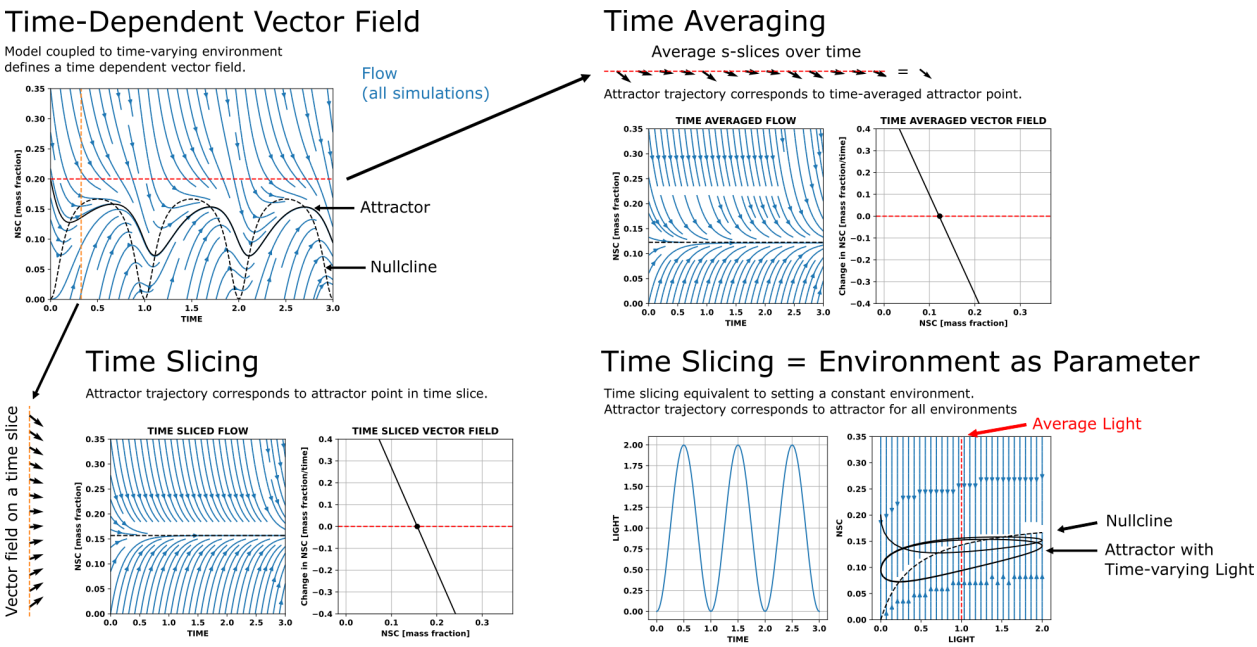

Figure 4.5: A time-dependent vector field cannot have true fixed points, having only attractors instead (solid black curve) which is not the same as its nullcline, the steady state fixed point through time (dashed black curve). Time-averaging a time-dependent vector field with an attractor (averaging by horizontal slices) reduces it to a time-independent one that can have true fixed points. However, each time-slice (vertical slices) corresponds a time-independent vector field with the environment held constant; if this time-independent vector field has fixed points for all environments (a nullcline exists for all environments), then the time-dependent vector field will have the same number of attractors; it will be also have fixed points when time-averaged. Thus, studying how changing the environment time-dependent vector field may be analyzed as a time-independent one with transient hysteresis resulting from the changing environment. The distance between the attractor (black curve) and the nullcline (dashed black curve) depends on the convergence rate/feedback strength.

hysteresis is small when relaxation is faster or slower than the fixed point moves (fast or slow relaxation), as the observed NSC value is well-described by a function of the environment. For fast relaxation, NSC remains close to a moving fixed point (nullcline) while for slow relaxation, NSC remains close to an average defined by the average environment (by the averaging theorem in Guckenheimer and Holmes, 1983); deviations from this average are small even if the fixed point moves, because NSC is almost constant at shorter time scales. In between these extremes, the system is dominated by neither and the hysteresis is maximal in this sense.

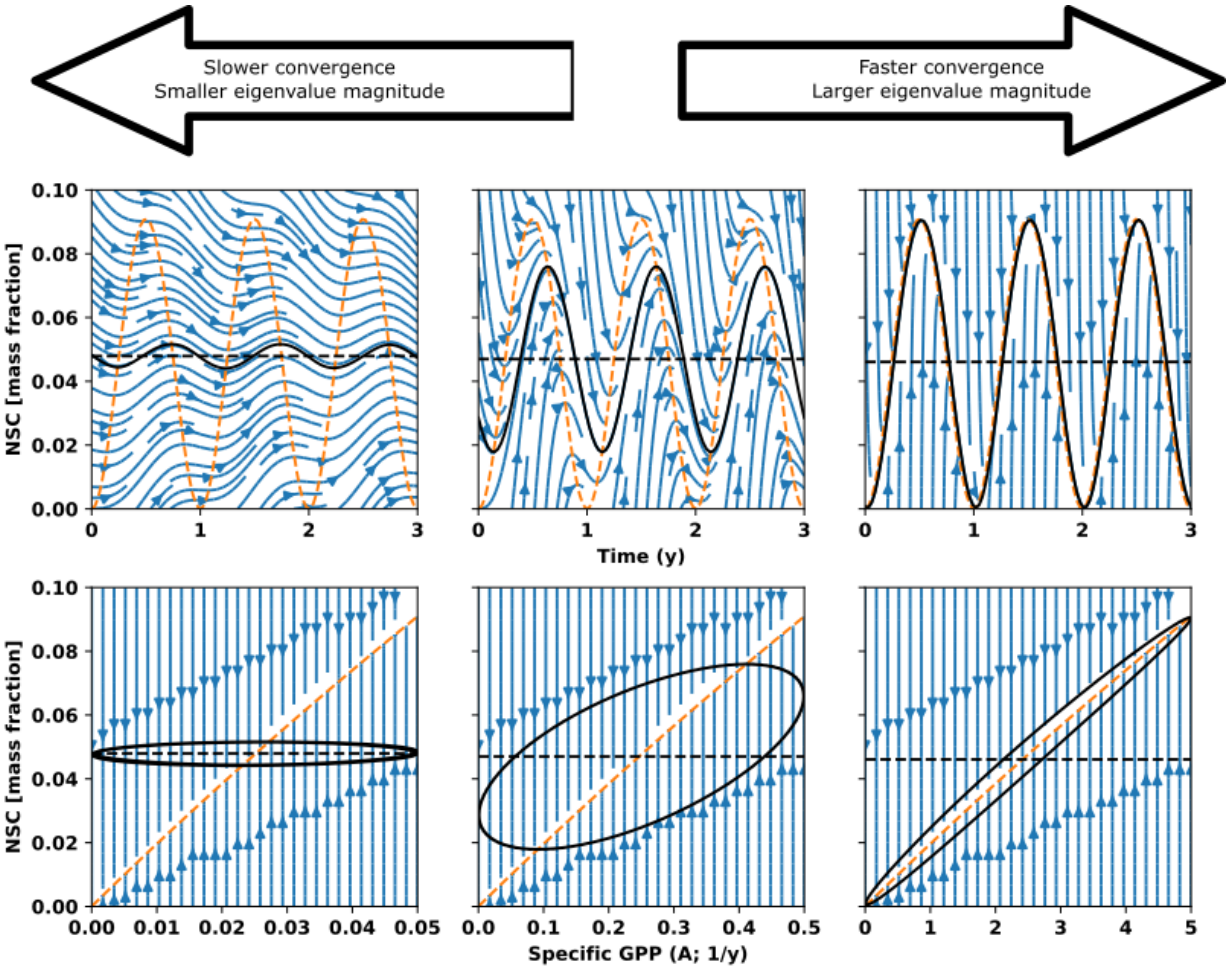

Figure 4.6: Comparison of systems with the steady state (NSC nullcline) through time, but different relaxation times. Going left to right, the relaxation time decreases by 10× for each panel (the system's convergence speeds up by 10×; the eigenvalue's modulus increases by 10×). When the system responds slower than the environment changes (left column), the attractor (black solid) remains near an average value (black dashed), while at the opposite extreme, the attractor is almost the same as the nullcline (orange dashed). In this example, specific gross primary production is typically greater in ecosystems with less biomass, thus the convergence rate likely varies with biomass.

4.3 Results

To turn to the modeling of nonstructural carbohydrate dynamics, we identify the essential structure of nonstructural carbohydrate dynamics in ecosystem models by determining the number and location of fixed points, their stability, and how they change with the environment. As suggested by Fig. 4.1, one can begin with a set of processes and pools (box and arrow diagram; Fig. 4.1a), posit kinetics (Fig. 4.1b), then study the resulting vector field (Fig. 4.1d) and fixed points (Fig. 4.1c,e). Alternatively, one begins by positing certain dynamics such as a single stable fixed point (Fig. 4.1e) and representative vector fields (Fig. 4.1d), then determines what supply and demand or kinetics must look like (Fig. 4.1b,c) or if additional processes or pools are needed to generate the hypothesized dynamics (Fig. 4.1a). The interplay the top-down and bottom-up approaches with observational facts gives insight into the necessary structure for a model to reproduce the essential physical phenomena. Using these ideas, we can identify what box and diagram figures must look like for nonstructural carbohydrate dynamics, what restrictions are created by kinetics assumptions, and how models differ in dynamics rather than variation in the functional form of kinetics or parameterizations.

4.3.1 Equating net primary production with growth prevents dynamic NSC

All models of nonstructural carbohydrate dynamics begin with a mass balance equation (4.4)(e.g., Fig. 4.1a); compare with (4.1)-(4.3). The change in nonstructural carbohydrates y is the net imbalance in photosynthesis A (or gross primary productivity; GPP), plant respiration R, and growth G (4.4). We consider these three processes for simplicity without loss of generality as additional processes do not modify our arguments. We assume units mass carbon per land area per time.

$$\dot{y} = \underbrace{A - R}_{\text{NPP}} - G \tag{4.4}$$

The direct barrier to dynamic nonstructural carbohydrates within many ecosystem models is that many such models equate net primary productivity (NPP) with growth, that is $A - R = G$; supply is assumed to always equal demand. In terms of mass balance, the growth rate G cannot represent changes in plant carbon mass. The plant's mass increases when carbon is absorbed from its environment by photosynthesis and lost by respiration or tissue loss (litter, root turnover). Instead, growth is the conversion of nonstructural carbohydrates into other forms of biomass. The assumption $A - R = G$ implies nonstructural carbohydrates are constant and has several additional problems, such as implying growth is negative whenever $\text{NPP} < 0$. Relaxing this assumption allows for dynamic nonstructural carbohydrates but creates a new problem. The growth rate G can now independent of photosynthesis and respiration, and must be determined by some other rule. This rule must relate A, R, and G such that the time-average of $A-R-G$ goes to zero over time for y to remain bounded. That is, $\bar{A}-\bar{R}-\bar{G} = 0$, where $\bar{G} = \lim_{t\to\infty} 1/t \int_0^t G dt$ is the time-averaged growth rate (alternatively, using the Fourier transform $\hat{G}$ of G, $\bar{G} = \hat{G}(0)$). Otherwise, nonstructural carbohydrates will accumulate to infinity if $\bar{A} - \bar{R} - \bar{G} > 0$ and will deplete to zero

if $\bar{A} - \bar{R} - \bar{G} < 0$. In summary, the inclusion of dynamic nonstructural carbohydrates within ecosystem models requires solving the conceptual problem of how to ensure that photosynthesis, respiration, and growth become tightly coupled at long time scales while remaining independent of each other at short time scales.

The solution is guaranteeing that equation (4.4) possesses a stable fixed point, in all fixed environments (time-slicing). Note that at any fixed point, $A - R = G$ holds; hence it is equivalent to assuming this steady state holds exactly at all times. These processes must possess stabilizing feedbacks—their rates must depend on the amount of nonstructural carbohydrates present. To illustrate with an example, suppose $R = R_0 y$ and $G = G_0 y$, where R_0, G_0 may depend on any number of environmental variables or other parameters. Inserting into equation (4.4) yields equation (4.5) which has a stable steady state: $y^* = A/(R_0 + G_0)$.

$$\dot{y} = A - R_0 y - G_0 y \tag{4.5}$$

When A, R_0, and G_0 are constant, nonstructural carbohydrates will tend toward y^*. When $y > y^*$, growth and respiration rates will exceed photosynthesis decreasing nonstructural carbohydrates. When $y < y^*$, photosynthesis will exceed growth and respiration rates increasing nonstructural carbohydrates. In either case, as the amount of nonstructural carbohydrates changes, the rate of growth and respiration approaches the amount of photosynthesis. This feedback between nonstructural carbohydrates and their supply and demand means that $\bar{A} - \bar{R} - \bar{G}$ tends to zero, and because this outcome happens for values of A, R_0, and G_0, it happens regardless of environmental forcing and other details of photosynthesis, respiration, and growth. Nonstructural carbohydrates will only ever deplete completely if $A = 0$, meaning the model cannot be driven into negative nonstructural carbohydrates. This equation allows for dynamic nonstructural carbohydrates and for respiration and growth rates to vary independently of photosynthesis[2] while coupling all three quantities at long time scales, a feature that not all models reproduce. Note that assuming respiration and growth rates depend on the amount of available nonstructural carbohydrates has some experimental support (Collins et al., 2021; Högberg et al., 2001; Sevanto et al., 2014). What this argument shows is that nonstructural carbohydrates can coordinate nonstructural carbohydrate supply and demand if a feedback (or kinetics) exists. Without this coordination, imbalances in the average difference in supply and demand lead to aphysical behavior, such as depletion beyond zero or accumulation to infinity.

4.3.2 The need for stabilizing feedbacks

With healthy scientific skepticism, one might question the necessity of this feedback. Perhaps, the average carbon balance could be regulated via some other means. Regardless of the details, the regulation must involve some feedback with nonstructural carbohydrates. To see why, consider Fig. 4.7 which compares the dynamics of equation 4.4 with and without stabilizing feedback. Both version are time-average stable (average $\dot{y} \to 0$), but only stabilizing feedback creates a structurally stable attract. With the stabilizing feedback, each time-slice now has stable fixed point whereas without, no fixed point exists to draw tra-

[2] At least in terms of carbon balance. Other couplings are not precluded.

jectories together. Having this fixed point leads to an average balance between supply and demand that adjusts to changing environments (Fig. 4.7). Without it, note that not only to trajectories never come together (Fig. 4.7 right), many trajectories cross zero. Without any feedback, nonstructural carbohydrates easily drift up and down as their amount has no effect on their accumulation or depletion.

More formally, we argue the upward and downward motion of model's flow in nonstructural carbohydrate (Fig. 4.7 right) must cancel out on average ($\dot{y} = 0$ on average) because if otherwise, the NSC mass y becomes unstable, tending to infinity. While A, R, and G can be chosen so that this time-average holds, almost any change in them will fail to keep y balanced[3], causing NSC mass to either accumulate or deplete over time. Furthermore, as Fig. 4.7 illustrates, even if model parameters are tuned to ensure stability for a certain set of observed environments (e.g., the historical climate record), the balance would be lost under almost any perturbation in the environment—any variation in the flowlines—unless the model contains feedbacks ensuring balance. The model contains no structure to reestablish balance when perturbed, and no structure to modify changes in NSC when NSC is low (note trajectories sufficiently close to $y = 0$ become negative). Without stabilizing feedbacks, future NSC remains sensitive to the initial amount of NSC; differences in the initial amount translate to large differences. The structural stability of the stable fixed point eliminates these undesirable effects (Fig. 4.7). In addition to its properties for modeling, the stable fixed point implies that nonstructural carbohydrates recover to their original value when the environment (and thus photosynthesis, respiration, and growth) returns to its original conditions, whereas without feedback, any depletion in nonstructural carbohydrates requires a period of additional surplus from the environment to correct because the supply and demand do not adjust to refill nonstructural carbohydrates.

These reasons are why most models do have some feedback, even if not explicitly stated or studied. For instance, the Earth Energy Exascale Earth System Land Model (ELM v1.0 Burrows et al., 2020), which is based on the Community Land Model (CLM v4.5; Oleson et al., 2013) contains a plant nonstructural carbon storage pool (CS_{xs} in Oleson et al., 2013) and its development reflects the need for structural stability. Note this pool is a deficit pool, tracking a carbon "debt" incurred when NPP is negative but is repaid over a fixed timescale when NPP is positive. While the negative formulation seems artificial, if the model contains the correct essential dynamics, then a transformation from the negative debt to positive mass will exist[4]. The authors briefly state that the reason for a negative deficit pool is "to eliminate the need to know in advance what the total maintenance respiration will be" (Oleson et al., 2013). They add that deficit adjusts allocation "until the supply of carbon into the pool balances the demand for carbon leaving the pool in a quasi-steady state" (Oleson et al., 2013). In constructing ELM, the authors confronted the need for structural stability. Analyzing their scheme within the theoretical framework here identifies the source of stability and problems with this scheme.

We plot the dynamics of this scheme in Fig. 4.8. Let y (gC m^2) denote this debt, then storage is described by $\dot{y} = \min(A - R_m, -12y)$ where only maintenance respiration is considered R_m so that when $A - R_m < 0$, debt accumulates. When $A - R_m > 0$, some carbon is allocated to pay back the

[3]Using their Fourier transforms, we must have $\hat{A}(0) - \hat{R}(0) - \hat{G}(0) = 0$, which is a measure zero subset of $\mathbb{R}^3$.

[4]For example, one can add a constant, representing an initial amount of nonstructural carbohydrates, to convert the pool to a positive so long as the pool is never depleted.

debt, up to a maximum storage allocation rate proportional to the size of the debt (i.e., $-12y$). Although not visible in Fig. 4.8, growth (and associated growth respiration) only occurs when $A - R_m > -12y$, so changes in $A - R_m$ can cause delayed changes in growth rates. Whenever $A - R_m < 0$, y decreases without bound and the system is unstable, while the system is structurally stable when $A - R_m > 0$. In Fig. 4.8, NPP oscillates from positive to negative values depending on the season (Fig. 4.8a) so the system oscillates between stable and unstable (time-slicing) but if on average over time $\bar{A} - \bar{R}_m > 0$ (Fig. 4.8b), stable but not structurally stable $\bar{A} - \bar{R}_m = 0$ (Fig. 4.8c), and unstable when $\bar{A} - \bar{R}_m < 0$ (Fig. 4.8d). Changes in the environment affecting photosynthesis or respiration shift the average, but with structural stability the system adjusts to a new attractor "quasi-steady state"; it is not allowing deficits but the fact that the deficit is repaid proportionally to its size (causing in the flowlines to converge).

This scheme fails to be structurally stable in all time-slices, because plant NPP can be, and regularly is, negative. Various experiments induce (or observe naturally induced) negative NPP by shading (Weber et al., 2019; Weber et al., 2018; Wiley et al., 2019), drought (Anderegg & Anderegg, 2013; Schönbeck et al., 2018; Sevanto et al., 2014), or both (Sapés et al., 2020). Experiments show that the above scheme fails to reproduce the correct fixed point structure: namely, $y^* = 0$ when $A = 0$. In particular, Weber et al., 2018 observe decreases in NSC concentrations $s \sim e^{-kt}$ for time t, consistent with Equation (4.5) when assuming $A = 0$ and linearizing about the fixed point $y^* = 0$ (and converting to mass fraction). Furthermore, Sevanto et al., 2014 (see their Fig. 5) observed that in leaf respiration declines to zero as leaf NSC declines to zero, roughly as $\frac{R}{m} \sim s/(s + K_m)$ or as $\frac{R}{m}\ s$ depending on shading (where m is total tissue mass). In conclusion, when $A = 0$, the fixed point must zero; but in ELM (v1.0), a carbon deficit builds without bound. These experiments suggest the fixed point tends smoothly to zero, while the model only has fixed points at zero and negative infinity, depending on $A - R_m$. No continuous transformation of this scheme converts two boundary fixed points into a smooth curve of fixed points, and any continuous transformation would conflict with its definition of the deficit in terms of a carbon budget. Thus, this scheme cannot produce smooth changes in steady state in a constant environment and fundamentally differs from observations.

In summary, the supply and demand in nonstructural carbohydrates must have feedbacks (AKA kinetics) which generate at least one stable fixed point to create the dynamic balancing that coordinates supply and demand over the long-term but allows for supply and demand to differ over the short-term. Without this dynamic balancing, models are likely to generate trajectories which correspond to plants building implausibly large carbon reserves or self-starving before reducing growth rates. To paraphrase Oleson et al., 2013, the structural stability of the stable fixed point eliminates the need to know the future environment in advance in order to coordinate carbon supply and demand. It also explains why even though observed nonstructural carbohydrate dynamics are quite dynamic, complete depletion of nonstructural carbohydrates is rare (Körner, 2003), and observations are consistent with this dynamic viewpoint. This observation provides a mathematical refinement of the argument that plants are likely to have active regulation in storage (Sala et al., 2012; Wiley & Helliker, 2012); without regulation, the model can generate nonsensical results. The nature of the feedback therefore corresponds to a description of nonstructural carbohydrate regulation.

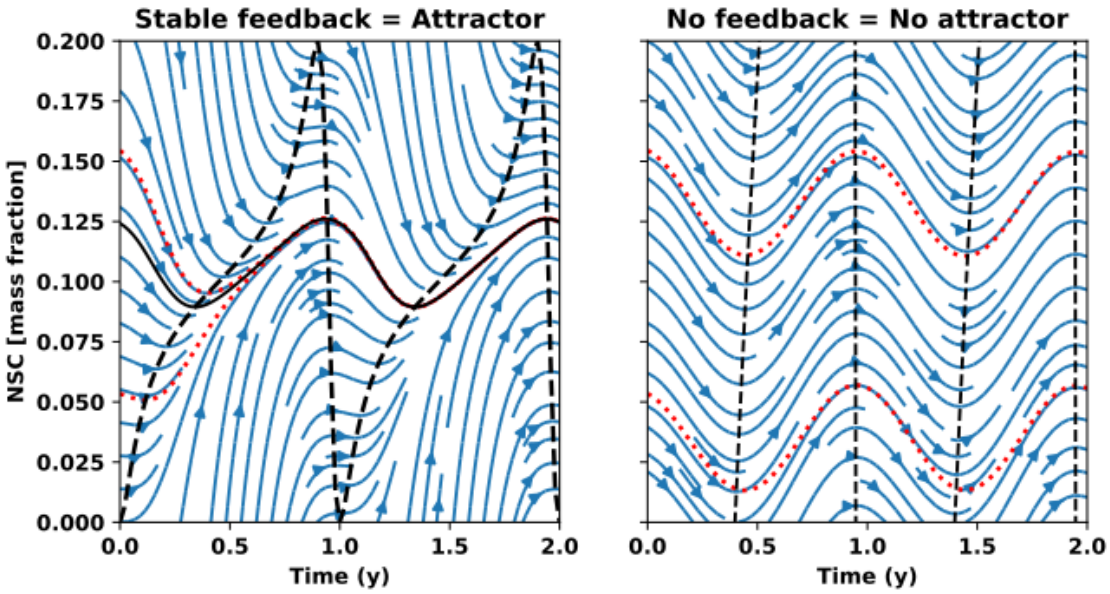

Figure 4.7: Comparison of streamplot of NSC dynamics with (left) and without (right) stabilizing feedback. The presence of a nullcline (black dashed) at all times leads to an attractor (black) toward which different simulations evolve (red dotted). Without these features, no attractor exists. Note very weak feedbacks resemble no feedback.

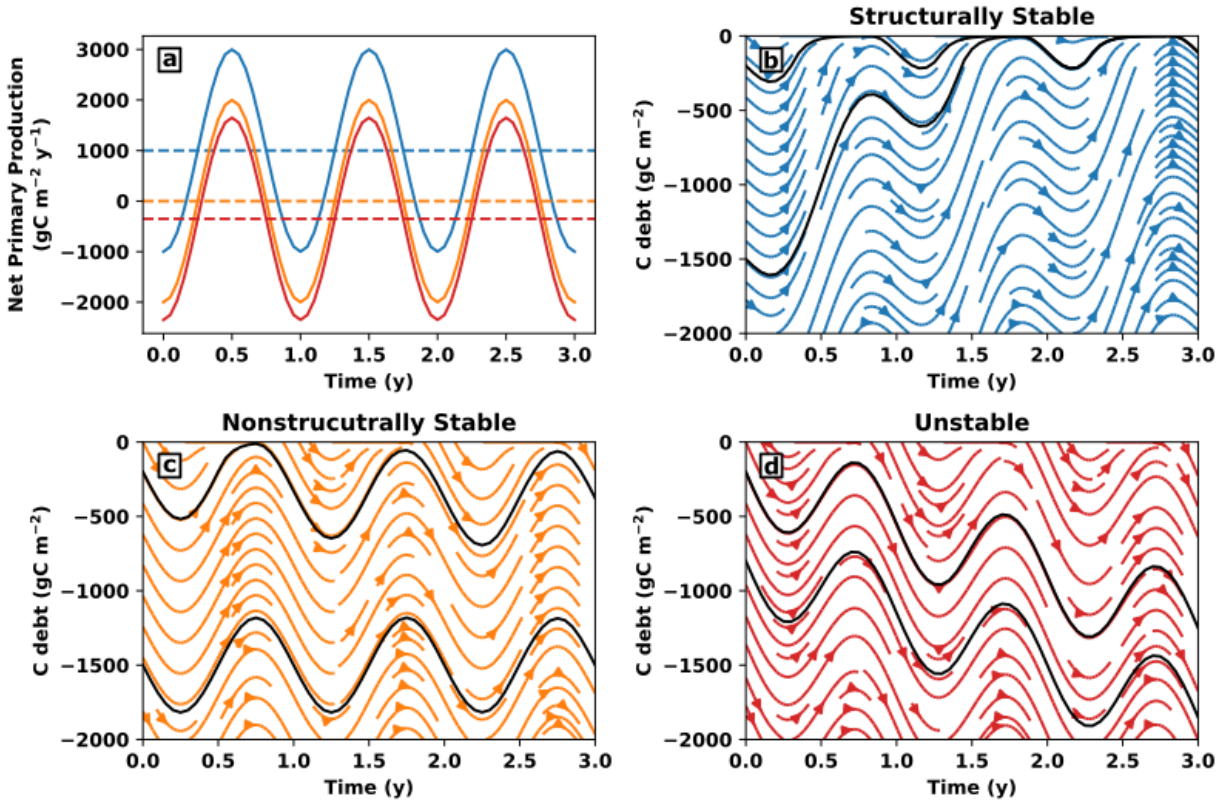

Figure 4.8: Stability of the carbon debt pool in ELM v1.0 / CLM (based on v4.5) (Burrows et al., 2020; Oleson et al., 2013) changes with average photosynthesis minus maintenance respiration $A - R_m$, stable when $A - R_m \geq 0$ (b,c) and unstable when $A - R_m < 0$ (d); To see the convergence rate, two simulations are highlighted in black. The convergence of flowlines in (b) is structurally stable but only because a feedback exists on average over time. Seasonality here results only from seasonal variation in net primary production (NPP).

4.3.3 NSC models differ widely in hysteresis and relaxation times

Comparing fixed points and relaxation times across models reveals structural differences that comparisons of simulated time-series may not. As discussed above, models with differences in relaxation times will exhibit different degrees of hysteresis from their nullcline (Fig. 4.6). In practice, models will differ along both dimensions and both properties are typically related.

For instance, consider the SUGAR (Jones et al., 2020) and CASSIA (Schiestl-Aalto et al., 2015; Schiestl-Aalto et al., 2019) models of seasonal NSC dynamics. Both contain a single NSC pool and relate its dynamics to photosynthesis, growth, and respiration. Within the resolution of available data, both models simulate seasonal NSC variation with similar magnitudes to observations in Furze et al., 2019[5]. These models have a similar conceptual basis (carbon mass balance) and the same box and arrow diagram (Fig. 4.1), but they differ in their kinetics (Fig. 4.1b,c) which yields differences in their responses. These models sit roughly at the extremes with CASSIA having extremely weak nonstructural carbohydrate feedback (left column in Fig. 4.6) while SUGAR has relatively strong feedback (mid-right column in Fig. 4.6), although Jones et al., 2020 also investigate the variation in feedback strength in their analysis of parameter variation.

To review the relevant parts of the SUGAR and CASSIA model, both define an equation similar to (4.4) (Equations 1, 1, and 4 in Jones et al., 2020; Schiestl-Aalto et al., 2015; Schiestl-Aalto et al., 2019, respectively). Jones et al., 2020 define a Michaelis-Menten like substrate dependence on NSC for growth and respiration.

$$\frac{G}{m} = G_0 \frac{s(1-s)}{K_m(1-s)+s} \qquad \frac{R}{m} = \underbrace{R_0 \frac{s(1-s)}{K_m(1-s)+s}}_{\text{maintenance}} + \underbrace{\frac{1}{3}G}_{\text{growth}} \tag{4.6}$$

Note (4.6) expresses the dependence in carbon mass fraction rather than in absolute mass as in Jones et al., 2020. The factor $1/3$ is the amount respiration needed per unit growth ($(1-Y_G)/Y_G$ in Jones et al., 2020). We collect several factors that do not depend on the amount of NSC into G_0 and R_0 for notational simplicity (these coefficients vary with temperature, using a Q10 response in Jones et al., 2020). Likewise, the CASSIA model defines growth and respiration as

$$\frac{G}{m} = G_0 \min\left\{1, \frac{1-\exp(\alpha m s)}{1-\exp(\alpha m_0 s_0)}\right\} \qquad \frac{R}{m} = \underbrace{R_0 \min\left\{1, \frac{1-\exp(\alpha m s)}{1-\exp(\alpha m_0 s_0)}\right\}}_{\text{maintenance}} + \underbrace{\frac{1}{3}G}_{\text{growth}} \tag{4.7}$$

The coefficients G_0, R_0 vary based on temperature, ontogenetic development stage, seasonal phenology, and soil moisture. Schiestl-Aalto et al., 2015 also track four separate structural biomass pools for the roots, stems (primary and secondary wood), and leaves so the growth and respiration rates are defined with some differences for each organ; however, the model contains only one NSC pool, and the growth and respiration substrate dependence has the same form (but variations in parameter values) across organs.

[5] Based on conversion to whole-plant starch carbon mass fractions.

Note both of these substrate dependences are saturating-type functions of NSC. These kinetics may then be inserted into Equation (2.1) to generate versions of Equation (2.2) as described in Chapter 2.

Both models generate one fixed point, but its dependence on the environment and the relaxation time (eigenvalue) differ between the two. While the values of both depend on the environment and parameters, in the CASSIA model nonstructural carbohydrates have a much weaker feedback than the SUGAR model. In the CASSIA model, nonstructural carbohydrates are less sensitive to short-term changes in carbon balance than in the SUGAR model. To illustrate, we plot the attractors for seasonal varying photosynthetic rates and the NSC fixed point (nullcline) by specific photosynthetic rate A/m (Fig. 4.9). Due to its lower substrate dependence, the CASSIA model exhibits greater sensitivity to changes in A/m in terms of its fixed point, indicating that small changes in photosynthesis lead to large responses in the balance between NSC supply and demand, but its longer relaxation time means that the attractor in centered around average values. Furthermore, short term variation in photosynthesis would have large effects on the nullcline but small ones on the actual NSC amount; relative to the nullcline, the model has large hysteresis. In contrast, the SUGAR model has little hysteresis and relaxes quickly into its steady state. Each model sits at the extremes of Fig. 4.6.

This comparison is not to say that either model is better. The correct fixed point and relaxation time for NSC dynamics are context-dependent, as many factors affect carbon balance. For instance, the CASSIA model attempts to capture seasonal phenology in temperate ecosystems in a way that the SUGAR model does not, which was developed for tropical and subtropical ecosystems. Even if reparameterized, winter-dormancy leads to a low relaxation time in winter. Additionally, in a previous work, we argue that the relaxation times are expected to vary by plant mass (Oswald & Aubrey, 2020) (see Chapter 2). While both models are consistent with this expectation, growth and respiration scale with plant mass in the SUGAR model, and only reductions in specific photosynthetic rate modify the dynamics as mass accumulates. On the other hand, the amount of NSC has almost no effect on growth and respiration rates for large plants in the CASSIA model.

Our analysis complements the analyses presented in Jones et al., 2020 and Schiestl-Aalto et al., 2015. For example, Jones et al., 2020 developed their NSC model to work within the Joint UK Land Earth System (JULES) model and perform comparisons with it. In the JULES model, effectively the relation $A - R - G = 0$ holds and it becomes the steady state for the SUGAR model (Jones et al., 2020). Thus, relative to the JULES model, the SUGAR model dampens the effect of carbon imbalances, exhibiting hysteresis as described here. Jones et al., 2020 observed that higher NSC increases the dampening effect by comparing simulations over several orders of magnitude their parameter f_{NSC} which controls how quickly growth and respiration saturate (see their Fig. 2). In fact, the relaxation time changes by almost three orders of magnitude in these simulations. Thus, at one extreme, their model has fast relaxation and remains near a fixed point, so carbon demand remains close to carbon supply ($A \approx R + G$) whereas at the other extreme of slow relaxation, growth and respiration respond little to changes in NSC. Thus, the buffering effect of NSC is greatest when growth and respiration do not depend much on NSC, thus effectively decoupling them from photosynthetic fluctuations.

Likewise, Schiestl-Aalto et al., 2015 found that the NSC pool dampens growth and respiration responses to photosynthesis. However, they conclude growth and respiration rates must include a dependence on past photosynthetic production to correctly reproduce interannual variation in growth due to interannual variation in photosynthesis (Fig. 8 in Schiestl-Aalto et al., 2015). This dependence is a kind of delay variable in which current dynamics depend directly on past. This dependence is independent of any feedback via the NSC pool; however, it is possible for the NSC pool to mediate this delay without introducing a delay variable, reductions in photosynthesis mean less accumulation / more depletion of NSC than otherwise leading to reduced growth. The strength of this effect depends on how strong growth rates depend on NSC, and Schiestl-Aalto et al., 2015 assume a weak substrate dependence, effectively decoupling these processes. Thus, they conclude that NSC availability does not mediate this effect but in essence, they begin with that assumption. For NSC dynamics to mediate this response, the model would have to have a stronger substrate dependence (faster relaxation time), then fluctuations in photosynthesis would generate much larger fluctuations in NSC and thus in growth and respiration. This stronger coupling is observed in Jones et al., 2020. Moreover, as presented, the CASSIA model requires one to specify past photosynthesis to predict current growth rates, meaning that growth rates are never decoupled from past photosynthesis even at short time scales. It seems more likely that even if NSC is not responsible, then some other latent variable mediates the effect (i.e., lower production leads to a reduction in the current value of some latent variable that then yields a reduced growth rate). The fixed point of the NSC pool depends on its supply and demand, and because the supply and demand may depend on NSC availability, supply and demand become strongly coupled over longer time-scales while not being coupled at short time-scales. Our point is that if the NSC pool mediates a certain response then it must have a certain substrate dependence to generate the coupling effect. Assuming no substrate dependence is the same as assuming that the NSC pool does not mediate this effect. These properties provide an additional method for rejecting or validating models.

As additional comparison, consider the simple ELM (sELM) model (D. Lu & Ricciuto, 2019), a version of ELM for prototyping modifications to ELM (available from Dan Ricciuto, https://github.com/dmricciuto/simple_ELM/tree/master). For the sELM model, the carbon debt scheme in ELM v1 (Burrows et al., 2020) was replaced with positive NSC mass as the storage pool (`cstor`). The dynamical law for the new pool is in (4.8). The η is the fraction of assimilated carbon allocated to growth, and it depends on the nitrogen availability; the mortality term μ represents loss of material due to turnover in the plant population.

$$\dot{y} = \underbrace{\min\{(A - R_m)(1-\eta), A - R_m\}}_{\text{allocation to NSC}} - \underbrace{\mu y}_{\text{mortality}} - \underbrace{K(T)y}_{\text{excess respiration}} \tag{4.8}$$

While the steady state depends on changes in photosynthesis and respiration smoothly, the fixed point of this pool can be negative because maintenance respiration R_m is independent of y. Unlike the CASSIA or SUGAR models, no saturation occurs at high photosynthesis. The excess respiration term was added to prevent this pool from growing too large as otherwise, the mortality term is the only aspect of the model to control the size of this pool. However, both terms are generally small;$\mu \approx 0.035$ y^{-1} while

$K \in [1, 5]$ y^{-1} as temperature ranges. Thus, under $A - R_m > 0$, the ultimate size of this pool is $y^* = (A - R_m)(1 - \eta)/(\mu + K)$; assuming $\eta \approx 0.8$, y^* is 4-25% of $A - R_m$ so more than 4-25% of true NPP. The relaxation time is long, similar to the CASSIA model, and much longer than typical values for the SUGAR model. Thus, like the CASSIA model but unlike the SUGAR model, the presence of NSC in the sELM model does not buffer respiration or growth rates to fluctuations in photosynthesis, nor mediate interannual variation. In fact, the case of sELM mirrors many pools of ecosystem models, where demand or outflow processes (outward arrows in Fig. 4.1a)

Although we focus on NSC dynamics, these techniques are applicable to ecosystem models in general. For instance, Luo et al., 2017 claim that the majority of terrestrial carbon cycling models may be summarized with an linear ordinary differential equation. Hysteresis is present in their analysis, and this hysteresis is governed by relaxation time (the inverse of the carbon residence time parameter is equal to the eigenvalue in their model) (Luo et al., 2017). For similar reasons, one expects ecosystem models to have structurally stable fixed points. Determining this fixed point structure, and the rate of convergence around it, may solve problems with model divergence under future climate projections as these aspects of the model will dominate the long-term responses.

In summary, the strength of feedbacks, which depends on both the overall magnitude of a flux and how much its rate varies with reactants or other signals, determines the strength of hysteresis. Weak feedbacks take a long time to become apparent as observed in both Schiestl-Aalto et al., 2015 and Jones et al., 2020. In practice, weak feedbacks often lead to more sensitive fixed points, changing the overall response.

4.3.4 Model construction from a dynamical view: Transient growth responses in a FACE experiment

Examining the geometric structure of a model is not only a method for analyzing existing models. It provides insights into the dynamical structure that a model must contain to reproduce a given experimental phenomenon. To illustrate, we present a short case study: how short term carbon feedbacks with long term nitrogen feedbacks generate transient growth responses.

The presence of storage pools for nitrogen and carbon allow for differences in transient responses and long-term ones, even within a simple two-state model of free amino-acids (labile nitrogen reserves) and nonstructural carbohydrates (labile carbon reserves). Before describing the model, we describe the phenomenon to explain. Certain free air carbon enrichment (FACE) experiments have seen a transient growth response, in particular the Oak Ridge National Laboratory's FACE as reported Norby et al., 2010 (Ainsworth & Long, 2005; Norby et al., 2001; Norby et al., 2022; Norby & Zak, 2011; R. S. Nowak et al., 2004). The rate of growth (e.g., diameter increment rate) is elevated immediately after the elevation of CO_2, relative to ambient CO_2 control groups, but this elevated growth rate is not sustained (Norby et al., 2001; Norby et al., 2010). Even with CO_2 levels maintained, the effect is strongest during the same growing season as enrichment and diminishes each year afterwards. After 10 years, the addition of nitrogen stimulated a similar increase in growth rates, which led to the conclusion that nitrogen availability limits growth while CO_2 is not limiting. This observation is among the strongest dynamical effects in this exper-

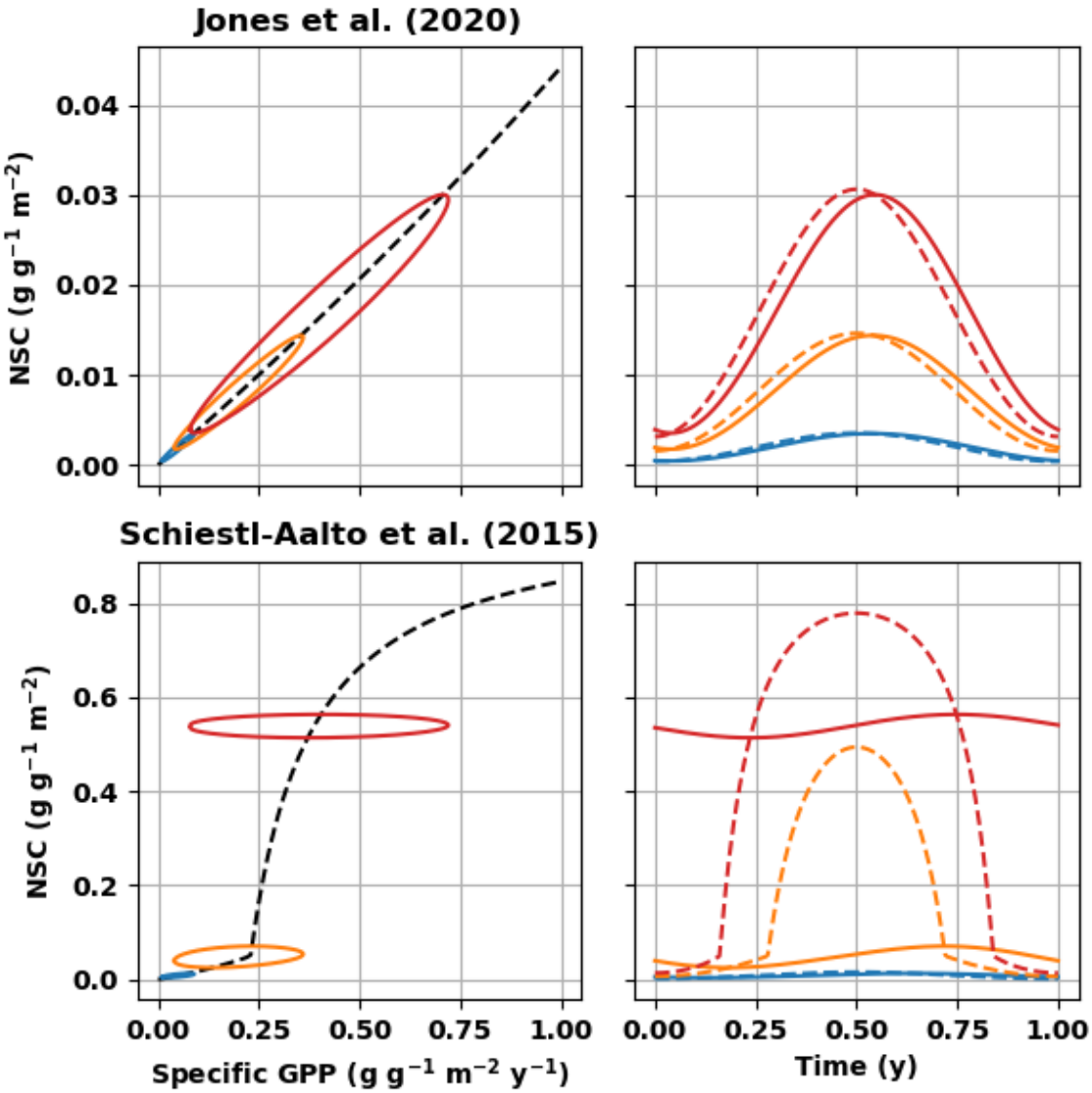

Figure 4.9: Comparison of the CASSIA (Schiestl-Aalto et al., 2015) and SUGAR (Jones et al., 2020) models for NSC responses. Left column is bifurcation diagram, showing the NSC fixed point (black dashed) by specific photosynthetic rate. Attractors for three different magnitudes of specific photosynthesis are shown (blue, orange, red solid curves). The time-series (right) also plots the corresponding nullcline (dashed curve). The diagrams were produced assuming temperature $= 25$ °C, and no water deficiency for both models. For the CASSIA, we used root growth and respiration parameters for whole-plant averages (for simplicity); a maximum growth rate is assumed (no reduction due to development stages); we also assumed a plant with a total dry biomass $= 160$ kg (as concentrations are not reported); and no effect of past photosynthetic production is assumed (i.e., we use the constant L model from Schiestl-Aalto et al., 2015).

iment, and ecosystem models must be able to reproduce this behavior. Furthermore, this phenomenon is not present at all FACE experiments, therefore, a model must identify what conditions lead to transient growth responses. The geometric viewpoint provides a way to identify the essential structure required.

Let x, y denote the carbon and nitrogen mass of nonstructural carbohydrates and free amino-acids, respectively. Suppose the following carbon and nitrogen balance equations:

$$\dot{x} = A - R - G \qquad \text{nonstructural carbon balance} \tag{4.9}$$

$$\dot{y} = U - \gamma G \qquad \text{nonstructural nitrogen balance} \tag{4.10}$$

where A, R, G are rates of photosynthesis, respiration, and growth, respectively; and U is the rate of nitrogen assimilation and γ is the nitrogen:carbon ratio of structural tissues (Fig. 4.1a). As established, the feedbacks determine the dynamical structure. Two sources of information constrain possible feedbacks. The first is to reason about each process, its substrate dependences, and other local information (cf. Fig. 4.1b,c). The second is to choose feedbacks that create a structurally stable fixed point and two different time-scales, allowing for a short and long-term response to differ (cf. Fig. 4.1d,e). We may either start with local information to develop an *ansatz* for each process and then adjust based on the resulting fixed points and Jacobian or begin with determining the Jacobian about a fixed point to set dynamical properties, then choosing local process formulations consistent with other information. For instance, we note that respiration and growth must be zero when no carbon or nitrogen substrate is available, and that growth contributes to respiration via growth respiration. Using a Taylor series expansion about zero, we postulate $R = R_0 x + \varepsilon G$ and $G = G_0 xy$. This *ansatz* feedback is sufficient to create a fixed point; and no reason suggests additional fixed points or more complicated attractors are necessary. Linearizing gives (4.11).

$$\frac{\partial V^i}{\partial x^j} = \begin{bmatrix} -R_0 - \varepsilon G_0 y & -G_0 x \\ -\gamma G_0 y & -\gamma G_0 x \end{bmatrix} \tag{4.11}$$

Note that parameters are not constant, but one may determine their approximate magnitudes by the process rates, the fixed point, and the Jacobian that they generate. To explain why this system can produce transient growth responses, consider the geometric properties shown in Fig. 4.1o.

Consider the flow as shown by the flow lines (Fig. 4.1o). We easily see that the flow around the fixed point (red point) varies sharply with direction. For instance, the carbon and nitrogen nullclines—that is, the set of (x, y) such that $\dot{x} = 0$ or $\dot{y} = 0$, respectively—are plotted. These curves represent the respective steady state of carbon or nitrogen, while treating the other variable as known. Solving for (x, y) such that both $\dot{x} = \dot{y} = 0$—where the nullclines intersect—are the fixed points; as photosynthesis changes, the nullclines change position and this fixed point moves tracing out a curve. The contours of G, along which growth rates are constant, are also plotted.

Suppose carbon dynamics come into equilibrium much faster than nitrogen dynamics, meaning the system splits into two time-scales: first, the system moves the carbon nullcline, because carbon dynamics equilibrate faster, and then the system moves along the carbon nullcline as the nitrogen dynamics come into equilibrium (Fig. 4.1o). Using the Jacobian of the fixed point, we can identify such time scale

separations and its dependence on parameterization. The eigenvectors identify stable (resp. unstable) subspaces if the corresponding eigenvalue has real part < 0 (resp. > 0). These eigenvectors are tangent to stable (resp. unstable) manifolds which extend out from the fixed point, and in this case, mostly follow coordinate directions; the eigenvalues give the rate of convergence. Eigenvectors whose corresponding eigenvalues have a zero real part are tangent to center manifolds, whose stability cannot be determined from the Jacobian. When stable, the dynamics along the center manifold are much slower than along stable manifolds. In Fig. 4.10, the fixed point is a stable sink (both eigenvalues are real and negative), but the one eigenvalue is much closer to zero than the other, indicating the slower direction is an approximate center manifold. This separation of time scales can generate vanishing transient growth responses. In other words, we could approximate the short-term carbon dynamics by holding nitrogen constant; and we could approximate the long-term nitrogen dynamics by replacing nonstructural carbohydrates with their nullcline (the fixed point conditional on nitrogen). The latter approximation is similar to the center manifold approximation, and both approximations correspond to singular perturbation theory problems (Fenichel, 1979; Guckenheimer & Holmes, 1983; Wiggins, 1996)

The true utility comes from considering changes to the system. Suppose the system begins near a fixed point. When photosynthesis is increased by increased CO_2, the nullclines shift and fixed point moves; however, the time-scale separation persists so that NSCs respond more quickly increasing. This increase in NSCs but little change in amino-acids pushes the system to a higher growth rate (and usage of labile nitrogen reserves), but then higher growth rates depletes nitrogen stores until reaching a new fixed point. Critically, the fixed point moves along the contour of growth rates, hence the growth rates will not remain elevated after CO_2 enrichment. Moreover, if the movement of carbon nullcline due to an increase in photosynthesis is almost parallel to the contours of growth—that is, when $\partial G/\partial x \approx 0$—then no transient growth response will occur. The physical meaning is that carbon supply far exceeds nitrogen supply so that growth is more limited by lack of nitrogen than carbon. Note that nitrogen still limits growth in both cases, in that nitrogen additions would increase growth rates in both cases.

While this explanation is plausible given the transient growth responses observed in FACE experiments but not in severely nitrogen limited ecosystems, the salient feature is that it provides testable predictions which involve the dynamical structure of the model, rather than specific process formulations. For instance, nonstructural carbohydrates should increase and remain elevated in FACE experiments, and indeed starch accumulation is among the strongest responses across FACE experiments (Ainsworth & Long, 2005). Additionally free amino-acids should decrease, which could be compounded by decreases in mineralized soil nitrogen.

This example also illustrates the importance of structural stability. Any environmental change that affects one of the processes in (4.9)-(4.10), be it light, temperature, or CO_2 will disrupt the balance of NSC and free amino acids, generating a response for both substances as well as all downstream processes. For hyperbolic fixed points, we can calculate tangent vectors to the set of fixed points and environments using (4.12).

$$dV = \frac{\partial V}{\partial x}dx + \frac{\partial V}{\partial \theta}d\theta = 0 \quad \Longrightarrow \quad \frac{\partial x^*}{\partial \theta} = -\left(\frac{\partial V}{\partial x}\right)^{-1}\frac{\partial V}{\partial \theta} \tag{4.12}$$

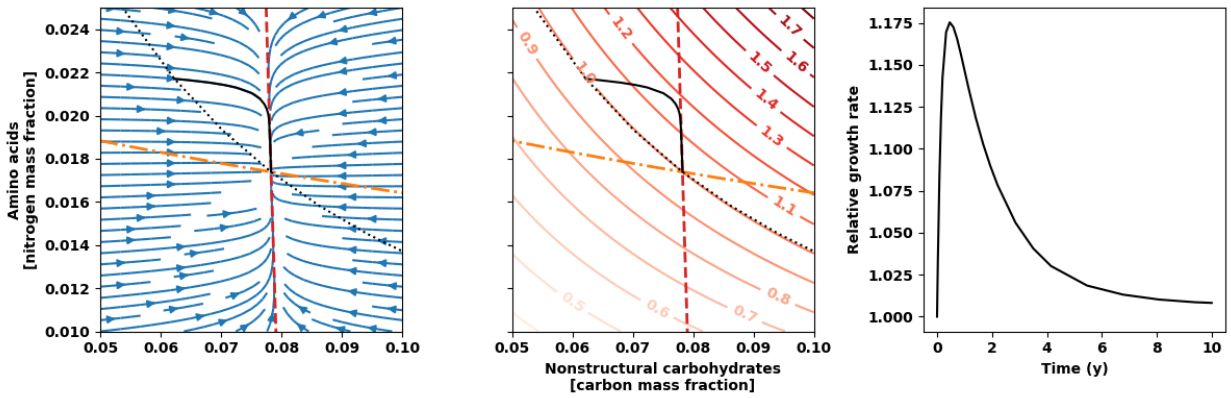

Figure 4.10: Structurally stable model for nonstructural carbon (NSCs) and nitrogen (free amino acids) predicts transient growth responses to CO_2 fertilization because of faster relaxation times for NSC dynamics than nitrogen storage. Streamplot (left) contains approximate center manifold along the NSC-nullcline (red dashed). Increasing photosynthesis by CO_2 fertilization moves the fixed point along a curve (black dotted) by shifting the NSC nullcline to the right and the amino acid nullcline (orange dashed-dotted) downward. Contours (middle, red solid gradient) show how growth rates (inset numbers show relative changes) vary with the amount of NSC and free amino acids. A simulation (black solid) is shown; and the resulting change in growth rates relative to initial (right).

This calculation involves inverting $J = \partial V/\partial x$ so no eigenvalues can be singular, and when small, the corresponding response is large. Thus, the fact that a model like ELM v4.5 or sELM have weak convergence or no convergence in their flowlines, depending on the environment conditions, indicates responses will be large or ill-defined. Any change in the processes shifts the fixed point, potentially leading to a differential short-term and long-term response. For instance, temperature increases would modify the nullclines and fixed point as well. Hence, having a structurally stable feedback obviates the need to specify all responses (or interactions of those responses).

In summary, to construct models that generate the dynamical properties observed in experiment (e.g., a transient growth response), we examine what feedbacks and other dynamical features (e.g., a time-scale separation) are required to generate such a response. Hypotheses about dynamical features correspond directly to hypotheses about what streamplot looks like, how the fixed points change, and whether there exist center manifolds. These features place constraints on the Jacobian and in turn on the kinetics of arrows in a box and arrow diagram. These constraints can be combined with other information or explored in experiments to identify how certain emergent behaviors (e.g., transient growth responses) arise from process kinetics.

4.3.5 Higher dimensions: Dynamic carbon allocation from transport dynamics

The development of dynamic carbon allocation represents an important objective in terrestrial ecosystem modeling (De Kauwe et al., 2014). In spatially explicit model, the same interaction between carbon and nitrogen around a structurally stable fixed point that generates a transient growth response also generates dynamic carbon allocation. Shifts in the carbon or nitrogen uptake change the distribution of NSC and free amino acids, which in turn modify growth rates. With the correct feedback, the long-term effect can be to shift carbon allocation. This idea is not new (Dewar, 1993; Johnson et al., 1991; Thornley, 1972, 1991), but this idea is under-explored in ecosystem modeling. In these models, dynamic carbon allocation between the root and shoot emerges from the interaction of other processes. This emergent property is contained with the essential dynamics of each model, so that even though each of these models differs in complexity and detail, they retain this property. Before concluding, we discuss how the geometry of flow provides a means to describe this emergent property.

To review the relevant details, these models assume a set of carbon and nitrogen mass balance equations, similar to (4.9)-(4.10) but with transport processes.

$$\dot{x}_i = A_i - R_i - G_i + \sum_j I_{ij} F_j \tag{4.13}$$

$$\dot{y}_i = \underbrace{U_i - \gamma G_i}_{\text{local}} + \underbrace{\sum_j I_{ij} \tilde{F}_j}_{\text{transport}} \tag{4.14}$$

Here, I is an oriented graph incidence matrix that defines the connectivity of plant organs and specifies a direction. The sign of the transport fluxes F and $\tilde{F}$ is relative to this orientation (positive = with, negative = against). Note that $\sum_i I_{ij} = 0$ and that $A_i = 0$ for non-photosynthetic tissues and $U_i = 0$ for non-nitrogen absorbing tissues. The local dynamics may defined as in (4.9), (4.10) but we need only assume that the local dynamics contain a stable fixed point. The transport process has the form $F = -IKI^T x$ and $\tilde{F} = -I\tilde{K}I^T y$ where I^T is the transpose and $K, \tilde{K}$ are diagonal matrices, representing the conductance between each organ. Effectively, the transport process is a weighted Laplacian, equalizing adjacent organs.

The transport process must be much faster than the internal local dynamics if the distribution of NSC and amino acids varies slightly across the plant. Organs closer to leaves will have higher NSC concentrations than more distant, while organs closer to fine roots absorbing nitrogen will have higher free amino acid concentrations. To depict this distribution graphically, plot a graph of points for each organ with the NSC concentration as the x-axis and the free amino acid concentration as the y-axis (Fig. 4.11). Note the distribution is a fixed point in a higher dimensional space (dimension of $2n$ for n organs); plotted in 2D is a projection to this plane. Contours represent equal growth rates, while shading indicates limitation by carbon (red) or nitrogen (blue) (Fig. 4.11). Graphically, one sees that horizontal shifts in this distribution (overall decreases or increases in NSC) affect more strongly the carbon-limited growth rates in roots. Vertical shifts (overall decreases or increases in free amino acids) affect nitrogen-limited growth rates in leaves. To summarize, increases in carbon supply promotes root growth more than shoot growth, and

increases in nitrogen promote shoot growth more than root growth. However, this outcome only occurs when the distribution is such that certain organs are carbon limited while others are nitrogen limited. If the distribution in Fig. 4.11 were entirely contained within the red or blue regions, then the whole-plant is carbon or nitrogen limited and the change in carbon allocation will be less pronounced. Such shifts in allocation have been observed in some, but not all FACE experiments (De Kauwe et al., 2014; Norby & Zak, 2011).

While this scheme may not contain all mechanisms involved in shifting carbon allocation, it only needs to reproduce the overall emergent effect at a given time-scale. That said, the scheme produces dynamic carbon allocation shifts across any spatial resolution. For instance, while Thornley, 1972 and Dewar, 1993 only model shoot and root partitioning, the same scheme is used for five organs in Thornley, 1991. Plant models like Allen et al., 2005 and Schnepf et al., 2018 effectively include dozens or hundreds of compartments. Note also that Thornley, 1972 and Dewar, 1993 consider additional feedbacks whereby increased growth rates leads to a faster increase resource acquisition of the root or shoot due to relative changes in how fast each organ grows.

More importantly, the center manifold theorem provides a method for reducing more complex models to simplified versions. We briefly discuss two applications. First, actual transport of NSCs and amino acids is governed by phloem and xylem dynamics. To determine the correct flux responses, the details of these processes must be incorporated. Models of the phloem flow (Thompson & Holbrook, 2003) or coupled xylem-phloem flow (Daudet et al., 2002; Lacointe & Minchin, 2008) are more appropriate for modeling these dynamics over shorter time-scales ($\sim$ days) rather than the simplified Laplacian flow above. However, at longer time-scales, many details do not matter. Only the fixed point and center manifold (if one exists; otherwise the slowest stable manifold) matter for describing the response. In this example, the explicit phloem models generate a distribution of NSC and amino acids, given inputs such as photosynthesis, water potential, and so on. In this way, the scheme above could be determined as an approximation to a more detailed phloem flow model. We do lose information, and reducing the system to a center manifold or approximate center manifold generally means ignoring short-term responses in favor long-term ones. This method already sees use in biology, ecology, and ecosystem modeling, though usually known as "quasi-steady state" approximations. For example, Michaelis-Menten kinetics are derived by reduction to a center manifold; similar enzyme kinetics approximations are used in ecosystem models (Tang, 2015) and can as accurate as spatially explicit models (Wang & Allison, 2019). The center manifold theorem provides a systematic description of such approximations.

An important point is that we still only assume a single fixed point and analyze the near-linear behavior around it (the nonlinearity resulting from necessary constraints on kinetics). This dynamic shift in carbon allocation due to an emergent feedback is simple from the standpoint of dynamical systems, involving no bifurcations, multiple fixed points, or other more complex attractors. One could in principle posit models with thousands of pools and fluxes, but the overall dynamical behavior could be quite simple such as a single stable fixed point. In that case, such a model could be represented by much simpler ones without significant losses in predictive ability.

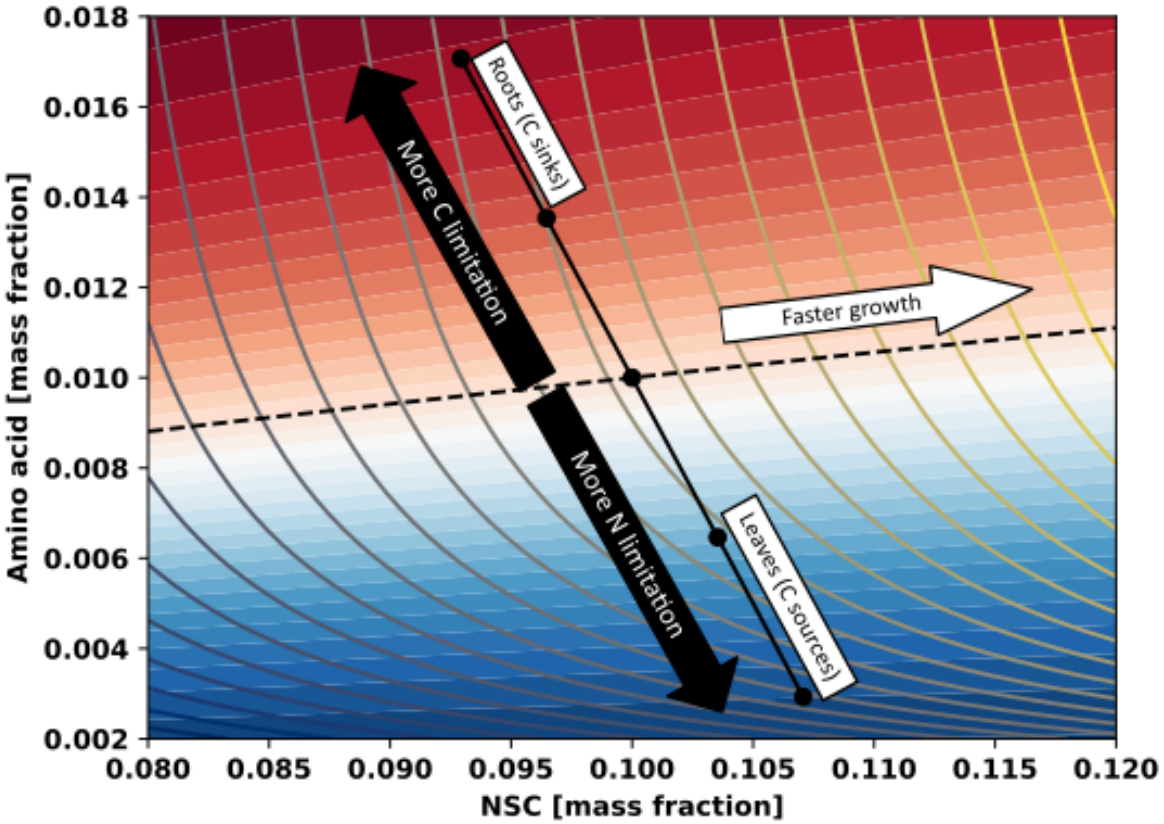

Figure 4.11: Distribution by organ (black dots) of nonstructural carbohydrates and free amino acids. Differences in nitrogen limitation (blue) and carbon limitation (red) lead to differential growth responses to external changes in carbon or nitrogen supply and demand, which shift the distribution.

In summary, complex emergent properties like differential shifts in carbon allocation could be understood as shifts in stable fixed points. Nonstructural carbohydrates can mediate shifts in carbon allocation without any additional complications. Geometric techniques provide a means to describe why models have (or do not have) certain emergent properties and often clues for how to simplify models.

4.4 Discussion

We have presented an approach to analyzing NSC dynamics for dynamic global vegetation models based on the geometry of their flow. Stabilizing feedbacks are necessary to allow short-term carbon imbalances

to generate dynamic NSC but also ensure that long-term carbon imbalances cancel out. The strength of these feedbacks controls the transient hysteresis to periodic fluctuations in the environment as well as the dampening effect that dynamic NSC can have. While published NSC models almost always include stabilizing feedbacks, the strength of these feedbacks and how the feedback changes with the environment varies considerably by model. Some models, like ELM, only achieve time-average stability and lack stabilizing feedbacks in certain environments altogether. If feedbacks are too weak, then the NSC dynamics effectively behave as if no stabilizing feedbacks are present. We have then shown that studying NSC-related feedbacks can lead model construction and shed light on important model structure. Investigation of the essential structure of models may clarify why models diverge in future climate scenarios, despite agreement in past climates (Lovenduski & Bonan, 2017). Furthermore, identifying the essential structure that models must capture facilitates their construction from experiments, even when these experiments occur under controlled or artificial circumstances. To conclude, we discuss some problems hinder the deployment of these techniques and compare the present approach to other "organizing principles".

To summarize this approach in three steps, given a model as a set of reactions and their kinetics (Fig. 4.1), first one identifies the position and number of fixed points (using a root finding algorithm). Second, to identify the stability of these fixed points and the strength of feedbacks as well as stable and center manifolds, one calculates the eigenvalues of the Jacobian and other derivatives. Third, one examines how the fixed points and eigenvalues vary as inputs (such as the environment) vary. The identification of bifurcations, where the number or stability of fixed points changes (e.g., two fixed points combining into one; a stable point becoming unstable), are of special interest. In essence, models with the same fixed point structure and stability are topologically equivalent and will have the same responses but may vary in degree (Fig. 4.6). In addition to identifying these features in a given model, one can prescribe or hypothesize a certain structure then construct a models or modify existing models according to that structure. Furthermore, low dimensional behavior may be derived from high dimensional models. This method applies geometry and topology to analyze dynamical systems (Guckenheimer & Holmes, 1983; Strogatz, 1994; Wiggins, 1996). Similar ideas have been employed elsewhere in the discussion of ecosystem dynamics (Scheffer et al., 2001) as well as in cell biology (Tyson et al., 2003).

A number of basic recommendations follow from this outline. While these calculations are relatively straightforward, current implementations of models often do not facilitate them. To employ a root solving algorithm to identify fixed points, or to determine derivatives by numerical differentiation or automatic differentiation, one must be able to vary starting conditions while fixing the environment or other external variables. To study the intrinsic responses of specific submodels, the submodel must be easily isolated and external inputs provided. These actions may require reformulation of the model's implementation to facilitate calculations with large models and to avoid translation errors. For instance, to produce Fig. 4.8, we reproduced the rule as described in ELM's documentation (Oleson et al., 2013) rather than using the current code because the current code would require modifications to make a certain piece directly accessible (although the results should be the same if the documentation and the model as implemented are the same).

Although our approach focuses on continuous time (i.e., using differential equations) rather than discrete time (i.e., using iterated maps), many ecosystem models are expressed in the latter. Conceptually, this difference poses no problem for the present approach as analogues between the two exist, and numerical integration converts differential equations into iterated maps; however, the stability of fixed points in the latter depends on the time step. Unless addressed, computer simulations may exhibit fundamental differences in their essential dynamics than the mathematical specification of a models.

A geometric approach is compatible with a number of other proposed approaches for ecosystem model construction, but the examination of fixed points and other stables of dynamics are often absent. A number of recent reviews on carbon allocation and "organizing principles of vegetation dynamics" (Franklin et al., 2012; Franklin et al., 2020) discuss optimality theory, evolutionary game theory, and self-organization. The presence or absence of fixed points and stabilizing feedbacks requires assumptions about dynamics, but not the optimality or evolution of plant physiology. Although traces are present, coordination theories (Maire et al., 2012; Prentice et al., 2014; N. G. Smith et al., 2019) effectively use assumptions about fixed point structure. Analyses of evolutionary dynamics and evolutionary game theory involve identifying fixed points and their stability (Brännström et al., 2013; M. A. Nowak & Sigmund, 2004; Page & Nowak, 2002). Self organization of vegetation and its effects on ecosystem function also involve the application of these concepts (Rietkerk, 2004; Rietkerk et al., 2021). Finally, while mostly absent from discussions of land surface modeling, a key objective is the development of model robustness (Prentice et al., 2015). Structural stability and topological conjugacy provide a formalism for model robustness. Consideration for the essential dynamics aids parameter selection by constraining good parameters to regions with certain dynamical features or by tuning parameters to tune the strength of stabilizing feedbacks.

To improve models, we must ask what their fundamental behavior is and how does it agree or disagree with reality. Efforts to represent ecosystem processes in ever greater detail may result in higher accuracy but will not result in greater insights. In particular, what fixed point structure and eigenvalues are necessary to capture the essential dynamics of these ecosystems? What feedbacks reproduce these features? For existing ecosystem models, analyzing these properties will lead to greater insight into the model. Given hypotheses about such properties, new experiments may be conducted to confirm or reject these hypotheses, thus informing model structure in manner that is not available from retrodiction on historical records.

Chapter 5

Conclusion

We have presented several works to advance the science of nonstructural carbohydrate dynamics. Within each we have discussed the implications of the results presented. Here, we elaborate on the broader implications of these results. To recall what main results, Chapter 2 introduces a mathematical framework to analyze seasonal nonstructural carbohydrate dynamics from the perspective of carbon balance. Several phenomena related seasonal dynamics are explored. Chapter 3 presents an experiment in which we simulated drought to perturb nonstructural carbohydrate dynamics to observe whether resources are shifted from growth to storage, even after drought. While growth rates were reduced after the simulated drought, no increase in nonstructural carbohydrates was observed. Chapter 4 studies the implementation of nonstructural carbohydrate dynamics into ecosystem models and what implications the insights required in Chapter 2 have for comparing and improving such models.

In Chapter 1, we reviewed the development of how contemporary studies conceive of nonstructural carbohydrate dynamics. The development of the theory presented in Chapter 2 speaks directly to this body of work, and it is worth commenting further on the connections. Roughly, we set the viewpoint of Körner, 2003 against that of Sala et al., 2012 and Wiley and Helliker, 2012. The basic difference in interpretation between these viewpoints is whether nonstructural carbohydrates, either in general or in specific cases, reflect the sink limitation of growth (Körner, 2003) or active storage (Sala et al., 2012; Wiley & Helliker, 2012). The critical insight that resolves these viewpoints is that stoichiometry is distinct from kinetics. Nonstructural carbohydrates must increase when supply exceeds demand, and decrease when demand exceeds supply: $\dot{s} = A(1 - s) - D(s)$ to cite Appendix A.3. Thus, decreases in demand by temperature or dehydration must increase the balance point (fixed point / nullcline) which leads to an increase in nonstructural carbohydrates when starting near the fixed point: lowering $D(s)$ will increase the fixed point for the same supply; in (2.2), $s^* = A/(A + U)$ and increases in U lead to decreases in s^*. This logic supports the reasoning of Körner, 2003, however, how supply and demand rate depend on the nonstructural carbohydrates, the supply and demand kinetics, does affect the responses as it changes how the fixed point varies with the environment: in other words, $D(s) = Us$ yields different fixed point sets than $D(s) = Vs/(0.01 + s)$, $D(s) = U\sqrt{2}$ or $D(s) = Vs^2/(0.1 + s^2)$. Thus, the kinetics allows for prioritization of storage over growth when nonstructural carbohydrates are low. For instance,

$D(s) = Us$ leads to a proportional decrease, whereas $D(s) = Vs^2/(K+s)$ requires more nonstructural carbohydrates to accumulate for demand comes into equilibrium with supply, thus yielding a prioritization of storage at low supply. The mathematical analysis also demonstrates that a natural but important time-separation exists. Supply and demand are independent at each moment in time in that supply and demand can change without affecting the other, but over longer time scales, the feedback couples supply and demand. The fixed point $A/(A+U)$ depends on both supply and demand related parameters, and then in turn determines supply and demand. For instance the demand at the fixed point becomes $AU/(A+U)$ (which is the same as supply). In this manner, supply and demand become coordinated. Although the exact details must still be elaborated, this analysis resolves the apparent theoretical conflict present in the literature.

The mathematical framework also explains when changes in supply and demand lead to increasing or decreasing nonstructural carbohydrates versus high or low nonstructural carbohydrates. Nonstructural carbohydrates increase whenever supply exceeds demand, or alternatively said, nonstructural carbohydrates increase whenever they are below the fixed point s^*, and vice versa. As explained in Chapter 2, local maxima and minima in time series always indicate intersections of the nullcline and the concentration of nonstructural carbohydrates, and thus they demarcate periods of accumulation and depletion. However, it is possible to observe periods of high but constant nonstructural carbohydrates or periods of low and constant concentrations. This outcome indicates that the fixed point is not changing (at least not dramatically) and that nonstructural carbohydrates concentrations are near their steady state. Although qualitative in nature, these insights do not depend on the additional details needed to calculate responses and may be directly employed to analyze experiments. Furthermore, such considerations suggest possible experiments. For instance, Fig. 14 in Körner, 2003 shows a near-linear decline in nonstructural carbohydrates with increasing seasonal mean temperatures. This observation is consistent with an exponential increase in growth rates $U \propto e^{kT}$; for instance, Fig. 5.1 shows the fit assuming a Q10 response (U doubles for every 10 degree increase). The ratio A/U is adjusted to that the curve passes through one point, but no statistical fitting is performed. However, the derivation suggests that the pattern will be true in experiments (and possibly stronger given hysteresis). While likely not a perfect fit, the mathematical derivation does more than predict the direction (or sign) of an effect. Without any particular mathematical theory, one could predict that increasing growth rates via increasing temperatures would lead to lower nonstructural carbohydrates; however, the calculation provides a means to estimate the magnitude (or size) of the effect.

Our mathematical analysis also suggests that transient hysteresis is likely widespread and likely not limited to nonstructural carbohydrates. In Chapter 2, seasonal variations in nonstructural carbohydrates lag changes in their fixed point, creating the loops in the bifurcation diagrams. This phenomena is a form of transient hysteresis as the same environmental conditions do not produce the result except when the environment changes slowly. For instance spring concentrations might be higher than fall concentrations (or vice versa) even at the same temperatures without additional phenological effects. The observed concentration depends on the recent past (this phenomenon is sometimes called a legacy effect or memory, but it does not require any additional processes to occur which are often suggested by the use of those terms).

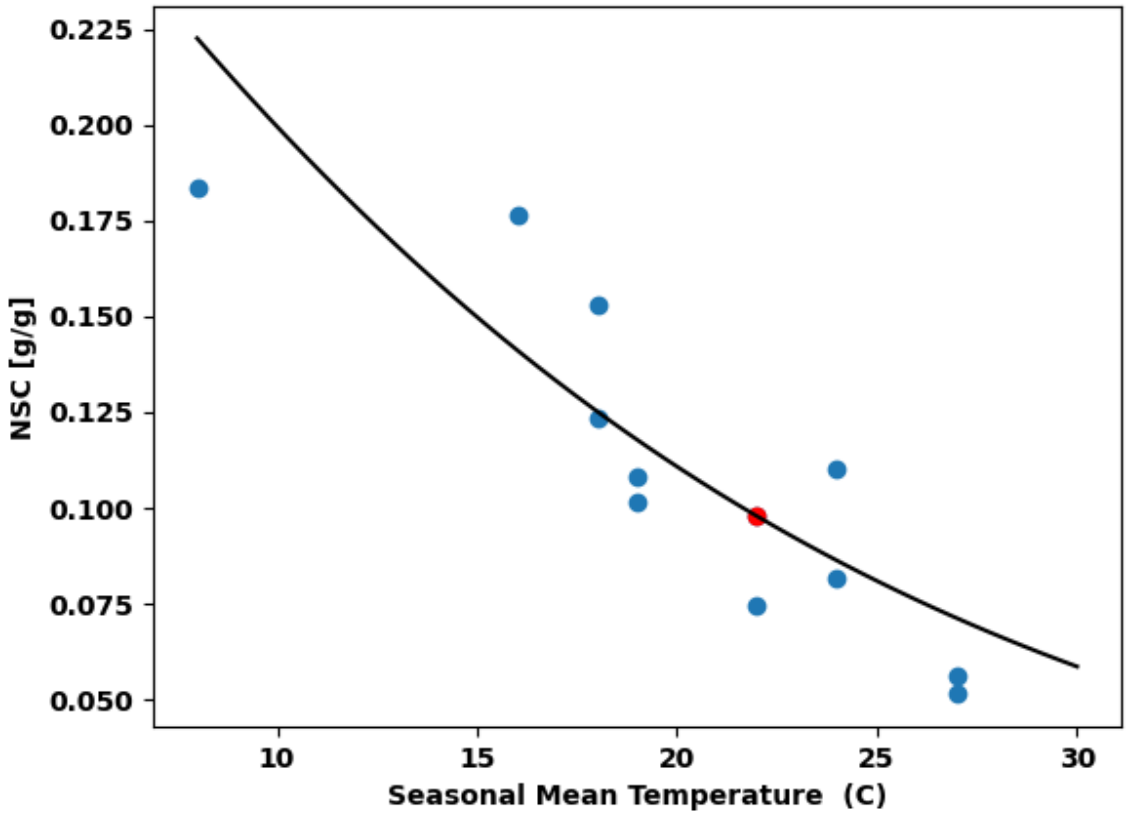

Figure 5.1: Comparison of data presented in Körner, 2003 with an Q10 temperature response based on the fixed point of Eq. (2.2). No least-squares minimization was performed; parameters were chosen to ensure the curve passes through the red point.

This hysteresis is transient because it results from the constant movement of the fixed point and would otherwise disappear; persistent hysteresis results from bifurcation of the stable fixed point into multiple stable fixed points, and these multiple possible outcomes for the same conditions do not disappear even if the environment is constant. We only mention it, however, as persistent hysteresis and bifurcations involving persistent hysteresis are often necessary to create switch-like systems (Tyson et al., 2003) and therefore may play some role in the seasonal phenology of nonstructural carbohydrates. We must mention two consequences of hysteresis for experiments. The first is that hysteresis means that causal relationships may appear weak because hysteresis means that plotting a driving variable and observations of nonstructural carbohydrate dynamics should form loops rather than functions (cf. Fig. 2.4-2.5). With low temporal resolutions, hysteresis looks like statistical noise (Fig. 5.2). The second consequence is hysteresis must be considered when studying responses to changing conditions as it may take some time for changes to reach their maximum.

Certainly, our analysis is not without flaws or avenues for extension. The principal extensions are to determine how whole-plant concentrations interacts with local spatial dynamics and the partitioning between sugar and starch. A few thoughts on achieving these extensions were discussed in Chapter 2. Gibon, Bläsing, et al., 2004 present a comparison of starch-producing wild-type and starch-less *pgm* mutants of *Arabidopsis*, which clearly shows that sugar concentrations normally remain despite large fluxes in and out, while starch concentrations increase and decrease throughout the day. This intuition is sufficient insight to build a minimal model and to study in what manner the two-state system involving starch and sugar can be reduced to a one-state system as well as what differing changes in sugars and starch indicate. Similarly, Lacointe and Minchin, 2008 present a model of phloem and xylem transport and their coupling which is sufficient to determine how phloem transport and loading interact with starch and sugar partitioning. Analyzing these phenomena may explain aspects of sugar and starch dynamics, in turn enlightening what dynamics represent whole-plant changes in carbon balance rather than local ones.

Without extensions, the analysis in Chapter 2 is however still salient for the interpretation of the experiment presented in Chapter 3. In essence, we observed reductions in average growth rates due to simulated drought. For our winter drought treatment, it would appear that although growth normally does not occur in winter, the winter drought reduced growth in the following summer growing season, whereas the summer drought had an immediate effect on growth rates. The proximate causes of this growth reduction and its delay relative to water stress remain to be explained.

We did not observe differences in nonstructural carbohydrates (neither starch or sugars) and certainly no differences that correspond to the growth rate reductions. This experiment would appear to contradict the standard paradigm of a growth-storage tradeoff, but it is more probable that any difference in nonstructural carbohydrates is rather small. Hysteresis likely plays no role because the estimated relaxation time is less than a month and probably much less. As discussed in Chapter 3, even overestimating the effect of drought on photosynthesis and growth, yields at most change around 0.01-0.02 $\mathrm{g\,g^{-1}}$. In reality, the difference would have been smaller than that and therefore likely beyond undetectable. The inability to sample the same plant's entire starch pool repeatedly at high frequency means that various sources of noise contaminate the signal (if there). Our mathematical theory suggests that studies on small plants could

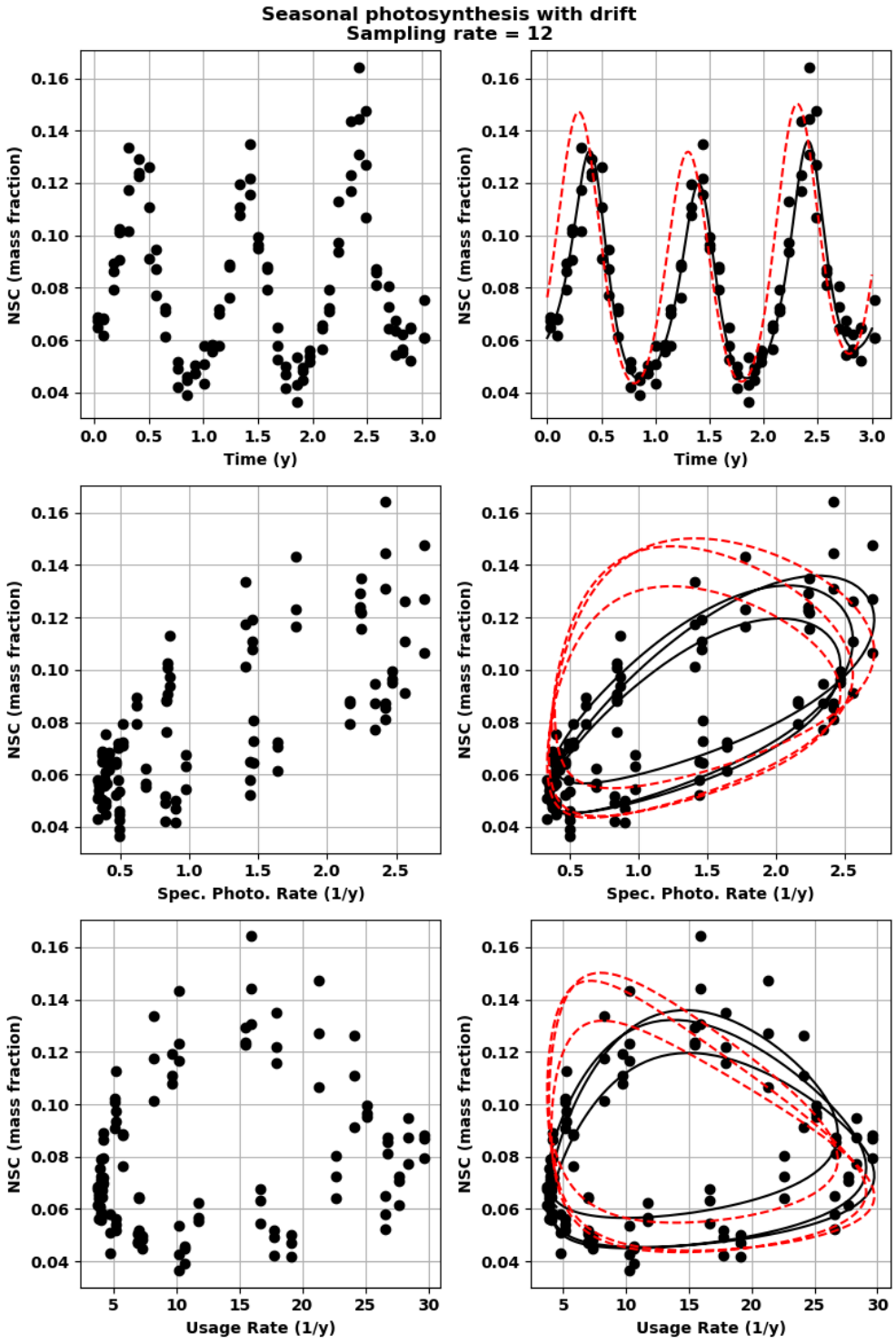

Figure 5.2: Hysteresis resembles statistical noise; hypothetical data generated to show the weakness of scatterplot (left) relationships despite knowing the exact drivers in the model. With sufficient noise and less sampling, the loops (middle, lower rows) would not be apparent.

observe conflicting signals when photosynthetic (or demand rates) do not scale proportional with plant mass. Since our plants' mass increased by 3-5× their initial mass and the largest plants were potentially pot-limited in root growth, these effects may have been larger than drought related effects. Air temperature and plant mass appeared to explain the temporal trends in whole-plant starch concentrations in our experiment; the former is a proxy for metabolism and respiration rates. We observed lower starch concentrations when temperatures were higher as expected; and on average, temperatures slightly decreased over time, which would result in the overall increase in starch. These temperature-related changes could, however, be coincidental. What our theory predicts is that the same temperature-related relationships would be observed when comparing plants grown under different, but constant temperature regimes.

Although applicable to other experiments, the basic ideas in Chapter 2 are a useful tool for experiments like in Chapter 3. Not only can we estimate direction of effects, also their magnitude (which is important when opposing effects are present). It provides a method for determining whether hysteresis may be present, and a method of determining the expected nature of mechanistic relationships (e.g., what temperature-dependent changes ought to look like) which aids interpretation of whether those effects are present or not.

Chapter 3 also illustrates experiment difficulties common to a great many experiments on nonstructural carbohydrates (cf. Blumstein et al., 2022, Sapés et al., 2021, Sevanto, 2014). Our experiment contained a large number of plants and measurements relative to similar experiments in the field, and yet our experiment likely had trouble detecting small effects due to limited sampling frequency, the inability to resample individuals, and the limited sample size. Since tissue must be removed to determine nonstructural carbohydrate concentrations by chemical extraction, removing more tissue (up to the entire plant) provides a more robust measurement of whole-plant nonstructural carbohydrate status at the expense of more work and limiting the ability for the same plant to be resampled. Unlike growth rates which could be calculated for each individual plant in our study, we could only determine changes in population averages. The ability to resolve temporal dynamics is more sensitive to the frequency of sampling, with high frequencies allowing greater resolution, but higher temporal resolution means more plants or smaller tissue samples per time increasing the uncertainty for individual measurements. It seems unlikely that these problems will ever be overcome without the development of new technologies to take measurements non-destructively. For instance, Quentin et al., 2017 present a method using infrared light spectroscopy to measure tissue samples without chemical extraction, and this method is much faster than chemical extraction and may be as accurate. It is possible that spectral or nuclear resonance techniques could be applied *in vivo*; but it is unclear if such methods will be feasible for large scale "routine" measurements. Carbon isotope labeling is a related technique but, by itself, does not produce information about specific compounds. It alone cannot be used to determine whether growth or storage occurred.

Our theory suggests that a focus on shorter term experiments (e.g., diurnal and weekly time-scales) may be more fruitful as the sampling frequency may better match the dynamics. It also suggests that a focus on comparing constant environments or step changes in environments rather than dynamic environments may be easier to determine from limited experimental data. For instance, see Wiley et al., 2019 for a constant environment (with before and after type measurement); see Weber et al., 2018 for a step-like environment

changes (albeit not perfectly as the illuminated plants experienced a day-night cycle). Gibon, Bläsing, et al., 2004 present an example of detailed daily measurements and Gersony et al., 2020 and Tixier et al., 2018 present field experiments on diurnal variations in nonstructural carbohydrates. However, experiments to assess non-temporal patterns such as those in Körner, 2003 and Fig. 5.1 remain rare. This type of experiments may be easier to conduct given current limitations of experimental measurements.

The development of a mathematical description of nonstructural carbohydrate dynamics also addresses a need in applying the basic science of plant physiology to ecosystem modeling. As reviewed by Merganičová et al., 2019, many vegetation models, which form the core of many ecosystem models, lack a number of known processes regarding carbon allocation and often employ simplistic schemes that do not appear to be a correct description. We argue that the reason is in part that while many experiments seem to show more complex behavior than what models employ, a summary or description does not exist in mathematical form, and such mathematical formulations must exist to be employed in computer simulation. Given the results of Chapter 2, Chapter 4 discusses how this mathematical formulation translates to ecosystem modeling. However, our work is not the first to attempt such a translation as various models of carbon allocation and nonstructural carbohydrates have now been published.

Having a mathematical formulation is only part of the solution. First, a mathematical description of nonstructural carbohydrates must be compatible with ecosystem model. Second, and more critically, many questions in the basic science of nonstructural carbohydrate are yet to be resolved. Thus, it is not a mere problem of expressing the basic science in mathematical terms, but discovering what hypotheses form a good description of nonstructural carbohydrate dynamics. Moreover, limitations of current measurements mean that it is difficult to only "learn" patterns from data (such as by machine learning). In this aspect, nonstructural carbohydrate modeling is a microcosm of ecosystem modeling as ecosystem function involves many difficult-to-measure processes, the historical record is limited, and interest is focused on responses to climate change, which by its nature means the past may not predict the future.

The development of Chapter 2 provides some insight into solutions to these problems. Nonstructural carbohydrate supply and demand contain many processes, but much of the mathematical derivation holds under rather weak conditions. In essence, we can assume that the kinetics of supply and demand are such that the feedback creates a single stable fixed point per environment (and other parameters). In this manner, we can make hypotheses regarding the dynamical behavior which remain true (or approximately so) under various possible forms of kinetics. In Chapter 4, we explain how this method of analyzing nonstructural carbohydrate dynamics and its interaction yields insights into model behavior.

For instance, models invariably add some feedback to nonstructural carbohydrate supply and demand (usually demand) to keep simulations within acceptable bounds, but models differ significantly in how and to what degree. The CASSIA model (Schiestl-Aalto et al., 2015) and the SUGAR model (Jones et al., 2020) are a nice example pair. Both sets of authors analyze their respective models in terms of source-sink limited growth. Schiestl-Aalto et al., 2015 found that nonstructural carbohydrates could not mediate the source-driven growth or nonstructural carbohydrate dynamics because variations in photosynthesis did not propagate to growth, while the same variations in photosynthesis do propagate to growth in the SUGAR model (Jones et al., 2020); however, both sets of authors consider their models to simulate source-

driven nonstructural carbohydrates or source limited growth and sink-driven nonstructural carbohydrates or sink limited growth, and yet their models produce different results. We explain that the strength of the feedback differs significantly between the two models, despite similar sets of processes; we also argue that the presence of feedback is trivial as its absence leads to unphysical behavior. The question is not whether variations in photosynthesis create variations in nonstructural carbohydrates (especially starch), because they do, or whether variations in temperature creates variations in growth and respiration rates which in turn creates variations in nonstructural carbohydrates, because this is also true; the question is what feedbacks are present, what is the nature of the fixed points, and the convergence rate.

We also illustrate how this way of thinking can lead to an explanation for transient responses. For instance, the interaction between short-term and long-term relaxation times. We present a simple system that has a short-term carbon dioxide fertilization but is long-term limited by nitrogen. This result is consistent with certain observations from free air carbon dioxide enrichment experiments. Like with hysteresis, such differential responses could be common with long-term responses overriding short-term responses. This process is crucial for determining whether models fail to capture processes due to missing processes or misspecified ones. From the standpoint of theory, we have shown that carbon limitation and nitrogen limitation of forest growth rate have technical difficulties when not treated carefully.

To conclude, the present work makes a small contribution to the science of nonstructural carbohydrates in land plants. We have shown that a mathematical analysis can explain seemingly difficult to describe phenomena like hysteresis. We have shown that this analysis can be applied to experiments and could prove useful in their design and interpretation. We also have shown that because nonstructural carbohydrates sit at the interaction of all plant carbon-related processes, this idea may prove useful in explaining ecosystem function and responses to climate change. We hope that our fellow scientists will find this work thought-provoking and that it will prove useful in their own scientific endeavors.

Appendix A

Additional Notes on Chapter 2

A.1 Carbon Mass Fraction vs. Biomass Fraction

To clarify a possible source of confusion; in experiments, NSC mass and plant mass include all mass and not only the carbon mass. In theoretical calculations, tracking the carbon mass independent of other elements is convenient since doing so removes the dependence on the mass of other elements. Whether carbon or biomass is used matters little in practice as the corresponding conversion factor is typically close to unity. To demonstrate, the conversion factor is the ratio of NSC concentration in carbon mass fraction to NSC concentration in mass fraction; using the definition we see that the conversion factor is:

$$\text{conversion factor} = \frac{\text{carbon mass of NSC}}{\text{mass of NSC}} \div \frac{\text{carbon mass of plant}}{\text{mass of plant}} \approx 1$$

Plant biomass is $\approx$ 45% C by mass (Epstein, 1972, 2005; Ma et al., 2018) while by mass, starch is 42% C, sucrose 42% C, glucose 40% C, and fructose 40% C; so, the conversion factors are about 0.933 and 0.889, respectively. Although plant biomass does not have a constant carbon mass fraction, plants are mostly composed of carbohydrates which are roughly 40–45% C by mass so theoretical calculations in terms of carbon mass may be converted without accounting for other elements with small errors. This conversion is a smooth change of coordinates and has no effect on essential properties of the dynamics: e.g., fixed points, their eigenvalues, etc.

A.2 Full derivation of Equation 2.1

The amount of water in the bucket (Fig. 2.1a) can be measured in mass or concentration. Likewise, NSC concentrations are expressible as either mass or concentrations. Recall that if NSC mass is y kg carbon and for a plant with biomass m kg carbon, then the NSC concentration is $y = ms$ by definition (this definition differs from experimental measurements, see Appendix A.1). This definition holds for any NSC compound (sugars, starch, etc.). Differentiating with respect to time as rearranging to isolate $ds/dt = \dot{s}$

yields Equation (2.1).

$$\dot{y} = \frac{d}{dt}(ms) = m\dot{s} + s\dot{m} \implies \dot{s} = \frac{\dot{y}}{m} - s\frac{\dot{m}}{m}$$

It is also possible to express $\dot{s}$ in terms of structural and non-structural mass fraction. Let x be the amount of structural carbon biomass such that $m = x + y$, then substituting $\dot{m} = \dot{x} + \dot{y}$ into Equation (2.1) yields

$$\dot{s} = \frac{\dot{y}}{m}(1 - s) - s\frac{\dot{x}}{m}$$

Intuitively, the change in concentration is equal the changes in NSC mass and non NSC mass weighted by the current concentration. This formulation adds no additional insight not contained in Equation (2.1) but may prove useful in certain analyses. These equations are equally applicable to sugar, starch, or total NSC as they are statements about mass fractions only.

Intuitively, Equation (2.1) says change in starch concentration depends on two terms. The first $\dot{y}/m$ is the rate of net starch supply and demand relative to total mass—the per-mass rate of net starch mass change—while the second "dilution" term $s\dot{m}/m$ reflects the fact that processes which increase carbon biomass but not starch mass dilute the starch, lowering its concentration. Likewise, processes which increase both starch mass and biomass increase starch concentration but with necessarily diminishing returns as the starch concentration increases. With no other changes to plant mass, increasing starch mass at a rate of 1 kg per unit time increases starch concentration at a rate of $1 - s$ per unit time, meaning the rate of starch concentration increase decreases as starch concentrations increase. This feedback results from expressing dynamics in concentrations. Changing the size of the bucket affects the relative amount but not the absolute amount of water in the bucket (Fig. 2.1a), and the dilution term accounts for this change.

While Equation (2.1) contains no additional dynamical information beyond carbon mass balance, expressing mass balance in these terms scales units with mass (i.e., nondimensionalizing the units), facilitating the comparison of starch dynamics between 50 g saplings and 50 kg trees. Inserting equations for $\dot{y}$ and $\dot{m}$ into Equation (2.1) yields starch supply and demand relative to total mass. As a result, mass dynamics are implicit in starch dynamics of Equation (1) without loss of generality. In practice, one must calculate mass dynamics to determine the exact starch supply and demand rates relative to mass, but when relative changes in plant mass are small (i.e., small percent changes), the mass dynamics may be safely ignored (see Appendix A.8).

A.3 Full Derivation of Equation 2.2

To derive Equation (2.2) from (2.1), suppose a simple mass balance model. Let P be the rate of photosynthesis measured in kg C per year, let R be the rate of respiration, and let L be the rate of mass loss due to tissue loss (e.g., litter production). Let G be the rate of growth, defined as the conversion from NSC carbon mass to structural carbon mass.

$$\dot{y} = P - R - G$$

where we assume no NSC mass is lost in tissue loss (without loss of generality). In our analogy, this equation is the change in absolute water amount in the bucket (Fig. 2.1a). Note that G does not change the total mass, so the rate of change in total mass is

$$\dot{m} = P - R - L$$

This equation reflects how bucket's size changes in our analogy (Fig. 2.1a), necessary for calculating how concentrations change. Inserting these relations into Equation (2.1) yields

$$\dot{s} = \frac{P}{m}(1-s) - \frac{R}{m}(1-s) - \frac{G}{m} + s\frac{L}{m}$$

where all rates are now rates per dry mass: e.g. P/m is the photosynthetic rate per mass, R/m is the rate of respiration per mass, etc. In the main text, we set $A = P/m$ for ease of notation. We have not yet applied any assumptions beyond carbon mass balance. Note that any additional terms will have the form of one of the existing terms, depending on how the process affects NSC mass and on how the process affects total mass. If positive for both, then a new term will have the same form as photosynthesis $P/m\,(1-s)$; if negative for both, then it will the same as respiration$-R/m\,(1-s)$; if the term does not affect total mass, then it will have the same form as growth $-G/m$ (up to a change of sign); and if the term affects total mass but not NSC mass, then it have the same form as litter sL/m (up to a change of sign).

The first term we call the supply term, and it depends on the specific photosynthetic rate $A = P/m$ (rate of photosynthesis relative to mass; photosynthesized per kg biomass per time) weighted by $1-s$, reflecting the fact that photosynthesis increases NSC mass and total mass simultaneously and would appear twice in Equation (2.1) as part of $\dot{y}$ and $\dot{m}$; however, this dependence exists for stoichiometric reasons and does not imply that absolute photosynthetic rates vary with NSC mass in any way; however, such a dependence may be important but is not assumed here.

To derive equation (2.2), we must obtain some kind of feedback. Except for $P/m(1-s)$, we combine all other terms into a single term $D(s)$ which we call the demand rate. With the exception of the litter term (which is typically small), all terms other than photosynthesis reduce the NSC concentration.

$$\dot{s} = A(1-s) - D(s)$$

To generate a steady state, the demand rate must be a function of NSC concentrations; for reasons explained below, we must assume that additional dynamical information is not needed. All terms inside the demand rate must vanish for stoichiometric reasons when $s = 0$ as NSC is a reactant or substrate in those processes. This observation suggests that linearization about $s = 0$ is a useful simplification. Doing so yields Equation (2.2), thus, letting $D'(s) = \partial D/\partial s$ we have $D(s) = D(0) + D'(0)\,s + O(s^2)$ (Taylor series expansion) but $D(0) = 0$; let $U = D'(0)$ and substitute yields Equation (2). This definition makes the usage rate U well-defined for any possible demand function. Using big O notation:

$$\dot{s} = A(1-s) - D(s) = A(1-s) - Us + O\left(s^2\right)$$

Although not explicitly written, U is still allowed to depend on time, and this time-dependence captures the influence of the environment or other processes. This approximation improves as NSC concentrations s become low (asymptotically valid as $s \to 0$) and has been used in other studies to simplify calculations (e.g.Dewar, 1993).

This linearization greatly simplifies analysis, because it makes calculating the steady states (nullcline) and response rate trivial; it also enforces a single stable fixed point, without any additional work. To illustrate, suppose we use the demand function in Jones et al., 2020 where we convert the plant carbon expenditure (U in their notation) in their calculations by plant mass and substituting the structural and non-structural carbon mass in terms of total mass and concentration. Thus, we obtain:

$$\dot{s} = A\left(1-s\right) - \left(R_0 + \gamma G_0\right)\frac{\left(1-s\right)^2 s}{s + K_1\left(1-s\right)} - G_0\frac{\left(1-s\right)s}{s + K_2(1-s)}$$

Note that in their paper R_0 and G_0 depend on temperature. Although potentially more accurate, this expression is more complex and difficult to manipulate. If we apply the linearization about $s = 0$, then we obtain:

$$\dot{s} = A\left(1-s\right) - \left(\frac{R_0 + \gamma G_0}{K_1} + \frac{G_0}{K_2}\right)s$$

In our notation, $U = \left(\frac{R_0+\gamma G_0}{K_1} + \frac{G_0}{K_2}\right)$. One may verify the accuracy of this approximation (e.g., by comparing integral cures, fixed points, etc.), using the parameter values reported in Jones et al., 2020, and see that this approximation is quite good. Of course, additional accuracy should not be sacrificed for many calculations, but Equation (2.2) facilitates understanding why more complicated models behave the way they do.

A.4 Generality of Equation 2.2 and additional notes on dynamical system theory

The linearization used to derive Equation (2.2) is convenient, but one may wonder about its generality; under what circumstances would Equation (2.2) provide a poor description of NSC dynamics? To discuss this point, we must introduce several concepts from the mathematical theory of dynamical systems. This theory provides several techniques for analyzing how dynamical systems behave at long time-scales. The concepts of attractor, nullcline, and response rate come from this field, especially the geometric viewpoint. For more information about dynamical systems theory, Strogatz, 1994 is an excellent introduction, requiring little background of readers other than some multivariable calculus. Although less introductory, Wiggins, 1996 and Guckenheimer and Holmes, 1983 are excellent references for dynamical systems theory. For additional background on differential topology, see Lee, 2003.

In essence, the approach in Strogatz, 1994, Wiggins, 1996, and Guckenheimer and Holmes, 1983 is to use geometry and topology to determine the long-term behavior of a dynamical system and how that behavior varies with system parameters. As stated in the main text, we may visualize the set of starch

concentrations and times as a plane. We may then visualize the rate of change $\dot{s} = f(s)$ as a vector field; for each starch concentration, draw an arrow with pointing $\dot{s}$ units in the s-direction and 1 unit in the t-direction(see the streamplots Fig. 2.1c, d). As time passes, different initial concentrations are mapped to other concentrations; we visualize this mapping as the flow of water or stream (hence the name streamplot). Each streamline corresponds to an integral curve, that is the result of simulation from a particular starting position.

While the vector field defines a rate of change for all positions, the long-term behavior of most vector fields is a subset of all possible values. This set toward which the system eventually tends is called the attractor (or ω-limit set); its shape determines what the long-run behavior is like. For instance, if it is a point, then the system tends to a particular value and stays there. If it is a loop or curve, then the system will tend toward a particular periodic oscillation. More complex, fractal shapes give chaotic dynamics. Even when attractors have complex shapes, the vector field will have some fixed points (i.e., steady states, points s where $f(s) = 0$) which characterize its behavior; at these points, the system stops changing. Stable fixed points are attractors (vector field points inward at this point) while unstable fixed points are repulsors (vector field points outward at this point). In higher dimensions, fixed points can be neither attractor or repulsor, with attraction and repulsion changing with direction. Analytically, fixed points are classified using the eigenvalues and eigenvectors of the derivative of the vector field (i.e., its Jacobian). In the main text, the response rate is the one eigenvalue of the Jacobian. The Jacobian measures how the vector field changes around a point, and all interesting behavior occurs around fixed points.

Several theorems justify the assertion that all interesting behavior happens around fixed points. For instance, the "canonical form of vector field at regular points" theorem or Theorem 9.22 in Lee, 2003 effectively states that smooth vector fields near regular points (points which are not fixed) look like a set of parallel arrows. The Hartman-Grobman theorem states that around a fixed point, the flow of a vector field is homeomorphic to the flow of its linearization (i.e., using its Jacobian) if the real part of all eigenvalues is not zero (Theorem 1.3.1 in Guckenheimer and Holmes, 1983). In other words, the Hartman-Grobman effectively means that linearization captures the qualitative behavior around a fixed point. Furthermore, dynamical properties are conserved under smooth coordinate transformations, meaning that models describing the same dynamics can be expressed using different variables, units, or other changes in structure. Features such as the number of fixed points and whether they are attracting or repelling (i.e, their stability) are structurally stable meaning that they persist even when the vector field is perturbed by other vector fields (i.e., even when the model has errors in its representation of the true dynamics).

The stable manifold theorem (Theorem 1.3.1 in Guckenheimer and Holmes, 1983) and the center manifold theorem (Theorem 3.2.1 in Guckenheimer and Holmes, 1983; Theorem 1.1.3 in **Wiggins1996**) partition the space around a fixed point into a stable subspace (attracting), an unstable subspace (repelling), and a center subspace (either no motion or motion determined by higher order, nonlinear terms); these subspaces then extend to manifolds. Manifold means a smooth object like line, curve, surface, sphere, and so on. At long timescales, the dynamics remain dominated by the center manifold (if one exists). In many cases, an approximate center manifold exists if one stable subspace is much slower than another.

Most texts treat time-independent vector field whereas our model is time-dependent due to changing environmental conditions; however, we can add time as an additional geometric variable. For this reason, our model is not technically 1-dimensional despite only describing a single NSC pool. The streamplots in Fig. 2.1 show the 2D vector field. Note that no fixed points exist because time always flows forward; however, the time-dependence is an environmental dependence and does not reflect the intrinsic dynamics. Holding environmental conditions constant yields a 1-dimensional system whose dynamics contain the intrinsic response; for a constant environment, Equation (2.2) always has a single stable fixed point even as A and U vary. Over time, changes in the environment change that stable fixed point, but the system retains an attractor because the number and stability of fixed points never change. This feedback determines the intrinsic NSC response. In this sense, the regulation is simple despite generating complex dynamics.

With this brief summary of facts, we return to circumstances under which Equation (2.2) is a poor description of the dynamics. By the canonical form theorem and the Hartman-Grobman theorem, Equation (2.2)will have the same qualitative behavior as any other 1-dimensional system with a single steady state; however, the magnitude of lag and hysteresis may change. The Hartman-Grobman theorem only guarantees a homeomorphism that maps orbits onto orbits, but not necessarily with the same time parameterization (i.e., topological equivalence), hence differing amounts of hysteresis. However in this case, if the eigenvalue agrees $-(A+U) = f'(s^*)$ with another system, a coordinate transformation which converts one system into the other will exist; in fact, this relation may be used as an alternate definition for the usage rate U to ensure that Equation (2.2) agrees with another system up to coordinate transformation. Furthermore, a coordinate transformation that linearizes the system is possible; normal form theory may be used to solve for such coordinate transformations (**Wiggins1996**; Guckenheimer & Holmes, 1983). In principle, errors in Equation (2.2) can be corrected using a coordinate transformation under these conditions.

A.5 Additional discussion on the dynamics of sugar and starch partitioning

The derivation presented in Note S2-S3 treats sugars and starch together; however, the derivation can be modified to analyze how starch and sugar dynamics interact. This analysis helps identify under what conditions Equation (2) applies to starch dynamics.

Let x be the amount of sugars and let y be the amount of starch, then assume the following mass balance equations:

$$\frac{dx}{dt} = P - R - G - F + H \qquad = V_x(x,y) \tag{A.1}$$

$$\frac{dy}{dt} = F - H \qquad = V_y(x,y) \tag{A.2}$$

where F is the starch formation rate and H is the hydrolysis rate; P, R, G are photosynthesis, respiration, and growth, respectively. We can apply Equation (2.1) to re-express sugar and starch in terms of concen-

trations, but that is unnecessary (it corresponds to a change of coordinates). Roughly, the approximation we make is that $\dot{y} \approx P - R - G$ and $\dot{x} \approx 0$. We assume that this system has at most one fixed point (x^*, y^*) then consider the Jacobian of this system at this fixed point.

$$J = \begin{bmatrix} \frac{\partial V_x}{\partial x} & \frac{\partial V_x}{\partial y} \\ \frac{\partial V_y}{\partial x} & \frac{\partial V_y}{\partial y} \end{bmatrix}$$

By the center manifold theorem, the dynamics around this fixed point are classified by the eigenvalues λ_1, λ_2. If $\mathrm{Re}\,(\lambda_i) \neq 0$, then the dynamics along the corresponding eigenvector u_i looks like $u_i e^{t\lambda_i}$; $\mathrm{Re}\,(\lambda_i) < 0$ indicates a stable direction (the dynamics look like a sink along this axis); while $\mathrm{Re}\,(\lambda_i) > 0$ indicates an unstable direction. If $\mathrm{Re}\,(\lambda_i) = 0$, then the Jacobian does not provide enough information to determine stability; higher order terms determine stability, but the dynamics will be strictly slower than exponential. If a center manifold exists at this fixed point, then the dynamics will resemble the dynamics restricted to the center manifold at long time-scales. The dynamics on the center manifold have lower dimension; in this case, our 2-dimensional coupled system becomes identical to a 1-dimensional system at long time scales if there is a center manifold. As before, we assume that external variation in time does not change these properties. However, we do not need to assume an exact center manifold, if both eigenvalues have negative real parts, but one is much closer to zero than the other, then the smaller eigenvalue corresponds to an approximate center manifold (approximate center manifolds are a geometric version of singular perturbation theory). The presence of an approximate center manifold corresponds to a time-scale separation (the smaller eigenvalue corresponds to the long time scale). One can then specify positions on the center manifold (and therefore dynamics along the center manifold) using sugar, starch, or total NSC concentrations.

For simplicity, one can assume that starch synthesis and hydrolysis happen at rates much greater than photosynthesis, respiration, and growth. Doing so causes the approximate center manifold to align closely the starch direction, so that the center manifold is defined by

$$\frac{dx}{dt} = P - R - G - F + H = V_x\,(x, y) = 0$$

While dynamics along the center manifold correspond to

$$\frac{dy}{dt} = F - H = V_y\,(x, y) = P - R - G$$

If certain feedbacks in starch synthesis and hydrolysis keep sugar concentrations near a constant value, then an approximate center manifold must exist.

A.6 Additional discussion on spatial NSC dynamics

Experimental observations of NSC dynamics often come from individual tissues and do not represent whole-plant NSC concentrations. Observed dynamics may then reflect NSC translocation in addition to

photosynthesis, respiration, and growth. The derivation in Appendix A.3 may be applied to the starch dynamics of an individual tissue, if translocation is included; however, a 1D model cannot represent differences in dynamics across tissues. Multiple pools are needed, but mass balance is straightforward to apply; effectively, one assumes a network of buckets that exchange water rather than an individual bucket. The dynamics of how these buckets exchange water determines the spatial dynamics in addition to whole-plant balance processes; the correct dynamics depends on phloem function, loading, and unloading.

As with sugar partitioning, several reasons justify ignoring spatial dynamics as long as the whole-plant starch is the observable of interest (and certain time-scale approximations hold). The previous section describes how a coupled system of sugar and starch dynamics may be reduced to a 1-dimensional system using an approximate center manifold. Likewise, a time-scale separation in which the NSC translocation occurs faster than seasonal photosynthesis, respiration, and growth rates means that spatial dynamics come to steady state faster than seasonal variations perturb that steady state, meaning that tracking spatial distribution of NSC is redundant information. If that steady state is uniform across the plant body (e.g., Potkay et al., 2022; Thornley, 1991) then seasonal variations would be similar across the plant body; differences in metabolism or steady state could create non-uniform gradients and differences in starch dynamics by organ, but the overall rate of growth and starch dynamics remain well-approximated by Equation (2.2) if the system reduces to a 1-dimensional approximate center manifold.

To illustrate, let y_1 and y_2 be the amount of starch in two different organs (e.g., leaf and root); we then suppose the following mass balance equations:

$$\dot{y}_1 = P_1 - R_1 - G_1 - T_{1\to 2} \tag{A.3}$$

$$\dot{y}_2 = P_2 - R_2 - G_2 + T_{1\to 2} \tag{A.4}$$

The rate of net transport is $T_{1\to 2}$. Note that $P_2 = 0$ if it is a non-photosynthetic tissue. As before, we can convert this system to concentrations. Again, we also assume a single fixed point then consider the Jacobian J. If an eigenvalue is much closer to zero than all others, it corresponds to an approximate center manifold. We may then parameterize the center manifold using whole-plant starch is $y = y_1 + y_2$. If the center manifold points along this line, we end up with the above 2-dimensional dynamical system projected to one dimension:

$$\dot{y} = P_1 + P_2 - (R_1 + R_2) - (G_1 + G_2)$$

Transport disappears from mass balance because it conserves the amount of starch. Making transport much faster than the whole-plant carbon balance will lead to this situation; otherwise dynamics along the center manifold may not correspond exactly to whole-plant carbon imbalance (some transport terms will remain) but the system still simplifies to one-dimension.

A.7 Calculating the limit cycle in simulations of Equation 2.2

If A and U are periodic functions of time, solutions to Equation (2.2) tend to a stable limit cycle. These solutions to Equation (2.2) may be expressed in the following integral representation. We set $r(t) = A(t) + U(t)$ and define $R(t) = \int_0^t r(t)\,dt$, then:

$$s(t) = e^{-R(t)}\left[C + \int_0^t e^{R(\tau)} A(\tau)\,d\tau\right]$$

The integral constant C depends on the initial value; setting $C = 0$ and calculating the resulting integral yields the limit cycle. In simulations, we calculate this integral numerically using several applications of the discrete Fast Fourier Transform (FFT) algorithm; we describe our calculation procedure below. Note while the integral representation is still valid for non-periodic A and U, our method only applies to periodic A and U. This method was used to determine the exact NSC concentrations in all simulations. This algorithm quickly determines the limit cycle. We verified our implementation using standard numerical integration algorithm (backwards differentiation formula).
To calculate the limit cycle of Equation (2.2) with periodic A and U using the above integral representation:

1. Select N equally spaced time-points: in years, $t_n = n/N$ for $n \in \{0, \ldots, N-1\}$.
2. Sample each function: $A_n = A(t_n), U_n = U(t_n)$
3. Let $r_n = A_n + U_n$ and compute its FFT: $\hat{r}_k = \mathcal{F}[r_n]$
4. Set $\bar{r} = \hat{r}_0$; this is the time-average of r.

   Depending on the implementation of FFT used, a normalization may be required. For instance, we used the python library `numpy.fft` (version 1.19.4) to compute the FFT and with default settings, $\bar{r} = \hat{r}_0/N$ to normalize the FFT by signal length.
5. Integrate $r - \bar{r}$ by $\hat{R}_k = \hat{r}_k/(ik\omega)$ for $k > 0$. For $k = 0$, set $\hat{R}_0 = 0$.

   A and U are periodic, so antiderivatives of $\int r(t)\,dt$ are periodic except for the average:

   $$\int r(t)\,dt = \bar{r}t + \int (r(t) - \bar{r})\,dt$$

   Note sign conventions for the FFT differ, so exchanging $i \mapsto -i$ in the appropriate formulae may be necessary for certain implementations. The fundamental angular frequency ω sets the time-scale depends on the time units but $\omega = 2\pi$ if t is measured in years.
6. Compute the IFFT (inverse transform) of $\hat{R}_k$ to obtain $R_n = \mathcal{F}^{-1}\left[\hat{R}_k\right]$.
7. Set $G_n = A_n e^{R_n}$ and then compute its FFT: $\hat{G}_k = \mathcal{F}[G_n]$.

8. Set $\hat{u}_k = \hat{G}_k / (\bar{r} + ik\omega)$ (convolution theorem).

9. Finally, compute the IFFT of $\hat{u}_k$ and multiply the result by e^{R_n} to obtain the NSC concentration (in mass fraction):

$$s_n = e^{-R_n} \mathcal{F}^{-1} [\hat{u}_k] = e^{-R_n} \mathcal{F}^{-1} \left[\frac{\hat{G}_k}{\bar{r} + ik\omega} \right]$$

A.8 Mass invariant specific-photosynthetic rate is a good approximation when mass change is small

In the main text, we analyzed seasonal starch dynamics without consideration of how simultaneous variations in plant mass might influence those dynamics. We justified this approach with the assumption that specific photosynthetic rates and usage rates only vary due to changing environmental conditions and not changes in plant size; however, we proceeded to present evidence that specific photosynthetic rates likely decline with increasing plant mass which contradicts this assumption. Here, we discuss when this assumption remains asymptotically valid.

The assumption is still approximately true over sufficiently short periods of time and has precedents in other works (Dewar, 1993). Without loss of generality, we perform an asymptotic analysis for photosynthesis only. Suppose that $P(t, m)$ is the photosynthetic rate (units mass/time) as a function of time (e.g., environmental changes) and plant mass; we note that $A = P/m$ for the specific photosynthetic rate in the main text. The assumption we wish to justify is that $P(t, m)/m = P(t, m_0)/m_0$ where $m_0 = m(t_0)$ is the plant mass at a specific time. In other words, the specific photosynthetic rate scales exactly with plant mass. Performing a first-order Taylor series expansion on $P(t, m)/m$ in m where we let $P' = \partial P / \partial m$:

$$\frac{P(t, m)}{m} = \frac{P(t, m_0)}{m_0} + \left(\frac{P'(t, m_0)}{m_0} - \frac{P(t, m_0)}{m_0^2} \right) (m - m_0) + \dots$$

This second term must be small for a valid approximation, and rearranging we see that this is the case if $m/m_0 \approx 1$ over the time period of the analysis.

$$\frac{P(t, m)}{m} = \frac{P(t, m_0)}{m_0} + \left(P'(t, m_0) - \frac{P(t, m_0)}{m_0} \right) \left(\frac{m - m_0}{m_0} \right) + \dots$$

Using big O asymptotic notation:

$$\frac{P(t, m)}{m} = \frac{P(t, m_0)}{m_0} + O\left(\frac{m - m_0}{m_0} \right)$$

The error in this approximation scales with the percent change in plant mass $(m - m_0)/m_0$.

Table A.1: Time average values used in Fig.2.3

Biome	$\bar{A}$
Evergreen forest	0.0855
Deciduous forest	0.1124
Mixed forest	0.11
Shrubland	0.1563
Savanna	0.3638
Grassland	1.699
Cropland	1.875

Alternatively, consider Equation (2.1):

$$\dot{s} = \frac{\dot{y}}{m} - s\frac{\dot{m}}{m}$$

If $\dot{m}/m$ is small, then above equations reduces approximately to $\dot{s} = \dot{y}/m$, and NSC concentrations reflect NSC mass dynamics. The relative mass increment $\dot{m}/m$ is small when mass dynamics are near their fixed point, which corresponds to canopy trees near their maximal size. Additionally, mass dynamics tend to be slow (longer response times) relative to NSC dynamics such that NSC dynamics approach equilibrium much faster than mass dynamics; this time-separation is easier to verify in simple models (Thornley, 2011). Therefore, a version of center manifold reduction applies here. In that case, the mass dynamics correspond to the approximate center manifold while the NSC dynamics form motion along a stable manifold.

A.9 Simulation Details

In this section, we describe the exact functions for A and U used to create each figure.

A.9.1 Scenario 1: Fig. 2.3

Specific photosynthetic rates A for Fig. 2.3 in the main text was produced using the GPP estimates by biome in Fig. 7a from Xiao et al., 2010. We fit a smoothed periodic cubic spline to the GPP estimates, call it $f\left(t\right)$. The smoothed periodic cubic spline was rescaled so that its time-average $\bar{A}$ matches the corresponding biome in Table 1 based on data from Saugier et al., 2001 and presented in Table 6.6 from Chapin et al., 2011; however, the list of biomes is not the same and we combined certain biomes. Table A.1 gives the values used in Fig. 2.3. Let $\bar{f} = \int_0^1 f\left(t\right) dt$ denote the time-average of the cubic splines for a

year. Thus, specific photosynthetic rate was:

$$A(t) = \frac{\bar{A}}{\bar{f}} f(t)$$

While U is constant, it differs by biome to keep NSC concentrations around 10%. Let $\bar{s} = 0.1$ be the target NSC concentration, then

$$U = \frac{1 - \bar{s}}{\bar{s}} \bar{A} = 9\bar{A}$$

A.9.2 Scenario 1: Fig. 2.4

Specific photosynthetic rates A for Fig. 2.4 in the main text was produced using a clear sky model for seasonal variation in light, based on Landsberg, 2011. We assume photosynthesis (and thus specific photosynthetic rates) has a saturating light response given as:

$$A = \frac{\alpha\beta I A_{\max}}{\alpha\beta I + A_{\max}}$$

where $\alpha = 0.1$, $A_{\max} = 0.4$, and $\beta = 3600 \times 24 \times 10^{-6}$. The coefficient β converts units J s^{-1} m^{-2} to MJ d^{-1} m^{-2} so that I is measured in units J s^{-1} m^{-2}. We used an estimate of the daily average irradiance I to eliminate daily variations in irradiance. Seasonal variations in irradiance are based on variation in the sun's position in the sky (solar declination and latitude on Earth).

$$I = I_c \underbrace{[1 + 0.033\cos(2\pi t)]}_{\text{orbital variation}} \underbrace{[H \sin\delta \sin\phi + \cos\delta \cos\phi \sin H]}_{\text{daily average cosine of zenith}}$$

Where δ is the solar declination, ϕ is latitude, and H is the hour angle of sunrise/sunset; time t is measured in years. We set $I = 0$ whenever the above value is less than zero.

$$\cos H = \text{clip}(-\tan\delta \tan\phi)$$

The argument of the clip function can be outside the range of the cosine (corresponding to latitudes and seasons when the sun never sets or never rises) so the clip function restricts the range to $[-1, 1]$.

$$\text{clip}(x) = \min[1, \max(-1, x)]$$

Seasonal variation in solar declination was assumed to be:

$$\sin\delta = -0.4\cos\left[2\pi\left(t + \frac{10}{365.24}\right)\right]$$

While U is constant, it differs by latitude to keep NSC concentrations around 10%. If $\bar{s} = 0.1$ be the target NSC concentration, then

$$U = \frac{1-\bar{s}}{\bar{s}}\bar{A} = 9\bar{A}$$

A.9.3 Scenario 2: Fig. 2.5

The seasonal variation in U in Fig. 2.5 is given by

$$U = 0.1 + \exp\left[-\alpha\cos\left(2\pi\left(t + \frac{10}{365.24}\right)\right)\right]$$

where the amplitude α was varied to increase the seasonal variation. We used $\alpha = 1.04$, 2.00, 2.83, and 3.46 for Fig. 2.5a-d, respectively. While A is constant, it was adjusted to keep NSC concentrations around 10%. If $\bar{s} = 0.1$ be the target NSC concentration and $\bar{U}$ as the annual average U:

$$A = \frac{\bar{s}}{1-\bar{s}}\bar{U} = 19\bar{U}$$

A.9.4 Scenario 3: Fig. 2.6

Specific photosynthetic rates A for Fig. 2.6 was produced using a clear sky model for seasonal variation in light, based on Landsberg, 2011; it is the same as in Fig. 2.4.

$$U = U_0 + 2\alpha\frac{\text{expit}\,(z) - 0.5}{\text{expit}\,(1) - \text{expit}\,(-1)} \qquad \text{where} \quad z = \cos\left(2\pi\left(t-\theta\right)\right)$$

where U_0, α, and θ roughly correspond to the average, amplitude, and phase respectively. The expit function is

$$\text{expit}\,(x) = \frac{1}{1+e^{-x}}$$

For Fig. 2.6, we set $U_0 = 19\bar{A}$ and $\alpha = 19\,(2/3)\,\bar{A}$ where $\bar{A}$ is the average specific photosynthetic rate $\bar{A}$. The phase θ is varied from 0 for Fig. 2.6b,f,j; 0.25 for Fig. 2.6c,g,k; and 0.5 for Fig. 2.6d,h,l.

A.9.5 Fig. 2.7

To generate Fig. 2.7, we used the following A and U where r was varied between 4, 2, 1, 0.5, and 0.1 to create the same nullcline with different response rates.

$$A = r\,(0.35\text{expit}\,(z)) \qquad \text{where} \quad z = -5\cos\left(2\pi t\right)$$

$$U = r\,(1 + 3.15\text{expit}\,(z)) \qquad \text{where} \quad z = -5\cos\left(2\pi t\right)$$

Where the expit function is

$$\operatorname{expit}(x) = \frac{1}{1 + e^{-x}}$$

Bibliography

Adams, H. D., Zeppel, M. J. B., Anderegg, W. R. L., Hartmann, H., Landhäusser, S. M., Tissue, D. T., Huxman, T. E., Hudson, P. J., Franz, T. E., Allen, C. D., Anderegg, L. D. L., Barron-gafford, G. A., Beerling, D. J., Breshears, D. D., Brodribb, T. J., Bugmann, H., Cobb, R. C., Collins, A. D., Dickman, L. T., … Mcdowell, N. G. (2017). A multi-species synthesis of physiological mechanisms in drought-induced tree mortality. *Nature Ecology & Evolution*, *1*(9), 1285–1291. https://doi.org/10.1038/s41559-017-0248-x

Ainsworth, E. A., & Long, S. P. (2005). What have we learned from 15 years of free-air CO2 enrichment (FACE)? a meta-analytic review of the responses of photosynthesis, canopy properties and plant production to rising CO2. *New Phytologist*, *165*(2), 351–372. https://doi.org/10.1111/j.1469-8137.2004.01224.x

Allen, M. T., Prusinkiewicz, P., & Dejong, T. M. (2005). Using l-systems for modeling source-sink interactions, architecture and physiology of growing trees: The l-peach model. *New Phytologist*, *166*(3), 869–880. https://doi.org/10.1111/j.1469-8137.2005.01348.x

Anderegg, W. R. L., & Anderegg, L. D. L. (2013). Hydraulic and carbohydrate changes in experimental drought-induced mortality of saplings in two conifer species. *Tree Physiology*, *33*(3), 252–260. https://doi.org/10.1093/treephys/tpt016

Angeli, D. (2009). A tutorial on chemical reaction network dynamics. *European Journal of Control*, *15*(3-4), 398–406. https://doi.org/10.3166/ejc.15.398-406

Arora, V. K., Boer, G. J., Friedlingstein, P., Eby, M., Jones, C. D., Christian, J. R., Bonan, G., Bopp, L., Brovkin, V., Cadule, P., Hajima, T., Ilyina, T., Lindsay, K., Tjiputra, J. F., & Wu, T. (2013). Carbon–concentration and carbon–climate feedbacks in CMIP5 earth system models. *Journal of Climate*, *26*(15), 5289–5314. https://doi.org/10.1175/jcli-d-12-00494.1

Aspinwall, M. J., King, J. S., Booker, F. L., & Mckeand, S. E. (2011). Genetic effects on total phenolics, condensed tannins and non-structural carbohydrates in loblolly pine (pinus taeda l.) needles. *Tree Physiology*, *31*(8), 831–842. https://doi.org/10.1093/treephys/tpr073

Aubrey, D. P., Mortazavi, B., O'brien, J. J., Mcgee, J. D., Hendricks, J. J., Kuehn, K. A., Teskey, R. O., & Mitchell, R. J. (2012). Influence of repeated canopy scorching on soil CO2 efflux. *Forest Ecology and Management*, *282*, 142–148. https://doi.org/10.1016/j.foreco.2012.06.041

Aubrey, D. P., & Teskey, R. O. (2018). Stored root carbohydrates can maintain root respiration for extended periods. *New Phytologist*, *218*(1), 142–152. https://doi.org/10.1111/nph.14972

Babst, F., Friend, A. D., Karamihalaki, M., Wei, J., Arx, G. V., Papale, D., & Peters, R. L. (2021). Modeling ambitions outpace observations of forest carbon allocation. *Trends in Plant Science*, *26*(3), 210–219. https://doi.org/10.1016/j.tplants.2020.10.002

Baysdorfer, C., & Robinson, J. M. (1985). Sucrose and starch synthesis in spinach plants grown under long and short photosynthetic periods. *Plant Physiology*, *79*(3), 838–842. https://doi.org/10.1104/pp.79.3.838

Beer, C., Reichstein, M., Tomelleri, E., Ciais, P., Jung, M., Carvalhais, N., Rödenbeck, C., Arain, M. A., Baldocchi, D., Bonan, G. B., Bondeau, A., Cescatti, A., Lasslop, G., Lindroth, A., Lomas, M., Luyssaert, S., Margolis, H., Oleson, K. W., Roupsard, O., … Papale, D. (2010). Terrestrial gross carbon dioxide uptake: Global distribution and covariation with climate. *Science*, *329*(5993), 834–838. https://doi.org/10.1126/science.1184984

Blumstein, M., Gersony, J., Martınez-vilalta, J., & Sala, A. (2023). Global variation in nonstructural carbohydrate stores in response to climate. *Global Change Biology*. https://doi.org/10.1111/gcb.16573

Blumstein, M., & Hopkins, R. (2021). Adaptive variation and plasticity in non-structural carbohydrate storage in a temperate tree species. *Plant, Cell & Environment*, *44*(8), 2494–2505. https://doi.org/10.1111/pce.13959

Blumstein, M., Sala, A., Weston, D. J., Holbrook, N. M., & Hopkins, R. (2022). Plant carbohydrate storage: Intra- and inter-specific trade-offs reveal a major life history trait. *New Phytologist*, *235*(6), 2211–2222. https://doi.org/10.1111/nph.18213

Bonan, G. B. (2008). Forests and climate change: Forcings, feedbacks, and the climate benefits of forests. *Science*, *320*(5882), 1444–1449. https://doi.org/10.1126/science.1155121

Brännström, Å., Johansson, J., & Festenberg, N. V. (2013). The hitchhiker's guide to adaptive dynamics. *Games*, *4*(3), 304–328. https://doi.org/10.3390/g4030304

Burrows, S. M., Maltrud, M., Yang, X., Zhu, Q., Jeffery, N., Shi, X., Ricciuto, D., Wang, S., Bisht, G., Tang, J., Wolfe, J., Harrop, B. E., Singh, B., Brent, L., Baldwin, S., Zhou, T., Cameron-smith, P., Keen, N., Collier, N., … Leung, L. R. (2020). The DOE e3sm v1.1 biogeochemistry configuration: Description and simulated ecosystem-climate responses to historical changes in forcing. *Journal of Advances in Modeling Earth Systems*, *12*(9). https://doi.org/10.1029/2019ms001766

Bustan, A., Avni, A., Lavee, S., Zipori, I., Yeselson, Y., Schaffer, A. A., Riov, J., & Dag, A. (2011). Role of carbohydrate reserves in yield production of intensively cultivated oil olive (*o*lea europaea l.) trees. *Tree Physiology*, *31*, 519–530.

Buysse, J., & Merckx, R. (1993). An improved colorimetric method to quantify sugar content of plant tissue. *Journal of Experimental Botany*, *44*(267), 1627–1629. https://doi.org/10.1093/jxb/44.10.1627

Cannell, M. G. R., & Dewar, R. C. (1994). Carbon allocation in trees: A review of concepts for modelling. In *Advances in ecological research* (pp. 59–104). Elsevier. https://doi.org/10.1016/s0065-2504(08)60213-5

Chapin, F. S., Matson, P. A., & Vitousek, P. (2011, September 2). *Principles of terrestrial ecosystem ecology*. Springer New York. https://www.ebook.de/de/product/19111184/f_stuart_chapin_iii_pamela_a_matson_peter_vitousek_principles_of_terrestrial_ecosystem_ecology.html

Chapin, F. S., Schulze, E. D., & Mooney, H. A. (1990). The ecology and economics of storage in plants. *Annual review of ecology and systematics*, *21*(1), 423–447. https://doi.org/10.1146/annurev.es.21.110190.002231

Chiariello, N., & Roughgarden, J. (1984). Storage allocation in seasonal races of an annual plant: Optimal versus actual allocation. *Ecology*, *65*(4), 1290–1301. https://doi.org/10.2307/1938334

Cho, N., Kang, S., Agossou, C., Kim, E., & Lim, J.-h. (2022). Modeling temporal variations of non-structural carbohydrate (NSC) storages across biomes. *Forest Ecology and Management*, *508*, 120033. https://doi.org/10.1016/j.foreco.2022.120033

Chow, P. S., & Landhausser, S. M. (2004). A method for routine measurements of total sugar and starch content in woody plant tissues. *Tree Physiology*, *24*(10), 1129–1136. https://doi.org/10.1093/treephys/24.10.1129

Chung, Y., Gelman, A., Rabe-Hesketh, S., Liu, J., & Dorie, V. (2015). Weakly informative prior for point estimation of covariance matrices in hierarchical models. *Journal of Educational and Behavioral Statistics*, *40*(2), 136–157. https://doi.org/10.3102/1076998615570945

Cohen, D. (1966). Optimizing reproduction in a randomly varying environment. *Journal of Theoretical Biology*, *12*(1), 119–129. https://doi.org/10.1016/0022-5193(66)90188-3

Cohen, D. (1971). Maximizing final yield when growth is limited by time or by limiting resources. *Journal of Theoretical Biology*, *33*(2), 299–307. https://doi.org/10.1016/0022-5193(71)90068-3

Collins, A. D., Ryan, M. G., Adams, H. D., Dickman, L. T., Garcia-forner, N., Grossiord, C., Powers, H. H., Sevanto, S., & Mcdowell, N. G. (2021). Foliar respiration is related to photosynthetic, growth and carbohydrate response to experimental drought and elevated temperature. *Plant, Cell & Environment*, *44*(12), 3853–3865. https://doi.org/10.1111/pce.14183

Daudet, F., Lacointe, A., Gaudillère, J., & Cruiziat, P. (2002). Generalized münch coupling between sugar and water fluxes for modelling carbon allocation as affected by water status. *Journal of Theoretical Biology*, *214*(3), 481–498. https://doi.org/10.1006/jtbi.2001.2473

Davidson, A. M., Le, S. T., Cooper, K. B., Lange, E., & Zwieniecki, M. A. (2021). No time to rest: Seasonal dynamics of non-structural carbohydrates in twigs of three mediterranean tree species suggest year-round activity. *Scientific Reports*, *11*(1). https://doi.org/10.1038/s41598-021-83935-1

De Kauwe, M. G., Medlyn, B. E., Zaehle, S., Walker, A. P., Dietze, M. C., Wang, Y.-p., Luo, Y., Jain, A. K., El-masri, B., Hickler, T., Wårlind, D., Weng, E., Parton, W. J., Thornton, P. E., Wang, S., Prentice, I. C., Asao, S., Smith, B., Mccarthy, H. R., … Norby, R. J. (2014). Where does the carbon go? a model-data intercomparison of vegetation carbon allocation and turnover processes at two temperate forest free-air CO2enrichment sites. *New Phytologist*, *203*(3), 883–899. https://doi.org/10.1111/nph.12847

De Schepper, V., & Steppe, K. (2010). Development and verification of a water and sugar transport model using measured stem diameter variations. *Journal of Experimental Botany*, *61*(8), 2083–2099. https://doi.org/10.1093/jxb/erq018

Dewar, R. C. (1993). A root-shoot partitioning model based on carbon-nitrogen-water interactions and munch phloem flow. *Functional Ecology*, *7*(3), 356. https://doi.org/10.2307/2390216

Dewar, R. C. (2009). Maximum entropy production as an inference algorithm that translates physical assumptions into macroscopic predictions: Don't shoot the messenger. *Entropy*, *11*(4), 931–944. https://doi.org/10.3390/e11040931

Dietze, M. C., Sala, A., Carbone, M. S., Czimczik, C. I., Mantooth, J. A., Richardson, A. D., & Vargas, R. (2014). Nonstructural carbon in woody plants. *Annual Review of Plant Biology*, *65*(1), 667–687. https://doi.org/10.1146/annurev-arplant-050213-040054

Dinant, S. (2008). Phloème, transport interorgane et signalisation à longue distance. *Comptes Rendus Biologies*, *331*(5), 334–346. https://doi.org/10.1016/j.crvi.2008.03.001

Dubois, M., Gilles, K. A., Hamilton, J. K., Rebers, P. A., & Smith, F. (1956). Colorimetric method for determination of sugars and related substances. *Analytical Chemistry*, *28*(3), 350–356. https://doi.org/10.1021/ac60111a017

Enquist, B. J., & Niklas, K. J. (2002). Global allocation rules for patterns of biomass partitioning in seed plants. *Science*, *295*(5559), 1517–1520. https://doi.org/10.1126/science.1066360

Epstein, E. (1972). *Mineral nutrition of plants: Principles and perspectives*. New York, Wiley.

Epstein, E. (2005). *Mineral nutrition of plants : Principles and perspectives*. Sunderland, Mass, Sinauer Associates.

Farquhar, G. D., Caemmerer, S. V., & Berry, J. A. (1980). A biochemical model of photosynthetic CO2 assimilation in leaves of c3 species. *Planta*, *149*(1), 78–90. https://doi.org/10.1007/bf00386231

Fatichi, S., Leuzinger, S., & Körner, C. (2014). Moving beyond photosynthesis: From carbon source to sink-driven vegetation modeling. *New Phytologist*, *201*(4), 1086–1095. https://doi.org/10.1111/nph.12614

Fatichi, S., Pappas, C., Zscheischler, J., & Leuzinger, S. (2019). Modelling carbon sources and sinks in terrestrial vegetation. *New Phytologist*, *221*(2), 652–668. https://doi.org/10.1111/nph.15451

Fenichel, N. (1979). Geometric singular perturbation theory for ordinary differential equations. *Journal of Differential Equations*, *31*(1), 53–98. https://doi.org/10.1016/0022-0396(79)90152-9

Field, C. B., Behrenfeld, M. J., Randerson, J. T., & Falkowski, P. (1998). Primary production of the biosphere: Integrating terrestrial and oceanic components. *Science*, *281*(5374), 237–240. https://doi.org/10.1126/science.281.5374.237

Fondy, B. R., & Geiger, D. R. (1985). Diurnal changes in allocation of newly fixed carbon in exporting sugar beet leaves. *Plant Physiology*, *78*(4), 753–757. https://doi.org/10.1104/pp.78.4.753

Foster, T. E., Schmalzer, P. A., & Fox, G. A. (2014). Timing matters: The seasonal effect of drought on tree growth. *The Journal of the Torrey Botanical Society*, *141*(3), 225–241. https://doi.org/10.3159/torrey-d-13-00060.1

Fox, T. C., & Geiger, D. R. (1984). Effects of decreased net carbon exchange on carbohydrate metabolism in sugar beet source leaves. *Plant Physiology*, *76*(3), 763–768. https://doi.org/10.1104/pp.76.3.763

Franklin, O., Johansson, J., Dewar, R. C., Dieckmann, U., Mcmurtrie, R. E., Brannstrom, A., & Dybzinski, R. (2012). Modeling carbon allocation in trees: A search for principles. *Tree Physiology*, *32*(6), 648–666. https://doi.org/10.1093/treephys/tpr138

Franklin, O., Harrison, S. P., Dewar, R., Farrior, C. E., Brännström, Å., Dieckmann, U., Pietsch, S., Falster, D., Cramer, W., Loreau, M., Wang, H., Mäkelä, A., Rebel, K. T., Meron, E., Schymanski, S. J., Rovenskaya, E., Stocker, B. D., Zaehle, S., Manzoni, S., … Prentice, I. C. (2020). Organizing principles for vegetation dynamics. *Nature Plants*, *6*(5), 444–453. https://doi.org/10.1038/s41477-020-0655-x

Friedlingstein, P., Meinshausen, M., Arora, V. K., Jones, C. D., Anav, A., Liddicoat, S. K., & Knutti, R. (2014). Uncertainties in CMIP5 climate projections due to carbon cycle feedbacks. *Journal of Climate*, *27*(2), 511–526. https://doi.org/10.1175/jcli-d-12-00579.1

Furze, M. E., Huggett, B. A., Aubrecht, D. M., Stolz, C. D., Carbone, M. S., & Richardson, A. D. (2019). Whole-tree nonstructural carbohydrate storage and seasonal dynamics in five temperate species. *New Phytologist*, *221*(3), 1466–1477. https://doi.org/10.1111/nph.15462

Gabry, J., & Veen, D. (2022). *Shinystan: Interactive visual and numerical diagnostics and posterioranalysis for bayesian models* [R package version 2.6.0]. R package version 2.6.0. https://CRAN.R-project.org/package=shinystan

Galiano, L., Martínez-vilalta, J., & Lloret, F. (2011). Carbon reserves and canopy defoliation determine the recovery of scots pine 4 yr after a drought episode. *New Phytologist*, *190*(3), 750–759. https://doi.org/10.1111/j.1469-8137.2010.03628.x

Galvez, D. A., Landhausser, S. M., & Tyree, M. T. (2011). Root carbon reserve dynamics in aspen seedlings: Does simulated drought induce reserve limitation? *Tree Physiology*, *31*(3), 250–257. https://doi.org/10.1093/treephys/tpr012

Galvez, D. A., Landhäusser, S. M., & Tyree, M. T. (2013). Low root reserve accumulation during drought may lead to winter mortality in poplar seedlings. *New Phytologist*, *198*(1), 139–148. https://doi.org/10.1111/nph.12129

Gao, S., Liu, R., Zhou, T., Fang, W., Yi, C., Lu, R., Zhao, X., & Luo, H. (2018). Dynamic responses of tree-ring growth to multiple dimensions of drought. *Global Change Biology*, *24*(11), 5380–5390. https://doi.org/10.1111/gcb.14367

Gelman, A., Carlin, J. B., Stern, H. S., Dunson, D. B., Vehtari, A., & Rubin, D. B. (2014). *Bayesian data analysis*. CRC Press.

Gersony, J. T., Hochberg, U., Rockwell, F. E., Park, M., Gauthier, P. P. G., & Holbrook, N. M. (2020). Leaf carbon export and nonstructural carbohydrates in relation to diurnal water dynamics in mature oak trees. *Plant Physiology*, *183*(4), 1612–1621. https://doi.org/10.1104/pp.20.00426

Gibon, Y., Blaesing, O. E., Hannemann, J., Carillo, P., Höhne, M., Hendriks, J. H., Palacios, N., Cross, J., Selbig, J., & Stitt, M. (2004). A robot-based platform to measure multiple enzyme activities in arabidopsis using a set of cycling assays: Comparison of changes of enzyme activities and

transcript levels during diurnal cycles and in prolonged darkness[w]. *The Plant Cell*, *16*(12), 3304–3325. https://doi.org/10.1105/tpc.104.025973

Gibon, Y., Bläsing, O. E., Palacios-rojas, N., Pankovic, D., Hendriks, J. H., Fisahn, J., Höhne, M., Günther, M., & Stitt, M. (2004). Adjustment of diurnal starch turnover to short days: Depletion of sugar during the night leads to a temporary inhibition of carbohydrate utilization, accumulation of sugars and post-translational activation of ADP-glucose pyrophosphorylase in the following light period. *The Plant Journal*, *39*(6), 847–862. https://doi.org/10.1111/j.1365-313x.2004.02173.x

Goodrich, B., Gabry, J., Ali, I., & Brilleman, S. (2022). Rstanarm: Bayesian applied regression modeling via Stan. [R package version 2.21.3].

Granda, E., Camarero, J. J., Gimeno, T. E., Martınez-fernández, J., & Valladares, F. (2013). Intensity and timing of warming and drought differentially affect growth patterns of co-occurring mediterranean tree species. *European Journal of Forest Research*, *132*(3), 469–480. https://doi.org/10.1007/s10342-013-0687-0

Griffin, K. L., Winner, W. E., & Strain, B. R. (1996). Construction cost of loblolly and ponderosa pine leaves grown with varying carbon and nitrogen availability. *Plant, Cell and Environment*, *19*(6), 729–738. https://doi.org/10.1111/j.1365-3040.1996.tb00408.x

Guckenheimer, J., & Holmes, P. (1983). *Nonlinear oscillations, dynamical systems, and bifurcations of vector fields* (Vol. 42). New York, NY, Springer New York. https://doi.org/10.1007/978-1-4612-1140-2

Hartmann, H., Adams, H. D., Hammond, W. M., Hoch, G., Landhäusser, S. M., Wiley, E., & Zaehle, S. (2018). Identifying differences in carbohydrate dynamics of seedlings and mature trees to improve carbon allocation in models for trees and forests. *Environmental and Experimental Botany*, *152*, 7–18. https://doi.org/10.1016/j.envexpbot.2018.03.011

Hartmann, H., Bahn, M., Carbone, M., & Richardson, A. D. (2020). Plant carbon allocation in a changing world – challenges and progress: Introduction to a virtual issue on carbon allocation. *New Phytologist*, *227*(4), 981–988. https://doi.org/10.1111/nph.16757

Hartmann, H., & Trumbore, S. (2016). Understanding the roles of nonstructural carbohydrates in forest trees – from what we can measure to what we want to know. *New Phytologist*, *211*(2), 386–403. https://doi.org/10.1111/nph.13955

Hartmann, H., Ziegler, W., & Trumbore, S. (2013). Lethal drought leads to reduction in nonstructural carbohydrates in norway spruce tree roots but not in the canopy (A. Knapp, Ed.). *Functional Ecology*, *27*(2), 413–427. https://doi.org/10.1111/1365-2435.12046

Hayat, A., Hacket-pain, A. J., Pretzsch, H., Rademacher, T. T., & Friend, A. D. (2017). Modeling tree growth taking into account carbon source and sink limitations. *Frontiers in Plant Science*, *8*. https://doi.org/10.3389/fpls.2017.00182

Hinman, E. D., & Fridley, J. D. (2018). To spend or to save? assessing energetic growth-storage tradeoffs in native and invasive woody plants. *Oecologia*, *188*(3), 659–669. https://doi.org/10.1007/s00442-018-4177-4

Hoch, G., Richter, A., & Körner, C. (2003). Non-structural carbon compounds in temperate forest trees. *Plant, Cell and Environment*, *26*(7), 1067–1081. https://doi.org/10.1046/j.0016-8025.2003.01032.x

Hoch, G. (2015, August). Carbon reserves as indicators for carbon limitation in trees. In *Progress in botany* (pp. 321–346). Springer International Publishing. https://doi.org/10.1007/978-3-319-08807-5_13

Hoch, G., Popp, M., & Körner, C. (2002). Altitudinal increase of mobile carbon pools in *p*inus cembra suggests sink limitation of growth at the swiss treeline. *Oikos*, *98*(3), 361–374. https://doi.org/10.1034/j.1600-0706.2002.980301.x

Högberg, P., Nordgren, A., Buchmann, N., Taylor, A. F. S., Ekblad, A., Högberg, M. N., Nyberg, G., Ottosson-löfvenius, M., & Read, D. J. (2001). Large-scale forest girdling shows that current photosynthesis drives soil respiration. *Nature*, *411*(6839), 789–792. https://doi.org/10.1038/35081058

Hsiao, T. C. (1973). Plant responses to water stress. *Annual Review of Plant Physiology*, *24*(1), 519–570. https://doi.org/10.1146/annurev.pp.24.060173.002511

Hsiao, T. C., Fereres, E., Acevedo, E., & Henderson, D. W. (1976). Water stress and dynamics of growth and yield of crop plants. In *Ecological studies* (pp. 281–305). Springer Berlin Heidelberg. https://doi.org/10.1007/978-3-642-66429-8_18

Huang, J., Hammerbacher, A., Gershenzon, J., Dam, N. M. V., Sala, A., Mcdowell, N. G., Chowdhury, S., Gleixner, G., Trumbore, S., & Hartmann, H. (2021). Storage of carbon reserves in spruce trees is prioritized over growth in the face of carbon limitation. *Proceedings of the National Academy of Sciences*, *118*(33). https://doi.org/10.1073/pnas.2023297118

Huang, M., Wang, X., Keenan, T. F., & Piao, S. (2018). Drought timing influences the legacy of tree growth recovery. *Global Change Biology*, *24*(8), 3546–3559. https://doi.org/10.1111/gcb.14294

Iwasa, Y., Cohen, D., & Leon, J. (1984). Tree height and crown shape, as results of competitive games. *Journal of Theoretical Biology*, *112*, 279–297.

Iwasa, Y., & Cohen, D. (1989). Optimal growth schedule of a perennial plant. *The American Naturalist*, *133*(4), 480–505. https://doi.org/10.1086/284931

Jensen, K. H. (2018). Phloem physics: Mechanisms, constraints, and perspectives. *Current Opinion in Plant Biology*, *43*, 96–100. https://doi.org/10.1016/j.pbi.2018.03.005

Jensen, K. H., Berg-sørensen, K., Friis, S. M. M., & Bohr, T. (2012). Analytic solutions and universal properties of sugar loading models in münch phloem flow. *Journal of Theoretical Biology*, *304*, 286–296. https://doi.org/10.1016/j.jtbi.2012.03.012

Johnson, I. R., Melkonian, J. J., Thornley, J. H. M., & Riha, S. J. (1991). A model of water flow through plants incorporating shoot/root 'message' control of stomatal conductance. *Plant, Cell and Environment*, *14*(6), 531–544. https://doi.org/10.1111/j.1365-3040.1991.tb01524.x

Jones, S., Rowland, L., Cox, P., Hemming, D., Wiltshire, A., Williams, K., Parazoo, N. C., Liu, J., Costa, A. C. L. D., Meir, P., Mencuccini, M., & Harper, A. B. (2020). The impact of a simple representation of non-structural carbohydrates on the simulated response of tropical forests to drought. *Biogeosciences*, *17*(13), 3589–3612. https://doi.org/10.5194/bg-17-3589-2020

Kannenberg, S. A., Novick, K. A., & Phillips, R. P. (2017). Coarse roots prevent declines in whole-tree non-structural carbohydrate pools during drought in an isohydric and an anisohydric species. *Tree Physiology*, *38*(4), 582–590. https://doi.org/10.1093/treephys/tpx119

Kannenberg, S. A., & Phillips, R. P. (2019). Non-structural carbohydrate pools not linked to hydraulic strategies or carbon supply in tree saplings during severe drought and subsequent recovery (M. Ryan, Ed.). *Tree Physiology*, *40*(2), 259–271. https://doi.org/10.1093/treephys/tpz132

Keeling, C. D., Bacastow, R. B., Bainbridge, A. E., Ekdahl, C. A., Guenther, P. R., Waterman, L. S., & Chin, J. F. S. (1976). Atmospheric carbon dioxide variations at mauna loa observatory, hawaii. *Tellus*, *28*(6), 538–551. https://doi.org/10.1111/j.2153-3490.1976.tb00701.x

Klein, T., & Hoch, G. (2015). Tree carbon allocation dynamics determined using a carbon mass balance approach. *New Phytologist*, *205*(1), 147–159. https://doi.org/10.1111/nph.12993

Klinkhamer, P. G. L., Kubo, T., & Iwasa, Y. (1997). Herbivores and the evolution of the semelparous perennial life-history of plants. *Journal of Evolutionary Biology*, *10*(4), 529–550. https://doi.org/10.1046/j.1420-9101.1997.10040529.x

Knoblauch, M., Knoblauch, J., Mullendore, D. L., Savage, J. A., Babst, B. A., Beecher, S. D., Dodgen, A. C., Jensen, K. H., & Holbrook, N. M. (2016). Testing the münch hypothesis of long distance phloem transport in plants. *eLife*, *5*. https://doi.org/10.7554/elife.15341

Körner, C. (2003). Carbon limitation in trees. *Journal of Ecology*, *91*(1), 4–17. https://doi.org/10.1046/j.1365-2745.2003.00742.x

Körner, C. (2015). Paradigm shift in plant growth control. *Current Opinion in Plant Biology*, *25*, 107–114. https://doi.org/10.1016/j.pbi.2015.05.003

Kozłowski, J., & Wiegert, R. G. (1986). Optimal allocation of energy to growth and reproduction. *Theoretical Population Biology*, *29*(1), 16–37. https://doi.org/10.1016/0040-5809(86)90003-1

Kozlowski, T. T. (1992). Carbohydrate sources and sinks in woody plants. *Botanical Review*, *58*(2), 107–222. https://doi.org/10.1007/Bf02858600

Lacointe, A., & Minchin, P. E. H. (2008). Modelling phloem and xylem transport within a complex architecture. *Functional Plant Biology*, *35*(10), 772. https://doi.org/10.1071/fp08085

Landhäusser, S. M., Chow, P. S., Dickman, L. T., Furze, M. E., Kuhlman, I., Schmid, S., Wiesenbauer, J., Wild, B., Gleixner, G., Hartmann, H., Hoch, G., Mcdowell, N. G., Richardson, A. D., Richter, A., & Adams, H. D. (2018). Standardized protocols and procedures can precisely and accurately quantify non-structural carbohydrates. *Tree Physiology*. https://doi.org/10.1093/treephys/tpy118

Landsberg, J. J. (2011). *Physiological ecology of forest production : Principles, processes and models*. Amsterdam Boston, Elsevier/Academic Press.

Landsberg, J. J., & Waring, R. H. (1997). A generalised model of forest productivity using simplified concepts of radiation-use efficiency, carbon balance and partitioning. *Forest Ecology and Management*, *95*(3), 209–228. https://doi.org/10.1016/s0378-1127(97)00026-1

Landsberg, J. J. (2003). Modelling forest ecosystems: State of the art, challenges, and future directions. *Canadian Journal of Forest Research*, *33*(3), 385–397. https://doi.org/10.1139/x02-129

Le Roux, X., Lacointe, A., Escobar-gutierrez, A. J., & Le Dizes, S. (2001). Carbon-based models of individual tree growth: A critical appraisal. *Annals of Forest Science*, *58*(5), 469–506. https://doi.org/10.1051/forest:2001140

Lee, J. (2003). *Introduction to smooth manifolds*. New York, Springer.

Leuzinger, S., Manusch, C., Bugmann, H., & Wolf, A. (2013). A sink-limited growth model improves biomass estimation along boreal and alpine tree lines. *Global Ecology and Biogeography*, *22*(8), 924–932. https://doi.org/10.1111/geb.12047

Li, H., Hoch, G., & Körner, C. (2002). Source/sink removal affects mobile carbohydrates in *p*inus cembra at the swiss treeline. *Trees*, *16*(4), 331–337. https://doi.org/10.1007/s00468-002-0172-8

Lovenduski, N. S., & Bonan, G. B. (2017). Reducing uncertainty in projections of terrestrial carbon uptake. *Environmental Research Letters*, *12*(4), 044020. https://doi.org/10.1088/1748-9326/aa66b8

Lu, D., & Ricciuto, D. (2019). Efficient surrogate modeling methods for large-scale earth system models based on machine-learning techniques. *Geoscientific Model Development*, *12*(5), 1791–1807. https://doi.org/10.5194/gmd-12-1791-2019

Lu, Y., Gehan, J. P., & Sharkey, T. D. (2005). Daylength and circadian effects on starch degradation and maltose metabolism. *Plant Physiology*, *138*(4), 2280–2291. https://doi.org/10.1104/pp.105.061903

Luedtke, C. M. (2013, December). *Carbon dioxide fluxes and nonstructural carbohydrates in seedlings asinfluenced by heat, drought, and low light* (Master's thesis). University of Georgia.

Luo, Y., Shi, Z., Lu, X., Xia, J., Liang, J., Jiang, J., Wang, Y., Smith, M. J., Jiang, L., Ahlström, A., Chen, B., Hararuk, O., Hastings, A., Hoffman, F., Medlyn, B., Niu, S., Rasmussen, M., Todd-brown, K., & Wang, Y.-p. (2017). Transient dynamics of terrestrial carbon storage: Mathematical foundation and its applications. *Biogeosciences*, *14*(1), 145–161. https://doi.org/10.5194/bg-14-145-2017

Ma, S., He, F., Tian, D., Zou, D., Yan, Z., Yang, Y., Zhou, T., Huang, K., Shen, H., & Fang, J. (2018). Variations and determinants of carbon content in plants: A global synthesis. *Biogeosciences*, *15*(3), 693–702. https://doi.org/10.5194/bg-15-693-2018

Maire, V., Martre, P., Kattge, J., Gastal, F., Esser, G., Fontaine, S., & Soussana, J.-f. (2012). The coordination of leaf photosynthesis links c and n fluxes in c3 plant species (B. Bond-Lamberty, Ed.). *PLoS ONE*, *7*(6), e38345. https://doi.org/10.1371/journal.pone.0038345

Martínez-Vilalta, J., Anderegg, W. R. L., Sapés, G., & Sala, A. (2019). Greater focus on water pools may improve our ability to understand and anticipate drought-induced mortality in plants. *New Phytologist*, *223*(1), 22–32. https://doi.org/10.1111/nph.15644

Martínez-vilalta, J., Sala, A., Asensio, D., Galiano, L., Hoch, G., Palacio, S., Piper, F. I., & Lloret, F. (2016). Dynamics of non-structural carbohydrates in terrestrial plants: A global synthesis. *Ecological Monographs*, *86*(4), 495–516. https://doi.org/10.1002/ecm.1231

Mcdowell, N. G. (2011). Mechanisms linking drought, hydraulics, carbon metabolism, and vegetation mortality. *Plant Physiology*, *155*(3), 1051–1059. https://doi.org/10.1104/pp.110.170704

Mcdowell, N. G., & Sevanto, S. (2010). The mechanisms of carbon starvation: How, when, or does it even occur at all? *New Phytologist*, *186*(2), 264–266. https://doi.org/10.1111/j.1469-8137.2010.03232.x

Mcdowell, N. G., Fisher, R. A., Xu, C., Domec, J. C., Hölttä, T., Mackay, D. S., Sperry, J. S., Boutz, A., Dickman, L., Gehres, N., Limousin, J. M., Macalady, A., Martınez-vilalta, J., Mencuccini, M., Plaut, J. A., Ogée, J., Pangle, R. E., Rasse, D. P., Ryan, M. G., … Pockman, W. T. (2013). Evaluating theories of drought-induced vegetation mortality using a multimodel-experiment framework. *New Phytologist*, *200*(2), 304–321. https://doi.org/10.1111/nph.12465

Mcdowell, N. G., Pockman, W. T., Allen, C. D., Breshears, D. D., Cobb, N., Kolb, T., Plaut, J., Sperry, J., West, A., Williams, D. G., & Yepez, E. A. (2008). Mechanisms of plant survival and mortality during drought: Why do some plants survive while others succumb to drought? *New Phytologist*, *178*(4), 719–739. https://doi.org/10.1111/j.1469-8137.2008.02436.x

Merganičová, K., Merganič, J., Lehtonen, A., Vacchiano, G., Sever, M. Z. O., Augustynczik, A. L. D., Grote, R., Kyselová, I., Mäkelä, A., Yousefpour, R., Krejza, J., Collalti, A., & Reyer, C. P. O. (2019). Forest carbon allocation modelling under climate change (A. Polle, Ed.). *Tree Physiology*, *39*(12), 1937–1960. https://doi.org/10.1093/treephys/tpz105

Nemali, K. S., & van Iersel, M. W. (2006). An automated system for controlling drought stress and irrigation in potted plants. *Scientia Horticulturae*, *110*(3), 292–297. https://doi.org/10.1016/j.scienta.2006.07.009

Norby, R. J., Todd, D. E., Fults, J., & Johnson, D. W. (2001). Allometric determination of tree growth in a CO_2-enriched sweetgum stand. *New Phytologist*, *150*(2), 477–487. https://doi.org/10.1046/j.1469-8137.2001.00099.x

Norby, R. J., Warren, J. M., Iversen, C. M., Childs, J., Jawdy, S. S., & Walker, A. P. (2022). Forest stand and canopy development unaltered by 12 years of CO2 enrichment (D. Tissue, Ed.). *Tree Physiology*, *42*(3), 428–440. https://doi.org/10.1093/treephys/tpab107

Norby, R. J., Warren, J. M., Iversen, C. M., Medlyn, B. E., & Mcmurtrie, R. E. (2010). CO_2 enhancement of forest productivity constrained by limited nitrogen availability. *Proceedings of the National Academy of Sciences*, *107*(45), 19368–19373. https://doi.org/10.1073/pnas.1006463107

Norby, R. J., & Zak, D. R. (2011). Ecological lessons from free-air CO2 enrichment (FACE) experiments. *Annual Review of Ecology, Evolution, and Systematics*, *42*(1), 181–203. https://doi.org/10.1146/annurev-ecolsys-102209-144647

Nowak, M. A., & Sigmund, K. (2004). Evolutionary dynamics of biological games. *Science*, *303*(5659), 793–799. https://doi.org/10.1126/science.1093411

Nowak, R. S., Ellsworth, D. S., & Smith, S. D. (2004). Functional responses of plants to elevated atmospheric CO2- do photosynthetic and productivity data from FACE experiments support early predictions? *New Phytologist*, *162*(2), 253–280. https://doi.org/10.1111/j.1469-8137.2004.01033.x

Oleson, K., Lawrence, D., Bonan, G., Drewniak, B., Huang, M., Koven, C., Levis, S., Li, F., Riley, W., Subin, Z., Swenson, S., Thornton, P., Bozbiyik, A., Fisher, R., Heald, C., Kluzek, E., Lamarque, J.-f., Lawrence, P., Leung, L., … Yang, Z.-l. (2013). *Technical description of version 4.5 of the community land model (clm)* (tech. rep.). UCAR/NCAR. https://doi.org/10.5065/D6RR1W7M

Oswald, S. W., & Aubrey, D. P. (2020). Xeric tree populations exhibit delayed summer depletion of root starch relative to mesic counterparts. *Forests*, *11*(10), 1026. https://doi.org/10.3390/f11101026

Oswald, S. W., & Aubrey, D. P. (2023). Modeling starch dynamics from seasonal variations of photosynthesis, growth, and respiration. *Tree Physiology*. https://doi.org/10.1093/treephys/tpad007

Page, K. M., & Nowak, M. A. (2002). Unifying evolutionary dynamics. *Journal of Theoretical Biology*, *219*(1), 93–98. https://doi.org/10.1006/jtbi.2002.3112

Piper, F. I. (2011). Drought induces opposite changes in the concentration of non-structural carbohydrates of two evergreen nothofagus species of differential drought resistance. *Annals of Forest Science*, *68*(2), 415–424. https://doi.org/10.1007/s13595-011-0030-1

Piper, F. I. (2021). Putting non-structural compounds on the map of plant life history strategies: A commentary on schoonmaker et al. (S. Sevanto, Ed.). *Tree Physiology*, *41*(9), 1559–1562. https://doi.org/10.1093/treephys/tpab088

Potkay, A., Hölttä, T., Trugman, A. T., & Fan, Y. (2022). Turgor-limited predictions of tree growth, height and metabolic scaling over tree lifespans (M. Ryan, Ed.). *Tree Physiology*, *42*(2), 229–252. https://doi.org/10.1093/treephys/tpab094

Prentice, I. C., Liang, X., Medlyn, B. E., & Wang, Y.-p. (2015). Reliable, robust and realistic: The three r's of next-generation land-surface modelling. *Atmospheric Chemistry and Physics*, *15*(10), 5987–6005. https://doi.org/10.5194/acp-15-5987-2015

Prentice, I. C., Dong, N., Gleason, S. M., Maire, V., & Wright, I. J. (2014). Balancing the costs of carbon gain and water transport: Testing a new theoretical framework for plant functional ecology (J. Penuelas, Ed.). *Ecology Letters*, *17*(1), 82–91. https://doi.org/10.1111/ele.12211

Quentin, A. G., Rodemann, T., Doutreleau, M.-F., Moreau, M., & Davies, N. W. (2017). Application of near-infrared spectroscopy for estimation of non-structural carbohydrates in foliar samples ofEucalyptus globulusLabilladière (P. Millard, Ed.). *Tree Physiology*. https://doi.org/10.1093/treephys/tpw083

Quetin, G. R., & Swann, A. L. S. (2018). Sensitivity of leaf area to interannual climate variation as a diagnostic of ecosystem function in CMIP5 carbon cycle models. *Journal of Climate*, *31*(20), 8607–8625. https://doi.org/10.1175/jcli-d-17-0580.1

Richardson, A. D., Carbone, M. S., Keenan, T. F., Czimczik, C. I., Hollinger, D. Y., Murakami, P., Schaberg, P. G., & Xu, X. (2013). Seasonal dynamics and age of stemwood nonstructural carbohydrates in temperate forest trees. *New Phytologist*, *197*(3), 850–861. https://doi.org/10.1111/nph.12042

Rietkerk, M. (2004). Self-organized patchiness and catastrophic shifts in ecosystems. *Science*, *305*(5692), 1926–1929. https://doi.org/10.1126/science.1101867

Rietkerk, M., Bastiaansen, R., Banerjee, S., van de Koppel, J., Baudena, M., & Doelman, A. (2021). Evasion of tipping in complex systems through spatial pattern formation. *Science*, *374*(6564). https://doi.org/10.1126/science.abj0359

Rowe, D. B., Blazich, F. A., & Raper, C. D. (2002). *New Forests*, *24*(1), 39–51. https://doi.org/10.1023/a:1020551029894

Ruswick, S. K., O'Brien, J. J., & Aubrey, D. P. (2021). Carbon starvation is absent regardless of season of burn in liquidambar styraciflua l. *Forest Ecology and Management*, *479*, 118588. https://doi.org/10.1016/j.foreco.2020.118588

Sala, A., Woodruff, D. R., & Meinzer, F. C. (2012). Carbon dynamics in trees: Feast or famine? *Tree Physiology*, *32*(6), 764–775. https://doi.org/10.1093/treephys/tpr143

Sapés, G., Demaree, P., Lekberg, Y., & Sala, A. (2020). Plant carbohydrate depletion spreads via ectomycorrhizal networks impairing plant water relations. https://doi.org/10.1101/2020.08.03.234823

Sapés, G., Demaree, P., Lekberg, Y., & Sala, A. (2021). Plant carbohydrate depletion impairs water relations and spreads via ectomycorrhizal networks. *New Phytologist*, *229*(6), 3172–3183. https://doi.org/10.1111/nph.17134

Sapés, G., Roskilly, B., Dobrowski, S., Maneta, M., Anderegg, W. R. L., Martínez-Vilalta, J., & Sala, A. (2019). Plant water content integrates hydraulics and carbon depletion to predict drought-induced seedling mortality. *Tree Physiology*, *39*(8), 1300–1312. https://doi.org/10.1093/treephys/tpz062

Saugier, B., Roy, J., & Mooney, H. A. (2001). Estimations of global terrestrial productivity. In *Terrestrial global productivity* (pp. 543–557). Elsevier. https://doi.org/10.1016/b978-012505290-0/50024-7

Schaffer, W. M. (1983). The application of optimal control theory to the general life history problem. *The American Naturalist*, *121*(3), 418–431. https://www.jstor.org/stable/2461159

Scheffer, M., Carpenter, S., Foley, J. A., Folke, C., & Walker, B. (2001). Catastrophic shifts in ecosystems. *Nature*, *413*(6856), 591–596. https://doi.org/10.1038/35098000

Schiestl-Aalto, P., Kulmala, L., Mäkinen, H., Nikinmaa, E., & Mäkelä, A. (2015). CASSIA – a dynamic model for predicting intra-annual sink demand and interannual growth variation in Scots pine. *New Phytologist*, *206*(2), 647–659. https://doi.org/10.1111/nph.13275

Schiestl-Aalto, P., Ryhti, K., Mäkelä, A., Peltoniemi, M., Bäck, J., & Kulmala, L. (2019). Analysis of the NSC storage dynamics in tree organs reveals the allocation to belowground symbionts in the framework of whole tree carbon balance. *Frontiers in Forests and Global Change*, *2*. https://doi.org/10.3389/ffgc.2019.00017

Schnepf, A., Leitner, D., Landl, M., Lobet, G., Mai, T. H., Morandage, S., Sheng, C., Zörner, M., Vanderborght, J., & Vereecken, H. (2018). Crootbox: A structural–functional modelling framework for root systems. *Annals of Botany*, *121*(5), 1033–1053. https://doi.org/10.1093/aob/mcx221

Schönbeck, L., Gessler, A., Hoch, G., McDowell, N. G., Rigling, A., Schaub, M., & Li, M.-H. (2018). Homeostatic levels of nonstructural carbohydrates after 13 yr of drought and irrigation in pinus sylvestris. *New Phytologist*, *219*(4), 1314–1324. https://doi.org/10.1111/nph.15224

Schoonmaker, A. L., Hillabrand, R. M., Lieffers, V. J., Chow, P. S., & Landhäusser, S. M. (2021). Seasonal dynamics of non-structural carbon pools and their relationship to growth in two boreal conifer tree species (A. Mäkelä, Ed.), *41*(9), 1563–1582. https://doi.org/10.1093/treephys/tpab013

Schulze, W., Stitt, M., Schulze, E.-d., Neuhaus, H. E., & Fichtner, K. (1991). A quantification of the significance of assimilatory starch for growth of *a*rabidopsis thaliana l. heynh. *Plant Physiology*, *95*(3), 890–895. https://doi.org/10.1104/pp.95.3.890

Secchi, F., & Zwieniecki, M. A. (2011). Sensing embolism in xylem vessels: The role of sucrose as a trigger for refilling: Sensing embolism in poplar vessels. *Plant, Cell and Environment*, *34*(3), 514–524. https://doi.org/10.1111/j.1365-3040.2010.02259.x

Sevanto, S. (2014). Phloem transport and drought. *Journal of Experimental Botany*, *65*(7), 1751–1759. https://doi.org/10.1093/jxb/ert467

Sevanto, S. (2018). Drought impacts on phloem transport. *Current Opinion in Plant Biology*, *43*, 76–81. https://doi.org/10.1016/j.pbi.2018.01.002

Sevanto, S., McDowell, N. G., Dickman, L. T., Pangle, R., & Pockman, W. T. (2014). How do trees die? a test of the hydraulic failure and carbon starvation hypotheses. *Plant, Cell & Environment*, *37*(1), 153–161. https://doi.org/10.1111/pce.12141

Silpi, U., Lacointe, A., Kasempsap, P., Thanysawanyangkura, S., Chantuma, P., Gohet, E., Musigamart, N., Clement, A., Ameglio, T., & Thaler, P. (2007). Carbohydrate reserves as a competing sink: Evidence from tapping rubber trees. *Tree Physiology*, *27*(6), 881–889. https://doi.org/10.1093/treephys/27.6.881

Smith, A. M., & Stitt, M. (2007). Coordination of carbon supply and plant growth. *Plant, Cell & Environment*, *30*(9), 1126–1149. https://doi.org/10.1111/j.1365-3040.2007.01708.x

Smith, N. G., Keenan, T. F., Prentice, I. C., Wang, H., Wright, I. J., Niinemets, Ü., Crous, K. Y., Domingues, T. F., Guerrieri, R., Ishida, F. Y., Kattge, J., Kruger, E. L., Maire, V., Rogers, A., Serbin, S. P., Tarvainen, L., Togashi, H. F., Townsend, P. A., Wang, M., … Zhou, S.-X. (2019). Global photosynthetic capacity is optimized to the environment (S. Niu, Ed.). *Ecology Letters*, *22*(3), 506–517. https://doi.org/10.1111/ele.13210

Smith, S. M., Fulton, D. C., Chia, T., Thorneycroft, D., Chapple, A., Dunstan, H., Hylton, C., Zeeman, S. C., & Smith, A. M. (2004). Diurnal changes in the transcriptome encoding enzymes of starch metabolism provide evidence for both transcriptional and posttranscriptional regulation of starch metabolism in arabidopsis leaves. *Plant Physiology*, *136*(1), 2687–2699. https://doi.org/10.1104/pp.104.044347

Sperry, J. S., & Love, D. M. (2015). What plant hydraulics can tell us about responses to climate-change droughts. *New Phytologist*, *207*(1), 14–27. https://doi.org/10.1111/nph.13354

Stan Development Team. (2022). RStan: The R interface to Stan [R package version 2.21.7]. http://mc-stan.org/

Strogatz, S. H. (1994). *Nonlinear dynamics and chaos: With applications to physics, biology, chemistry, and engineering*. Addison-Wesley Pub.

Stroock, A. D., Pagay, V. V., Zwieniecki, M. A., & Holbrook, N. M. (2014). The physicochemical hydrodynamics of vascular plants. *Annual Review of Fluid Mechanics*, *46*(1), 615–642. https://doi.org/10.1146/annurev-fluid-010313-141411

Talbott, L. D., & Zeiger, E. (1993). Sugar and organic acid accumulation in guard cells of vicia faba in response to red and blue light. *Plant Physiology*, *102*(4), 1163–1169. https://doi.org/10.1104/pp.102.4.1163

Talbott, L. D., & Zeiger, E. (1998). The role of sucrose in guard cell osmoregulation. *Journal of Experimental Botany*, *49*(90001), 329–337. https://doi.org/10.1093/jexbot/49.suppl_1.329

Tang, J. Y. (2015). On the relationships between the michaelis–menten kinetics, reverse michaelis–menten kinetics, equilibrium chemistry approximation kinetics, and quadratic kinetics. *Geoscientific Model Development*, *8*(12), 3823–3835. https://doi.org/10.5194/gmd-8-3823-2015

Thompson, M. V., & Holbrook, N. (2003). Application of a single-solute non-steady-state phloem model to the study of long-distance assimilate transport. *Journal of Theoretical Biology*, *220*(4), 419–455. https://doi.org/10.1006/jtbi.2003.3115

Thornley, J. H. M. (1970). Respiration, growth and maintenance in plants. *Nature*, *227*(5255), 304–305. https://doi.org/10.1038/227304b0

Thornley, J. H. M. (1971). Energy, respiration, and growth in plants [Publisher: Oxford University Press]. *Annals of Botany*, *35*(142), 721–728. Retrieved September 22, 2022, from http://www.jstor.org/stable/42751963

Thornley, J. H. M. (1972). A balanced quantitative model for root: Shoot ratios in vegetative plants. *Annals of Botany*, *36*(2), 431–441. https://doi.org/10.1093/oxfordjournals.aob.a084602

Thornley, J. H. M. (1991). A transport-resistance model of forest growth and partitioning. *Annals of Botany*, *68*(3), 211–226. https://doi.org/10.1093/oxfordjournals.aob.a088246

Thornley, J. H. M. (2011). Plant growth and respiration re-visited: Maintenance respiration defined – it is an emergent property of, not a separate process within, the system – and why the respiration : photosynthesis ratio is conservative. *Annals of Botany*, *108*(7), 1365–1380. https://doi.org/10.1093/aob/mcr238

Tixier, A., Guzmán-Delgado, P., Sperling, O., Roxas, A. A., Laca, E., & Zwieniecki, M. A. (2020). Comparison of phenological traits, growth patterns, and seasonal dynamics of non-structural carbohydrate in mediterranean tree crop species. *Scientific Reports*, *10*(1). https://doi.org/10.1038/s41598-019-57016-3

Tixier, A., Orozco, J., Roxas, A. A., Earles, J. M., & Zwieniecki, M. A. (2018). Diurnal variation in nonstructural carbohydrate storage in trees: Remobilization and vertical mixing. *Plant Physiology*, 00923 2018. https://doi.org/10.1104/pp.18.00923

Tyson, J. J., Chen, K. C., & Novak, B. (2003). Sniffers, buzzers, toggles and blinkers: Dynamics of regulatory and signaling pathways in the cell. *Current Opinion in Cell Biology*, *15*(2), 221–231. https://doi.org/10.1016/s0955-0674(03)00017-6

von Caemmerer, S. (2013). Steady-state models of photosynthesis: Steady-state models of photosynthesis. *Plant, Cell & Environment*, *36*(9), 1617–1630. https://doi.org/10.1111/pce.12098

Walker, A. P., Kauwe, M. G. D., Bastos, A., Belmecheri, S., Georgiou, K., Keeling, R. F., McMahon, S. M., Medlyn, B. E., Moore, D. J. P., Norby, R. J., Zaehle, S., Anderson-Teixeira, K. J., Battipaglia, G., Brienen, R. J. W., Cabugao, K. G., Cailleret, M., Campbell, E., Canadell, J. G., Ciais, P., … Zuidema, P. A. (2021). Integrating the evidence for a terrestrial carbon sink caused by increasing atmospheric CO_2. *New Phytologist*, *229*(5), 2413–2445. https://doi.org/10.1111/nph.16866

Wang, B., & Allison, S. D. (2019). Emergent properties of organic matter decomposition by soil enzymes. *Soil Biology and Biochemistry*, *136*, 107522. https://doi.org/10.1016/j.soilbio.2019.107522

Weber, R., Gessler, A., & Hoch, G. (2019). High carbon storage in carbon-limited trees. *New Phytologist*, *222*(1), 171–182. https://doi.org/10.1111/nph.15599

Weber, R., Schwendener, A., Schmid, S., Lambert, S., Wiley, E., Landhäusser, S. M., Hartmann, H., & Hoch, G. (2018). Living on next to nothing: Tree seedlings can survive weeks with very low carbohydrate concentrations. *New Phytologist*, *218*(1), 107–118. https://doi.org/10.1111/nph.14987

Wiggins, S. (1996). *Introduction to applied nonlinear dynamical systems and chaos* (Corr. 3rd print). New York, Springer-Verlag.

Wiley, E., & Helliker, B. (2012). A re-evaluation of carbon storage in trees lends greater support for carbon limitation to growth. *New Phytologist*, *195*(2), 285–289. https://doi.org/10.1111/j.1469-8137.2012.04180.x

Wiley, E., King, C. M., & Landhäusser, S. M. (2019). Identifying the relevant carbohydrate storage pools available for remobilization in aspen roots (D. Tissue, Ed.). *Tree Physiology*, *39*(7), 1109–1120. https://doi.org/10.1093/treephys/tpz051

Woodruff, D. R. (2014). The impacts of water stress on phloem transport in douglas-fir trees. *Tree Physiology*, *34*(1), 5–14. https://doi.org/10.1093/treephys/tpt106

Woodruff, D. R., Bond, B. J., & Meinzer, F. C. (2004). Does turgor limit growth in tall trees? *Plant, Cell and Environment*, *27*(2), 229–236. https://doi.org/10.1111/j.1365-3040.2003.01141.x

Woodruff, D. R., & Meinzer, F. C. (2011). Water stress, shoot growth and storage of non-structural carbohydrates along a tree height gradient in a tall conifer. *Plant, Cell & Environment*, *34*(11), 1920–1930. https://doi.org/10.1111/j.1365-3040.2011.02388.x

Würth, M. K. R., Winter, K., & Körner, C. (1998). Leaf carbohydrate responses to CO_2 enrichment at the top of a tropical forest. *Oecologia*, *116*(1-2), 18–25. https://doi.org/10.1007/pl00013821

Xiao, J., Zhuang, Q., Law, B. E., Chen, J., Baldocchi, D. D., Cook, D. R., Oren, R., Richardson, A. D., Wharton, S., & Ma, S. (2010). A continuous measure of gross primary production for the conterminous united states derived from MODIS and AmeriFlux data. *Remote Sensing of Environment*, *114*(3), 576–591. https://doi.org/10.1016/j.rse.2009.10.013

Yin, X., & Struik, P. C. (2009). C3 and c4 photosynthesis models: An overview from the perspective of crop modelling. *NJAS - Wageningen Journal of Life Sciences*, *57*(1), 27–38. https://doi.org/10.1016/j.njas.2009.07.001